

Angefertigt am Helmholtz Zentrum München  
Abteilung Genvektoren  
Direktor: Prof. Dr. med. vet. Wolfgang Hammerschmidt



Dissertation zum Erwerb des Doktorgrades der Naturwissenschaften  
an der Medizinischen Fakultät  
der Ludwig-Maximilians-Universität München

**Generation and characterisation of new  
potential therapeutic antibodies targeting  
surface PRDX4**

vorgelegt von  
Julia Christina Hörmann

aus  
Landsberg am Lech

2022

Mit Genehmigung der Medizinischen Fakultät  
der Universität München

**Betreuer:** Prof. Dr. rer. nat. Reinhard Zeidler

**Zweitgutachter:** Prof. Dr. rer. nat. Rainer Glaß

**Dekan:** Prof. Dr. med. Thomas Gudermann

**Tag der mündlichen Prüfung:** 10. März 2023

## Eidesstaatliche Erklärung

Ich erkläre hiermit an Eides statt,  
dass ich die vorliegende Dissertation mit dem Titel

**„Generation and characterisation of new potential therapeutic antibodies targeting surface PRDX4“**

selbstständig verfasst, mich außer der angegebenen keiner weiteren Hilfsmittel bedient und alle Erkenntnisse, die aus dem Schrifttum ganz oder annähernd übernommen sind, als solche kenntlich gemacht und nach ihrer Herkunft unter Bezeichnung der Fundstelle einzeln nachgewiesen habe.

Ich erkläre des Weiteren, dass die hier vorgelegte Dissertation nicht in gleicher oder in ähnlicher Form bei einer anderen Stelle zur Erlangung eines akademischen Grades eingereicht wurde.

München, den 29. März 2023

Julia Christina Hörmann

---

Julia Christina Hörmann

*„The art and science of asking questions is the source of all knowledge.“*

Thomas Berger



# Contents

<b>List of Figures</b>	<b>V</b>
<b>List of Tables</b>	<b>VII</b>
<b>List of Abbreviations</b>	<b>IX</b>
<b>1 Abstract</b>	<b>1</b>
<b>2 Introduction</b>	<b>5</b>
2.1 Evolution of cancer . . . . .	5
2.1.1 Immunoavoidance of cancer cells . . . . .	6
2.1.2 The role of hypoxia in tumour progression . . . . .	8
2.2 Cancer therapy . . . . .	10
2.3 Antibodies in cancer immunotherapy . . . . .	11
2.3.1 Structure and function of antibodies . . . . .	11
2.3.2 Antibody effector mechanism . . . . .	14
2.4 Peroxiredoxin 4 . . . . .	15
2.5 Extracellular vesicles . . . . .	18
2.5.1 EVs in cancer . . . . .	20
2.6 Aim of this thesis . . . . .	22
<b>3 Materials</b>	<b>23</b>
3.1 General laboratory equipment . . . . .	23
3.2 General consumables . . . . .	26
3.3 Chemicals and Reagents . . . . .	29
3.4 General buffers and solutions . . . . .	33
3.5 Cell culture . . . . .	38
3.5.1 Cell culture media and additives . . . . .	38
3.5.2 Cell lines . . . . .	39
3.6 Antibodies . . . . .	41
3.7 Oligonucleotides . . . . .	46
3.7.1 Oligonucleotides for PRDX4 plasmid cloning . . . . .	46

## CONTENTS

---

3.7.2	Oligonucleotides for tPRDX4 detection in human cell lines . . . . .	47
3.7.3	Oligonucleotides for 5' RACE-PCR . . . . .	47
3.8	Plasmids . . . . .	49
3.9	Bacteria strain . . . . .	51
3.10	Commercial Kits . . . . .	52
3.11	Software . . . . .	53
3.12	Services and databases . . . . .	54
<b>4</b>	<b>Methods</b>	<b>57</b>
4.1	Cell biological methods . . . . .	57
4.1.1	Cell culture conditions . . . . .	57
4.1.2	Cryopreservation of cells . . . . .	58
4.1.3	Cell counting . . . . .	58
4.1.4	Isolation of PBMCs . . . . .	58
4.1.5	Transfection of cells . . . . .	59
4.2	Flow cytometry . . . . .	59
4.2.1	Epitope blocking assay . . . . .	59
4.2.2	Analysis of antibody $K_D$ . . . . .	59
4.3	Laser scanning confocal microscopy . . . . .	60
4.4	Microbiological methods - Transformation of bacteria . . . . .	60
4.5	Molecular biological methods . . . . .	61
4.5.1	Plasmid DNA purification from <i>Escheria coli (e. coli)</i> . . . . .	61
4.5.2	Isolation of RNA . . . . .	61
4.5.3	5' RACE-PCR to resolve antibody sequences . . . . .	62
4.5.4	Cloning of PRDX4 deletion constructs . . . . .	64
4.5.5	tPRDX4 plasmid construction . . . . .	66
4.5.6	PCR for tPRDX4 verification in human cell lines . . . . .	68
4.6	Protein biochemical methods . . . . .	70
4.6.1	Preparation of cell lysates . . . . .	70
4.6.2	Determination of protein concentration . . . . .	70
4.6.3	Subcellular fractionation of cell lysates . . . . .	70
4.6.4	Identification of antigen specificity of antibodies via IP . . . . .	71
4.6.5	Purification of His-tagged protein . . . . .	72
4.6.6	Biotinylation of cell surface . . . . .	72
4.6.7	SDS-PAGE . . . . .	73
4.6.8	Coomassie staining of PAA-gels . . . . .	73

---

4.6.9	Immunoblotting . . . . .	74
4.6.10	Dot blot . . . . .	74
4.6.11	ELISA for PRDX4 antibody clone testing . . . . .	75
4.7	Purification and characterisation of EVs . . . . .	75
4.7.1	Isolation via serial centrifugation . . . . .	75
4.7.2	Isolation and purification via iodixanol density gradient . . . . .	76
4.7.3	Quantification via NTA . . . . .	76
4.7.4	ELISA for detection of EVs in patient samples . . . . .	77
<b>5</b>	<b>Results</b>	<b>79</b>
5.1	Generation and characterisation of novel monoclonal antibodies . . . . .	79
5.1.1	Generation and selection of new mAbs targeting potential novel tumour antigens . . . . .	79
5.1.2	Identification of antibody specificity by mass spectrometry . . . . .	81
5.1.3	Discovery of PRDX4 as a new potential tumour antigen . . . . .	82
5.2	PRDX4 is expressed on the surface of various tumour cell lines . . . . .	87
5.3	PRDX4 is expressed on EVs . . . . .	94
5.4	PRDX4 antibodies are present in primary tumour samples . . . . .	96
5.5	CCDC47 is a novel interaction partner of PRDX4 . . . . .	97
5.6	Characterisation of PRDX4 antibodies . . . . .	100
5.6.1	Analysis of the PRDX4 antibody sequences by 5' RACE-PCR . . . . .	100
5.6.2	Evaluation of the PRDX4 antibodies binding site . . . . .	102
5.7	Humanisation of a PRDX4 antibody . . . . .	107
5.7.1	Testing the binding efficiency of different humanised HC and LC PRDX4 antibody sequences . . . . .	108
5.7.2	Measurement of the affinities ( $K_D$ ) of the humanised antibodies . . . . .	110
5.8	An alternatively spliced form of PRDX4 is expressed in human cancer cells . . . . .	112
5.8.1	Successful generation of antibodies targeting tPRDX4 . . . . .	114
5.8.2	Generated antibodies specifically detect tPRDX4 . . . . .	116
<b>6</b>	<b>Discussion</b>	<b>119</b>
6.1	Successful characterisation and humanisation of PRDX4 antibodies . . . . .	120
6.2	PRDX4 is a new potential tumour marker exclusively identified on the surface of tumour cells . . . . .	121
6.3	Autoantibodies targeting PRDX4 and EVs expressing PRDX4 are present in malignant patient samples . . . . .	123

## CONTENTS

---

6.4	Identification of tPRDX4 in human as potential testis cancer antigen . . . . .	125
6.5	CCDC47 is a novel interaction partner of PRDX4 . . . . .	126
<b>7</b>	<b>References</b>	<b>127</b>
<b>8</b>	<b>Appendix</b>	<b>151</b>
	<b>Danksagung</b>	<b>159</b>

## List of Figures

2.1	The hallmarks of cancer. . . . .	7
2.2	Schematic structure of an IgG antibody. . . . .	13
2.3	Possible modes of action for monoclonal antibodies to control tumour cell growth. . . . .	16
2.4	Biogenesis and secretion of extracellular vesicles. . . . .	20
4.1	Scheme of 5' RACE-PCR reaction steps. . . . .	62
5.1	Strategy for the generation and characterisation of new mAbs. . . . .	80
5.2	PRDX4 is the most prominent target after immunisation with EVs from malignant ascites. . . . .	81
5.3	Confirmation of PRDX4 antibody specificity by IP experiments. . . . .	83
5.4	IP experiments with HEK293T PRDX4-KO cell line also confirm PRDX4 antibody specificity. . . . .	84
5.5	All PRDX4 AB clones show similar surface staining on ES-2 cells in FC analysis. . . . .	86
5.6	Immunoblots of IP experiments performed with surface labelled cell lysates reveal PRDX4 surface expression. . . . .	87
5.7	Total PRDX4 levels are comparable among cell lines, but cell surface localisation differs significantly. . . . .	88
5.8	Heterogenous surface PRDX4 expression among different tumour cell lines as observed in LSCM. . . . .	90
5.9	Subcellular fractionation revealed PRDX4 enrichment in the plasma membrane fraction of surface PRDX4 positive cell lines. . . . .	92
5.10	PRDX4 is present on the surface of primary tumour cells isolated from ascites samples. . . . .	93
5.11	PRDX4 is present on EVs isolated from ascites samples. . . . .	95
5.12	PRDX4-specific antibodies are present in malignant ascites samples. . . . .	97
5.13	IP experiments revealing interaction between CCDC47 and PRDX4. . . . .	98
5.14	LSCM images show intracellular CCDC47 staining and heterogenous PRDX4 expression in different tumour cell lines. . . . .	99
5.15	Product of a successful 5' RACE-PCR of a PRDX4 antibody clone. . . . .	100
5.16	PRDX4 antibody bind to the same or near-by epitope. . . . .	103
5.17	The epitope of the PRDX4 antibody is located within exons2-7. . . . .	105
5.18	PRDX4 AB recognise an epitope within exons2-7 of PRDX4. . . . .	106

## LIST OF FIGURES

---

5.19	FC screening for humanisation of the 5H5 PRDX4 antibody. . . . .	109
5.20	$K_D$ of the top five humanised HC-LC combinations of antibody 5H5. . . . .	111
5.21	Expression of tPRDX4 in human cancer cells. . . . .	113
5.22	Strategy for the generation of tPRDX4 specific antibodies. . . . .	115
5.23	LSCM images show intracellular staining of tPRDX4. . . . .	116
5.24	IP experiments revealing specificity of the generated tPRDX4 antibody. . . . .	118
8.1	Computational analysis of PRDX4 exon1. . . . .	151
8.2	PRDX4 surface expression on different cell lines. . . . .	152
8.2	PRDX4 surface expression on different cell lines. . . . .	153
8.3	Dot blot of humanisation of antibody 5H5. . . . .	154

## List of Tables

3.1	Devices and equipment used in this thesis. . . . .	23
3.2	Consumables used during this thesis. . . . .	26
3.3	Used chemicals and reagents. . . . .	29
3.4	Prepared buffers and solutions. . . . .	33
3.5	Media and additives used for cell cultivation of human cell lines. . . . .	38
3.6	Cell lines cultivated during this thesis. . . . .	39
3.7	Directly labelled antibodies. . . . .	41
3.8	Commercial primary antibodies. . . . .	42
3.9	In-house produced primary antibodies. . . . .	43
3.10	Secondary antibodies. . . . .	45
3.11	Oligonucleotides used for the generation of PRDX4 plasmid constructs. . . . .	46
3.12	Oligonucleotides used for the detection of tPRDX4 in human cell lines. . . . .	47
3.13	Oligonucleotides for 5' RACE-PCR. . . . .	48
3.14	Oligonucleotides for 5' RACE-PCR antibody sequence validation. . . . .	48
3.15	Generated plasmids. . . . .	49
3.16	Plasmids purchased for PRDX4 antibody (OCA2E 5H5) humanisation. . . . .	50
3.17	Bacteria strain used in this thesis. . . . .	51
3.18	Kits used during this thesis. . . . .	52
3.19	Software used during this thesis. . . . .	53
4.1	Composition of standard media used for mammalian cell culture. . . . .	57
4.2	5' RACE-PCR program steps. . . . .	63
4.3	Substances for 5' RACE-PCR preparation. . . . .	63
4.4	Primer pair combinations for the generation of different PRDX4-deletion constructs. . . . .	64
4.5	PCR program steps for the generation of PRDX4 deletion constructs. . . . .	65
4.6	PCR reagents for the generation of PRDX4 deletion constructs. . . . .	65
4.7	Restriction digestion of vector and insert for the generation of a tPRDX4-GFP construct. . . . .	67
4.8	Reaction mix for dephosphorylation of vector DNA. . . . .	67
4.9	RT-PCR components. . . . .	68
4.10	PCR-reagents for the detection of tPRDX4. . . . .	69
4.11	PCR program for the amplification of tPRDX4. . . . .	69

## LIST OF TABLES

---

4.12	Composition of separating and stacking gel. . . . .	73
4.13	Zetaview settings for the measurement of EV concentration. . . . .	76
5.1	Overview of all potential PRDX4 antibody clones. . . . .	85
5.2	Identified protein sequences of PRDX4 antibody clones. . . . .	101
5.3	Calculated $K_D$ of the top five HC and LC combination for the humanisation of the PRDX4 antibody 5H5. . . . .	112
5.4	Sequencing results of five different cell lines reveal expression of tPRDX4 in cell lines and primary cancer cells. . . . .	114
8.1	Plasmid sequences of the evaluated backmutations for the humanisation of the OCA2E 5H5 antibody heavy chain. . . . .	155
8.2	Plasmid sequences of the evaluated backmutations for the humanisation of the OCA2E 5H5 antibody light chain. . . . .	156
8.3	Identified protein sequences of three tPRDX4 antibody clones. . . . .	157

## List of Abbreviations

5' RACE	5' Rapid amplification of cDNA ends
AA	amino acid
AB	antibody
ADCC	antibody-dependent cellular cytotoxicity
ADCP	antibody-dependent cellular phagocytosis
AGV	Department of gene vectors
AID	activation-induced cytidine deaminase
Akt	protein kinase B
APC	antigen presenting cell
APL	acute promyelocytic leukemia
APS	ammonium persulfate
ATP	adenosine triphosphate
ATP1A1	sodium potassium ATPase subunit 1 $\alpha$
BCA	bicinchoninic acid
Bis-Tris	bis(2-hydroxyethyl)iminotris(hydroxymethyl)methane
bp	base pair
BRCA1	breast cancer type 1 susceptibility protein
BSA	bovine serum albumin
CA	cellulose acetate
CAF	cancer-associated fibroblast
CCDC47	coiled-coil domain containing 47
CDC	complement-dependent cytotoxicity
cDNA	complementary DNA
CDR	complementarity-determining region
CNBr	cyanogen bromide
CSR	class switch recombination
CTA	cancer testis antigen
CTLA4	cytotoxic T-lymphocyte-associated antigen 4
D	diversity
DAPI	4',6-diamidino-2-phenylindole, dihydrochloride
DC	dendritic cell
dCTP	deoxycytidine triphosphate
DEPC	diethylpyrocarbonate
DMEM	Dulbecco's Modified Eagle Medium
DMSO	dimethyl sulfoxide
DNA	desoxyribonucleic acid

## LIST OF ABBREVIATIONS

---

dNTP	desoxynucleotide triphosphate
DPBS	Dulbecco's Phosphate-Buffered Saline
DSB	double strand break
DTT	dithiothreitol
e. coli	Escheria coli
ECL	enhanced chemiluminescent
ECM	extracellular matrix
EDTA	ethylenediaminetetraacetic acid
EGFR	epidermal growth factor receptor
EGTA	egtazic acid
ELISA	enzyme-linked immunosorbent assay
EMT	epithelial to mesenchymal transition
EpCAM	epithelial cell adhesion molecule
ER	endoplasmic reticulum
Ero1	ER oxidoredoxin 1
ERP44	endoplasmic reticulum resident protein 44
ESCRT	endosomal sorting complex responsible for transport
EV	extracellular vesicle
Fab	fragment antigen-binding
FC	flow cytometry
Fc	fragment crystallizable
FcR	Fc receptor
FCS	fetal calf serum
FDA	U.S. Food and Drug Administration
FDC	follicular dendritic cell
FR	framework region
GFP	green fluorescent protein
GPx4	phospholipid hydroperoxide glutathione peroxidase-4
GSP	gene specific primer
GST	glutathione-S-Transferase
GTPase	small guanosine triphosphatase
HC	heavy chain
HCMV	human cytomegalovirus
HEK	human embryonic kidney
HER2	human epithelial growth factor receptor 2
HIF1 $\alpha$	hypoxia induced factor 1 $\alpha$
HPRT1	hypoxanthine phosphoribosyltransferase 1
HRP	horseradish peroxidase
HSP	heat shock protein
ICAM-1	intercellular adhesion molecule 1

## LIST OF ABBREVIATIONS

---

ICB	Institute of Computational Biology
IFN $\gamma$	interferon $\gamma$
Ig	immunoglobulin
IL 1	interleukin 1
ILV	intraluminal vesicle
IP	immunoprecipitation
J	joining
K <sub>D</sub>	dissociation constant
kb	kilo base pair
KO	knock out
LB	lysogeny broth
LC	light chain
LDHA	lactate dehydrogenase A
LSCM	laser scanning confocal microscopy
MAB	Monoclonal antibody core facility
mAb	monoclonal antibody
MAC	membrane attack complex
MAGE A1	melanoma antigen family 1
MBP	maltose binding protein
MCE	mixed cellulose esters
MFI	mean fluorescence intensity
MHC	major histocompatibility complex
MoA	mode-of-action
MOPS	3-(N-morpholino)propanesulfonic acid
mRNA	messenger RNA
MS	mass spectrometry
MVB	multivesicular body
NEB	New England BioLabs GmbH
NHEJ	non-homologous end joining
NHS-PEG <sub>4</sub>	N-hydroxysuccinimide-polyethylene glycol
NK	natural killer
NSCLC	non-small-cell lung cancer
NTA	nanoparticle tracking analysis
OD	optical density
PAA	polyacrylamide
PBMC	peripheral blood mononuclear cell
PBS	phosphate-buffered saline
PCR	polymerase chain reaction
PD1	programmed cell death protein 1
PDIA6	protein disulfide isomerase 6

## LIST OF ABBREVIATIONS

---

Pei Max	polyethylenimine „Max“
Pen Strep	Penicillin Streptomycin
PFA	para-formaldehyde
PI3-kinase	phosphoinositide 3-kinase
PI3K	phosphatidylinositol 3-kinase
PMN	pre-metastatic niche
PRDX1	peroxiredoxin 1
PRDX4	peroxiredoxin 4
PROT	Research unit Protein Science
RIPA	radioimmunoprecipitation assay
RNA	ribonucleic acid
ROS	reactive oxygen species
rpm	rounds per minute
RPMI	Roswell Park Memorial Institute
RT-PCR	reverse transcriptase PCR
SDS	sodium dodecyl sulfate
SDS-PAGE	SDS-polyacrylamide gel electrophoresis
SEM	standard error of the mean
SFCA	surfactant-free cellulose acetate
SHM	somatic hypermutation
SNARE	soluble N-ethylmaleimide-sensitive factor attachment protein receptor
SRRM2	serine/arginine repetitive matrix 2
TAE	Tris acetate EDTA
TBS	Tris-buffered saline
TBS-T	Tris-buffered saline-Tween 20
TCA	tricarboxylic acid
TCR	T cell receptor
TdT	terminal deoxynucleotidyl transferase
TEMED	tetramethylethylenediamine
TGF $\beta$	transforming growth factor $\beta$
TMB	3,3',5,5'-Tetramethylbenzidine
TME	tumour microenvironment
TNF $\alpha$	tumour necrosis factor $\alpha$
tPRDX4	testis peroxiredoxin 4
TRIS	Tris-(hydroxymethyl)-aminomethane
Tween20	polysorbate 20
TXNDC5	thioredoxin domain-containing protein 5
UV	ultra violet
V	variable
VEGF	vascular endothelial cell growth factor

# 1 Abstract

Cancer is the second leading cause of death worldwide with an ever-growing number of people who are diagnosed with the disease. Classic therapeutic approaches are relatively unspecific, and are limited by severe adverse effects and acquired resistance to treatment, which often result in recurrent disease and death. Therefore, novel therapeutic strategies are urgently needed. Therapeutic antibodies offer a great potential as they bind their cognate antigens with high affinity and unsurpassed specificity. Some antibodies are now part of modern cancer therapeutic regimens, but an even broader application is still limited by the small number of known suitable target molecules on cancer cells. This holds true especially for solid tumours. This rises the demand to identify new targets, and for this, our group has developed an immunisation strategy based on extracellular vesicles (EVs) isolated from permanent human cancer cell lines, which turned out as an immunogenic source of known and unknown tumour associated antigens. This approach already led to the identification of interesting targets and the generation of the corresponding antibodies with clinical potential. In an attempt to identify completely new targets, we recently performed immunisations with EVs isolated from cancer patients, which can be considered as more authentic. Among others, this immunisations led to the generation of antibodies binding to peroxiredoxin 4 (PRDX4), a protein involved in the cell defense against oxidative stress and, so far, exclusively described as localised in the endoplasmic reticulum (ER) and the cytosol of cells. Much to our surprise, these antibodies detected the protein also on the surface of cancer cells, but not on normal cells.

This dissertation deals with the characterisation and humanisation of PRDX4-specific antibodies, the expression profile of surface PRDX4 on normal and malignant cells and their EVs. Furthermore, it describes, for the first time, the expression of a testis-specific splice variant of PRDX4 in human cancer cells, the presence of PRDX4-specific autoantibodies in patients, as well as the identification of a new PRDX4 interaction partner, CCDC47. In summary, it provides convincing data that qualify PRDX4 as a new potential biomarker and attractive target molecule.



# Zusammenfassung

Krebs ist die zweithäufigste Todesursache weltweit, wobei die Zahl der Betroffenen ständig steigt. Herkömmliche Behandlungsmethoden sind oft relativ unspezifisch, gehen oft mit schweren Nebenwirkungen einher und induzieren häufig eine Therapieresistenz. Langfristig führt dies zum Auftreten von Rezidiven und letztendlich zum Tod. Aus diesem Grund ist es dringend notwendig neue therapeutische Strategien zu entwickeln. Dafür bieten therapeutische Antikörper großes Potential, da sie in der Lage sind Tumorantigene gezielt zu binden. Einige werden daher bereits in modernen Therapieansätzen eingesetzt. Trotzdem wird in der Behandlung besonders von soliden Tumoren nur eine limitierte Anzahl tumorspezifischer Antigene angesprochen. Aufgrund dessen ist es essentiell neue Tumorantigene zu identifizieren. Dafür wurde eine neue Immunisierungsstrategie entwickelt, bei der extrazelluläre Vesikel (EVs), die von Tumorzelllinien sekretiert werden, als Quelle für verschiedenste bereits bekannte als auch für unbekannt Tumorantigene verwendet werden. Dadurch wurden bereits einige interessante neue Zielmoleküle identifiziert und die korrespondierenden Antikörper für potenzielle klinische Anwendungen generiert. In einem weiterführenden Ansatz wurden nun EVs, welche aus Proben von Krebspatienten isoliert wurden, für Immunisierungen verwendet. Dadurch wurden unter anderem Peroxiredoxin 4 (PRDX4)-spezifische Antikörper generiert. PRDX4 ist ein Protein, welches im zellulären Schutz gegen oxidativen Stress beteiligt ist und bis jetzt ausschließlich im endoplasmatischen Retikulum und im Zytosol von Zellen detektiert wurde. Überraschenderweise erkennen unsere Antikörper PRDX4 auf der Zelloberfläche von Tumorzellen, wohingegen gesunde Zellen keine Oberflächenexpression von PRDX4 aufweisen. In dieser Arbeit wurden PRDX4-spezifische Antikörper tiefgehender charakterisiert. In diesem Kontext wurde ein PRDX4 Antikörper humanisiert, sowie das Expressionsprofil von PRDX4 auf der Oberfläche von gesunden und malignen Zellen analysiert. Des Weiteren konnte zum ersten Mal die Expression einer hodenspezifischen Spleißvariante von PRDX4 in humanen Tumorzellen nachgewiesen werden. Zudem konnten Autoantikörper gegen PRDX4 in Tumorpatienten detektiert und das Chaperon CCDC47 als neuer Interaktionspartner von PRDX4 identifiziert werden. Zusammenfassend zeigen die Ergebnisse, dass PRDX4 auf der Oberfläche von Tumorzellen ein neues Zielmolekül und ein potentieller neuer Tumorbiomarker ist.



## 2 Introduction

### 2.1 Evolution of cancer

Cancer is one of the leading causes of death worldwide, accounting for around 19.3 million new cases and ten million deaths reported in 2020. Cancer is described as a heterogeneous disease comprising various subtypes, of which cancer of the breast, lung, colon and prostate are the most frequent ones. Furthermore, the incidence and mortality of cancer is steadily increasing due to demographic ageing and overall population growth [1, 2].

Tumour cells are characterised by abnormal growth and the potential to spread to adjacent cells, organs, and even remote parts of the body [3, 4]. Tumours are defined as a genetically diverse set of cells, which give rise to heterogenetic subpopulations [5]. The heterogeneity of tumours, somatic cell mutations, and clonal selection led to the concept of carcinogenesis as an evolutionary process, which is in line with the Darwinian concepts of somatic selection, diversification, and extinction [5–8].

Tumour cells arise from one benign cell and proliferate abnormally by means of clonal selection. This is initialised by a multi-step process that involves for example mutations, which led to genetic alterations that favor abnormal proliferation and therefore increase the tumour cells' capacity for survival, invasion and metastasis. This process is induced by the consequent activation of oncogenes or the inhibition of tumour suppressor genes [9, 10].

Hanahan and Weinberg define these mechanisms and arising features of tumours as the hallmarks of cancer (see Figure 2.1). Moreover, according to them, tumour cells manipulate existing protective molecular and cellular pathways to circumvent their original mode of action and turn them into tumour promoting modulators [11–13]. In normal tissues, cell proliferation is strictly controlled and orchestrated by multiple activating and suppressing signals. In contrast, cancer cells evolve the potential to proliferate autonomously and permanently. On the one hand, this is achieved by an increased production of growth factors that, upon binding, activate a variety of intracellular signalling pathways that regulate cell cycle progression and proliferation.

On the other hand, cancer cells disrupt negative feedback regulation of cell programs that suppress cell growth and proliferation processes by loss-of-function mutations in genes, which are generally referred to as tumour suppressor genes [11, 14, 15]. In addition, fast-proliferating tumour cells need to overcome apoptosis, that normally eliminates damaged cells by the use of a machinery of coordinated sensors and transducers at multiple checkpoints of the cell cycle. As a countermeasure, tumour cells develop a set of different apoptosis-avoiding mechanisms, for example by means of loosing the TP53 tumour suppressor protein [11, 16, 17].

When a tumour reaches a certain size, its supply with nutrients and oxygen becomes limited. Consequently, tumours induce the development of a new blood vasculature, to counteract this limitation and to allow further growth [18–20]. This phenomenon, termed neo-angiogenesis, is a highly complex and dynamic process and involves a variety of pro- and anti-angiogenic factors such as vascular endothelial cell growth factor (VEGF), a key player in this process that activates endothelial cell proliferation and vasodilatation of existing vessels [19, 21].

Yet another characteristic of most tumours are increased numbers of mutations, also termed genomic instability. These mutations arise from genotoxic stress, such as reactive oxygen species (ROS), ionising radiation or ultra violet (UV) light. Genomic instability is also induced due to loss-of-function mutations in desoxyribonucleic acid (DNA) repair genes. For example, germline mutations in breast cancer type 1 susceptibility protein (BRCA1), a protein involved in repair of double strand breaks (DSBs) is a predispose for breast and ovarian cancer with high penetrance [22, 23]. These mutations, which can be found in hereditary cancers provide strong support for the mutator hypothesis. According to this hypothesis, which was already published in 1976, tumour initiation and progression are the result of already existing genomic alterations within normal cells [7, 24, 25].

Additional hallmarks of cancer are mentioned in the context of the following sections and are summarised in Figure 2.1.

### 2.1.1 Immuno evasion of cancer cells

Cancer immune surveillance is an essential mechanism of the immune system to monitor and eliminate evolving tumour cells [26]. This process is called immunoediting and comprises three major phases. In the first phase, the elimination, the innate and adaptive immune responses manage to kill nascent tumour cells by the use of tumour specific CD4<sup>+</sup> and CD8<sup>+</sup> T cells upon presentation of tumour derived antigens by professional antigen presenting cells (APCs).

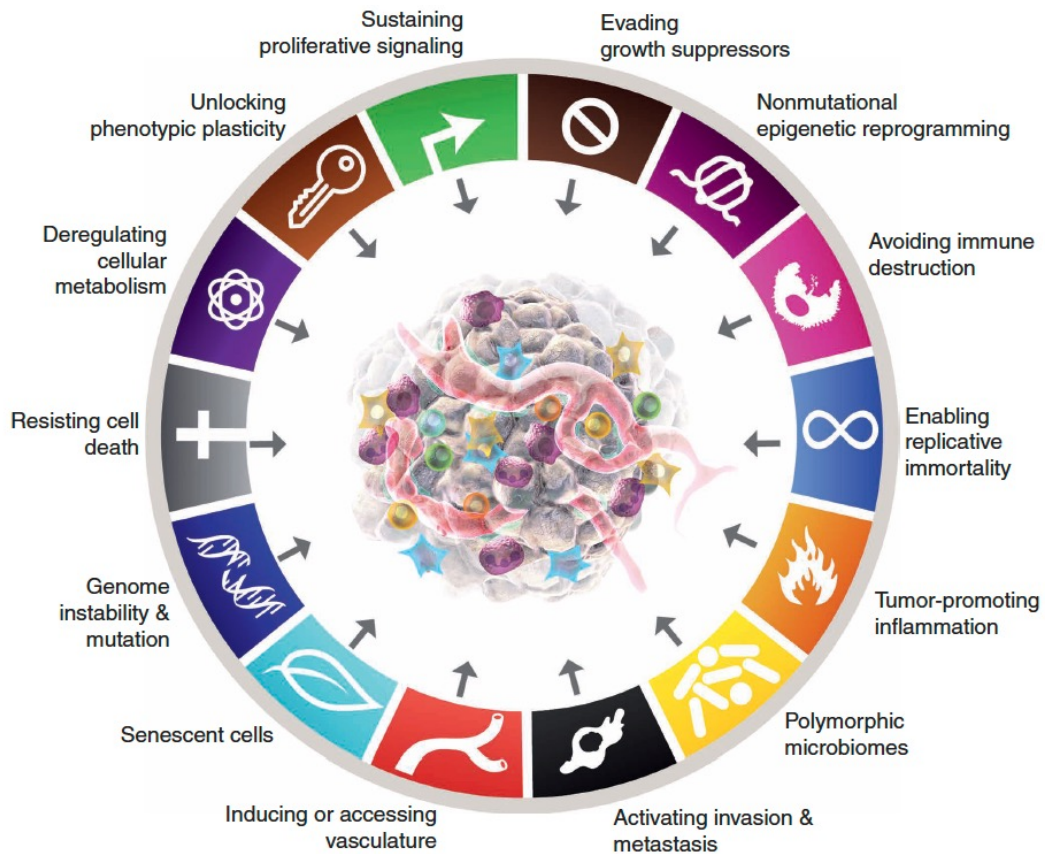


**Figure 2.1: The hallmarks of cancer.**

This illustration adapted from Hanahan and Weinberg summarises the currently 14 hallmarks of cancer [12].

Nevertheless, resistant clonal variants of the tumour cells can evolve by decreasing their immunogenicity. As a result, the immune system's ability to effectively recognise and eliminate the tumour cells is impaired. This second phase is called equilibrium.

If another round of immune responses fails to eliminate the emerging cancer cells, the phase of immune escape is reached, which will probably lead to clinical manifestation [26–28]. Tumour cells exhibit several strategies for immune evasion: they induce tolerance towards the developing tumour or they acquire resistance to being killed by activated immune effector cells. The immune system attacks and eliminates cancer cells in a series of iterative, stepwise events, which are summarised in the cancer immunity cycle [29]. Due to genomic instability, new tumour associated antigens or neoepitopes arise during tumour development. These anti-

gens are presented by APCs to T cells via the major histocompatibility complex (MHC)-I pathway. This results in priming and activation of an effector T cell response against these tumour antigens. Thereupon, activated effector T cells traffic to the tumour site, bind to cancer cells via T cell receptor (TCR)-MHC interaction and consequently kill their target cancer cell. This killing of the cancer cells leads to the release of additional tumour associated antigens and restarts the cycle. One of the main mechanisms used by tumour cells to evade immune recognition is the inhibition of antigen presentation, especially via the MHC-I pathway [29–32].

Apart from tumour cells, tumour infiltrating T cells and inflammatory immune cells also reside in a tumour’s neighbourhood. In combination with stromal cells and cancer-associated fibroblasts (CAFs), they form the tumour microenvironment (TME) [33]. As early as 1863, Rudolf Virchow proposed the link between inflammation and cancer, coining tumours as non-healing wounds [34, 35]. Inflammatory cells can potentially have an impact on tumour development by featuring both, pro- and anti-tumour effects. On the one hand, the expression of cytokines such as interferon  $\gamma$  (IFN $\gamma$ ), tumour necrosis factor  $\alpha$  (TNF $\alpha$ ) or interleukin 1 (IL 1) are pivotal in the process of tumour elimination. On the other hand, pro-tumorigenic inflammation promotes cancer progression by blocking the anti-tumour immunity. As a result, it remodels the TME toward a more tumour-permissive state by means of exerting direct tumour promoting signals onto epithelial and cancer cells [35, 36].

Nevertheless, cancer cells manage to escape the body’s immune response by suppressing almost every step of the cancer immunity cycle and to block the generation of tumour-reactive effector T cells. Cancer cells attain this by downregulating antigen presentation via MHC-I molecules, by upregulating membrane receptors that can trigger apoptosis in T cells, as well as by inducing immune tolerance [29, 32, 37].

### **2.1.2 The role of hypoxia in tumour progression**

The uncontrolled and excessive proliferation and expansion of tumours result in an increased oxygen demand. At the same time, the tumour’s oxygen supply is limited due to insufficient vasculature, leading to the creation of an oxygen deprived hypoxic milieu with oxygen levels of around 1%. In comparison, normal physiological oxygen levels (termed physoxia), although varying considerably among tissues, are in the range between 15% in lung aveoli and 5% in the liver [38–41]. Hypoxia is another common feature of solid tumours and typical

for the TME [42–44]. Since adaption to hypoxia plays a pivotal role in the progression of tumours, it is not surprising that many hallmarks of cancer are regulated by hypoxia.

Moreover, another important hallmark of cancer is the reprogramming of the tumour’s glucose metabolism, which was observed by Otto Warburg as early as 1924 [45]. Instead of metabolising glucose through the oxygen consuming tricarboxylic acid (TCA) cycle in order to produce adenosine triphosphate (ATP), cancer cells switch their glucose metabolism to the oxygen independent glycolysis even in the presence of oxygen. As a consequence, the produced pyruvate is converted into lactate for the generation of ATP. However, in terms of ATP generation, glycolysis is far less efficient: only two molecules of ATP are generated from one glucose molecule, whereas the TCA cycle generates 36 additional molecules of ATP from one glucose molecule. Consequently, cancer cells uptake enormous amounts of glucose. This reprogramming of the tumour’s metabolism is known as the Warburg effect [45–47]. Furthermore, physiological stressors such as hypoxia, acidosis, and leaky vasculature in the TME are one of the reasons for the altered metabolism of tumours. Under hypoxic conditions, hypoxia induced factor 1  $\alpha$  (HIF1 $\alpha$ ), which is the master regulator in hypoxia, can drive the stimulation of the glycolysis pathway, i.e. by increasing the extracellular glucose uptake via increased expression of glucose transporters such as GLUT1 and GLUT3 [48]. Increased glycolysis consequently generates enhanced pyruvate levels, which are usually redirected and processed in the TCA cycle. HIF1 $\alpha$  induces lactate dehydrogenase A (LDHA) to convert pyruvate to lactate, which is excreted from the cells into the extracellular space. In addition to clearing pyruvate from the cell, HIF1 $\alpha$  can downregulate oxidative phosphorylation within the mitochondria, thereby limiting the oxygen dependent ATP-production via the TCA cycle even further [39, 46–50].

Tumour metastasis is the process of cancer cell migration from the primary tumour site to distant locations within the body. Furthermore, metastasis is associated with enhanced angiogenesis and permeable, leaky blood vessels, which facilitate the extravasation and relocation of tumour cells. Moreover, it is also promoted by epithelial to mesenchymal transition (EMT), which is another hypoxia induced process in carcinoma cells [51–53]. EMT is an initial step where tumour cells cease the expression of adhesion molecules such as E-cadherin, and consequently acquire a more motile phenotype. This phenotype is characterised by mesenchymal-like gene expression such as N-cadherin. EMT is promoted by the master regulator transforming growth factor  $\beta$  (TGF $\beta$ ), which increases under hypoxic conditions [44, 52, 54–57]. Generally, intratumoral hypoxia is a negative prognostic indicator for most cancer patients as it induces a more aggressive tumour phenotype and fosters metastatic spread. Tumour cells adapting to hypoxic conditions are also more resistant to chemo- and radiotherapy [39, 58, 59].

## 2.2 Cancer therapy

Cancer remains a largely unsolved problem worldwide, although a variety of different cancer treatment strategies have been established and even more are in development. In order to improve the clinical prognosis of patients, treatment regimens are used in combination to increase their efficiency [4]. However, a permanent cure for the disease is still seldom or even unlikely for certain types of cancer such as pancreatic cancer or aggressive forms of brain cancer [60, 61]. Each type of treatment has its efficacy but also its limitations due to the fact that the induced resistance to treatment causes serious to even lethal side effects on account of off-target-toxicity in normal tissues [4, 62]. For this reason, recently developed treatment strategies such as metronomic chemotherapy, a type of chemotherapy with a more frequent and low-dose administration compared to conventional types of chemotherapy, aim at keeping the disease in check as long as possible without induction of resistance [63, 64]. Cytoreductive surgery is still considered the most effective treatment for solid tumours. However, this applies only as long as the cancer grows locally and has not yet spread to other organs [65]. Therefore, surgery is often combined with neoadjuvant or adjuvant chemo- or immunotherapy, which aim at destroying residual distant cancer cells and micrometastases [4, 63, 66].

Many emerging innovative therapies that are emerging exploit the immune system's potential to fight cancer cells and to initiate a self-sustaining cycle of cancer immunity. This is exemplified by the recently developed checkpoint inhibitors, which show stunning effects in a fraction of cancer patients. These molecules have become attractive targets for immunotherapeutic approaches [67].

These inhibitory checkpoint molecules, which regulate the interaction between T cells and APCs are generated upon T cell activation. Targets in question include, for example, the checkpoint molecules cytotoxic T-lymphocyte-associated antigen 4 (CTLA4), programmed cell death protein 1 (PD1), as well as its ligand PD-L1. CTLA4 downmodulates T cell activation in lymph nodes and PD1 is a co-inhibitory receptor, which, together with PD-L1, is expressed on activated T cells or stromal cells. By blocking CTLA4, PD1 or PD-L1 receptors with monoclonal antibodies (mAbs), the antitumour response in the TME can be restored [29, 32, 37, 67, 68].

Other prominent targets in tumour therapy are human epithelial growth factor receptor 2 (HER2) and epidermal growth factor receptor (EGFR), also known as HER1. Both are over-expressed in a wide range of malignancies and play pivotal roles in modulating proliferative mechanisms. Especially in breast cancers, 15 to 20 % of all cases show HER2 overexpression, which is associated with poor prognosis and higher recurrence rates [69–71].

Also, the blocking therapeutic antibodies Herceptin (Trastuzumab) and Erbitux (Cetuximab) that target HER2 and HER1, respectively, show therapeutic effects in some patients. Given their intrinsic biological properties like specificity and availability, antibodies are nowadays considered a preferred class of molecules for therapeutic interventions to cancer patients as well as for the treatment of autoimmune and infectious diseases [72–75].

### 2.3 Antibodies in cancer immunotherapy

Antibodies were discovered at the end of the 19th century by Behring and Kitasato. At that time, they described antibodies as neutralising substances against tetanus and diphtheria in animal models [76]. Antibodies are glycoproteins, which have the capacity to target molecular components in a specific fashion. Being produced by B cells, they play a central role in the immune system by recognising and neutralising antigens, as well as provoking cellular immune responses. It is therefore not surprising that they are about to become an integral part of novel therapeutic and diagnostic approaches alike [69, 77, 78].

#### 2.3.1 Structure and function of antibodies

In many species, including humans, antibodies are composed of four polypeptide chains, two identical heavy chains (HCs) and two light chains (LCs). Disulfide bridges link these chains together that collectively form the typical Y-shaped structure [79, 80]. The HCs and LCs each consist of a variable and a constant region. The former is responsible for the specificity of the antibody, while the latter determines the immunoglobulin (Ig) subclass and forms the so called fragment crystallizable (Fc)-region. The different Fc-regions thus determine the antibody's effector function as they provide these molecules with different binding affinities

for distinct cell-surface receptors on immune cells. Consequently, they decide whether or not the antibody can activate distinct players of the immune system to eliminate pathogens, such as macrophages, natural killer (NK) cells or mast cells. Furthermore, the Fc-region determines whether an antibody can be transcytosed through epithelial membranes at mucosal surfaces, and whether it can diffuse into tissues or polymerise to restore a greater avidity [78, 79, 81, 82].

The specificity of the fragment antigen-binding (Fab) region is provided by hypervariable complementarity-determining region (CDR) regions, which lie within the less variable framework regions of the HCs and LCs and evince the highest sequence variations within the antibody sequence. Each HC and LC variable region comprises three CDRs containing ten juxtaposed amino acids that form the antigen binding site [78–80]. As a result, the CDRs create the diversity of the antigen specificity.

Antibody diversity results from the process of somatic hypermutation (SHM) during antibody maturation upon VDJ-recombination. This process occurs during early B cell development and is a first step of diversification, where the variable region of an antibody is assembled from different juxtaposed variable (V), diversity (D) and joining (J) segments that are randomly selected from the germline pool [83–85]. It has been shown that the CDR3 of the heavy chain is of special interest as this region has in average the most contacts with the antigens and is located in the center of the binding site. This CDR-H3 possesses the highest structural diversity among all CDRs as this is the most hypervariable sequence encompassing the junctions between all three randomly combined  $V_H$   $D_H$  and  $J_H$  segments [82, 85, 86]. A schematic structure of an antibody with its specific domains is shown in Figure 2.2.

The Ig isotype is determined in mature B cells by a process called class switch recombination (CSR). During this process, different genes are excluded from the heavy chain locus in a conserved mechanism. Moreover, involving the activity of the enzyme activation-induced cytidine deaminase (AID) to induce double strand breaks, which are subsequently repaired by non-homologous end joining (NHEJ). As a consequence, the gene encoding the Ig constant region of the HC is replaced from  $C\mu$  to other HC constant genes ( $\alpha$ ,  $\gamma$ ,  $\delta$ , and  $\epsilon$ ) resulting in a class switch from IgM to IgA, IgG, IgD, or IgE. The constant domains of the LCs are encoded either by Ig  $\kappa$  or  $\lambda$  genes [79, 81, 87, 88].

Most antigens are highly complex, and they present numerous epitopes that can be processed and recognised by a large number of B lymphocytes. Each activated B lymphocytes consequently differentiates into an antibody secreting plasma cell. Consequently, the resulting antibody response is polyclonal. Antibodies produced by a single B lymphocyte are called monoclonal antibodies (mAbs) and they bind to one unique epitope [89].

Based on the paratope, epitopes can be divided in two major categories, namely conformational epitopes and the linear epitopes [90]. Their interaction with the antibody is provided by the epitope's 3D conformation that is predefined by the involved amino acid residues as well as the tertiary structure of the protein. Conformational epitopes are shaped by the interaction of discontinuous amino acid residues while a linear epitope results mainly from the primary structure of the involved continuous amino acid residues [91, 92]. It is known that as much as 90% of all B cell epitopes are conformational epitopes [90, 91].

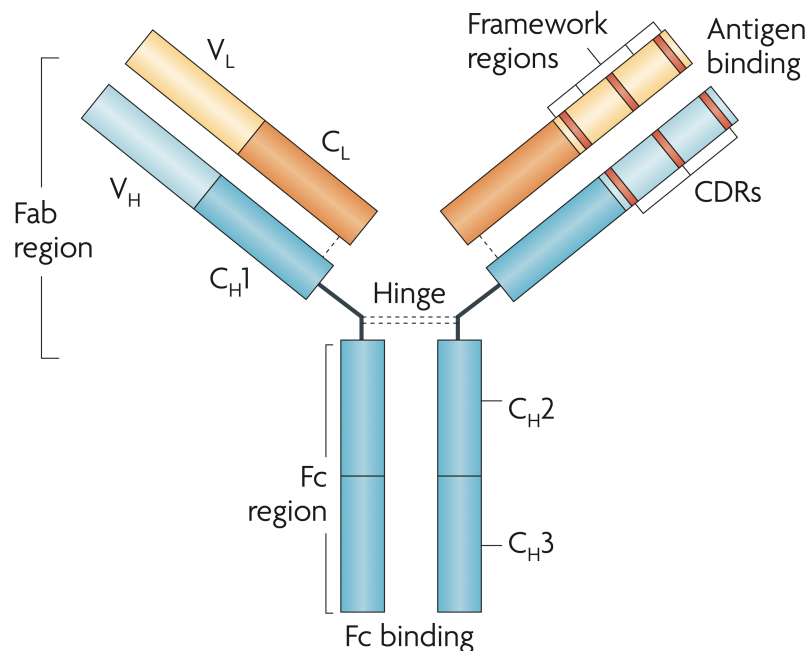


**Figure 2.2: Schematic structure of an IgG antibody.**

mAbs consist of two identical HCs and two LCs, which are linked by disulfide bridges. All chains comprise a variable and a constant part. The Fab-region of the antibody embodies the CDRs, which provide binding of the antibody to specific targets. The Fc part comprises constant parts of the HCs and thus serves as interaction site for other cells. The graphic is adapted from [75].

### 2.3.2 Antibody effector mechanism

Therapeutic mAbs are biopharmaceuticals that are nowadays commonly used for the treatment of cancer, as well as autoimmune and inflammatory diseases. Monoclonal antibodies offer a great opportunity for an efficient treatment as they are very specific and thus provoke relatively mild side effects. For this reason, mAbs directed against tumour associated antigens or neoantigens on the surface of tumour cells can induce their death by a variety of mechanisms [69, 93]. Furthermore, the therapeutic efficacy of mAbs relies on the nature of the targeted antigen, which should ideally be abundant and exclusively expressed on the surface of cancer cells and indispensable for their growth and survival. In addition, only minimal amounts of the antigen should be secreted, which could attenuate antibody binding to the tumour cell [69, 93].

One main mode-of-action (MoA) of therapeutic mAbs is the direct antagonist blockage of the function of the target molecule. Cetuximab is an example for such a mAb. It blocks the EGFR, which is overexpressed on many different types of cancer and triggers tumour cell proliferation and migration. Moreover, Cetuximab can also induce apoptosis of tumour cells [69, 78, 93, 94]. Not only tumour cells but also structures that support tumour progression such as the vasculature, the TME and the extracellular matrix (ECM) are potential targets when trying to stop tumour growth and to induce tumour cell death. [75, 93]. In addition, receptor agonist binding of mAbs can mediate reduced proliferation and apoptosis by activating intracellular downstream signalling. In example Theralizumab is a CD28 agonist antibody that can induce proliferation of regulatory T cells regardless of the signal received by TCRs [75, 95, 96].

Other, more indirect MoAs of mAbs involve the engagement of components of the immune system. The majority of mAbs activate the complement system and induce complement-dependent cytotoxicity (CDC), which leads to the formation of the membrane attack complex (MAC) and, consequently, to cell lysis [97]. Tumour cells opsonized by mAbs can be recognised by the immune system via interactions with the Fc receptors (FcRs), a receptor that interacts with the Fc part of an antibody. Immune effector cells equipped with FcRs are, for example, NK cells, which are the primary mediators of antibody-dependent cellular cytotoxicity (ADCC) [80, 98]. This recognition by NK cells leads to the release of cytotoxic factors such as perforin, granzymes or  $\text{TNF}\alpha$ , which subsequently mediate cell lysis of the target tumour cells [99]. Alternatively, opsonized tumour cells can also be phagocytosed by macrophages. This process is called antibody-dependent cellular phagocytosis (ADCP), and it involves the activation of the  $\text{Fc}\gamma\text{R}$  [98]. Another therapeutic antibody applied for

the treatment of breast cancer is Trastuzumab. It acts via direct binding to HER2 and hinders the receptor dimerization and consequently promotes proteolysis of the receptor through receptor-mediated endocytosis. As a result of this inhibition step, downstream signaling of HER2 is disrupted, which causes cell cycle arrest. In addition, Trastuzumab can mediate ADCC and ADCP [69, 100].

The previously described direct targeting of the immune system in order to enhance natural immune responses by means of antibodies binding to checkpoint inhibitors is another antibody effector mechanism. Furthermore, conjugated antibodies can be used to deliver toxic payloads, such as drugs, toxins, siRNAs or chemotherapeutic agents directly to the tumour site [80, 93]. In this approach, the payload is conjugated via chemical linkers to the heavy chain domain of an antibody. The ability of mAbs to internalize allows a more specific delivery of the cytotoxic agents, and consequently reduces systemic toxicity throughout the body as well [101]. All of these different MoAs of monoclonal antibodies are summarised and visualised in Figure 2.3.

Despite the many advantages, the clinical success of therapeutic antibodies has long been limited by the fact that animal-derived mAbs are immunogenic in humans. This means that the immune system raises antibodies, which neutralize the administered mAb. To overcome this obstacle, the technology of antibody humanisation has been developed. As a result of this technology, the immunogenicity of non-human antibodies can be significantly reduced. This happens due to the substitution of the rodent antibody backbone with a human antibody structure with only grafting the CDRs regions, which are providing the antibody's specificity. This result in humanized antibodies consisting to 85-90% of human sequences [102–106].

## 2.4 Peroxiredoxin 4

Peroxiredoxins are small redox proteins of a molecular size between 20 and 30 kDa that are ubiquitously expressed throughout the human body. The family of peroxiredoxins comprises six isoenzymes (PRDX1-6) of highly similar molecular structures. All of them exhibit a peroxidase activity and play a pivotal role in cellular defense mechanisms against ROS by catalysing the reduction of excessive  $H_2O_2$  to water through the thioredoxin system using thioredoxin as electron donor [108–110].

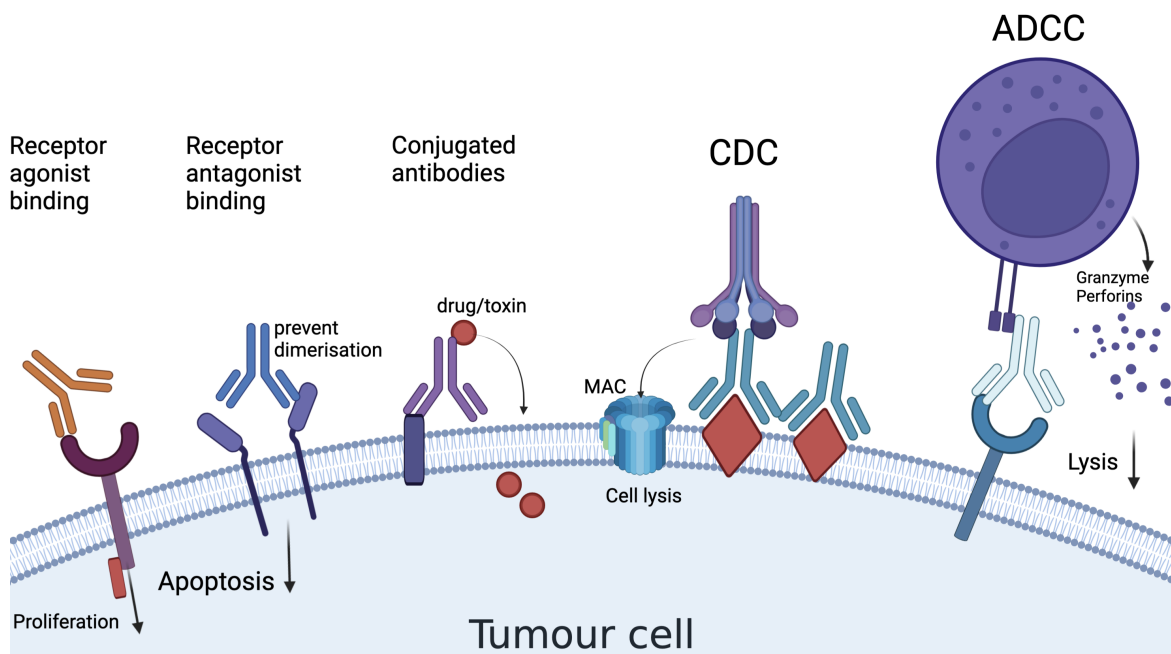


**Figure 2.3: Possible modes of action for mAbs to control tumour cell growth.**

Killing of tumour cells can be achieved by receptor agonist binding of mAbs to receptors, activating them and thus inducing apoptosis or reduced proliferation. It can also be mediated by receptor antagonist activity, such as blocking receptor dimerisation, kinase activation or downstream signalling through antibody binding. Conjugated mAbs can be used to deliver toxic payloads such as drugs, toxins, siRNAs or radioisotopes to the tumour cell and thus inducing cell death. Furthermore, tumour cells can be eliminated by the immune system by activating the complement system (by CDC) or by ADCC [75, 93]. Figure was created with BioRender.com [107].

PRDX1-6 are classified into three different subgroups according to their structure and catalytic mechanism [111]. PRDX1-4 are members of the typical 2-Cys class exhibiting high similarities across their catalytic domains and existing as homodimers and decamers associated by disulfide bridges during their catalytic action [111, 112]. PRDX5 and PRDX6 are monomeric enzymes with more divergent structures. PRDX5 belongs to the subgroup of atypical 2-Cys class, whereas PRDX6 is associated with the class of 1-Cys PRDXs, because it contains only a single conserved cysteine residue [110, 113–115].

Under physiological conditions, peroxidases regulate a variety of processes, such as the cellular protection against oxidative stress and signalling induced by  $H_2O_2$  [113, 116]. ROS like  $H_2O_2$  and nitric oxides, are toxic secondary products that can induce, for the most part, damage to DNA and thus genomic instability. However, they also induce damage to proteins and other types of macromolecules.

ROS may also affect EMT, angiogenesis and apoptosis by modulating the phosphoinositide 3-kinase (PI3-kinase)/protein kinase B (Akt) pathway [109, 117–119]. For this reason, it is not surprising that alternating PRDX levels were also found in a variety of different human cancers [109, 113, 116]. This stringent control of cellular ROS-levels, which are potent mutagens and promoters of carcinogenesis is therefore crucial for cells.

PRDX4 contains a unique N-terminal hydrophobic domain that is responsible for its localisation in the endoplasmic reticulum (ER), or its secretion [113, 120, 121]. PRDX4 plays an important role in correct folding of nascent proteins by coupling the  $H_2O_2$ -catabolism with oxidative protein folding to maintain the redox balance in the ER by metabolising  $H_2O_2$  produced by ER oxidoredoxin 1 (Ero1) and thus protect cells from the development of misfolded proteins [113, 122, 123]. Furthermore, PRDX4 has an important chaperone function. It operates in a versatile mechanism allowing a switch from its redox-dependent mode of action, where it appears as a homodimer, to higher multimeric forms like decamers. As a decamer, PRDX4 interacts with binding partners, such as stress-responsible kinases, membrane proteins or immune modulators [109, 124, 125]. As a chaperone in its decameric form, PRDX4 interacts with the protein disulfide isomerase 6 (PDIA6), a key foldase at the ER mediating oxidative folding of a wide range of ER proteins [109].

Overexpression of PRDX4 is found in multiple different cancer tissues, where it favours tumour initiation and propagates therapeutic resistance as well as a subsequent recurrent disease [113]. The accumulation of PRDX4 in tumours likely protects these cells from toxic effects of increased ROS-levels. Nevertheless, the mode of action of PRDX4 varies among different cancers. For example, in pancreatic cancer, different studies propose PRDX4 as potential tumour marker as its depletion of PRDX4 inhibits tumour growth [109, 126, 127]. Moreover, in lung cancer, PRDX4 contributes to the maintenance of anchorage independent colony formation, cell migration and invasion [109, 113, 128]. In contrast, a significant down-regulation of PRDX4 is reported for acute promyelocytic leukemia (APL) [109, 129]. Taken all this into consideration, PRDX4 is a promising potential new tumour biomarker. However, a more detailed knowledge of PRDX4's MoA in tumour cells is necessary [113].

Of interest, a splice variant of PRDX4 (testis peroxiredoxin 4 (tPRDX4)) that uses an alternative exon 1 located approximately 2 kb upstream of the classical exon 1 of the PRDX4 gene on the X chromosome has been identified recently in the testes of sexually mature mice [114, 130, 131]. tPRDX4 lacks the signal peptide and the unique N-terminal domain of PRDX4 but retains catalytic activity. tPRDX4 has been found to have a protective effect during spermatogenesis [114, 132, 133].

### 2.5 Extracellular vesicles

Intercellular communication is of fundamental importance and is mediated either by direct cell-cell contact, through the transfer of secreted molecules or by the intercellular transfer of EVs [134]. The secretion of EVs, which are nano-meter sized spherical particles, is an evolutionary conserved process that is detectable in cells from different eukaryotic organisms and prokaryotic cells alike [135]. EVs have been detected in nearly all body fluids including blood, urine, saliva, breast milk, amniotic fluid, ascites, cerebrospinal fluid, bile and semen [136–140].

Cell-derived EVs have been classified into subgroups based on their biogenesis and release pathway. Microvesicles, a relatively heterogeneous population of vesicles, are directly released from the plasma membrane via outward budding and fission of the cell membrane and have a size in between 20 nm and 1  $\mu$ m and contain cytoplasmic cargo consisting of proteins and various types of nucleic acids [140–142]. During apoptosis, the cell content is packaged in apoptotic bodies by outward blebbing of cell membrane in vesicles of a size between 50 nm and 2  $\mu$ m [135, 142–144]. Besides apoptotic bodies, also large EVs, so called oncosomes, can bud from the membrane. Oncosomes have a size of about 1-10  $\mu$ m and are primarily produced by malignant cells [142, 145]. Yet another subtype of EVs are exosomes, characterised by a size of in between 40 and 160 nm in diameter [146]. The biogenesis of exosomes involves a double invagination of the plasma membrane and the formation of so called multivesicular bodies (MVBs), which contain intraluminal vesicles (ILVs) (see Figure 2.4) [140, 146–150]. These intracellular MVBs can either follow the secretory pathway, whereby they fuse with the plasma membrane, resulting in the release of ILVs as exosomes via exocytosis, or the lysosomal pathway to their content into the lysosomal lumen for degradation [151, 152].

MVBs, possessing high levels of cholesterol and sphingomyelin are thereby targeted to the secretory pathway. In contrast, cholesterol poor MVBs are targeted for lysosomal degradation [148, 153]. Several proteins are involved in the exosome biogenesis, such as the endosomal sorting complex responsible for transport (ESCRT) machinery that is involved in sorting proteins into ILVs [154–157].

Furthermore, EVs are characterised by the expression of proteins involved in membrane transport and fusion, such as Rab proteins, the largest family of small guanosine triphosphatases (GTPases) regulating exosome docking and membrane fusion [158] and annexins, proteins that are involved in membrane trafficking and fusion [159]. EVs are also enriched with heat shock proteins (HSPs), and tetraspanins like CD9, CD63, CD81 and CD82 [135, 148, 152].

Upon their release from cells, EVs can act as intercellular messengers. Therefore, they interact with target cells to induce changes in their physiology by delivering their contents of proteins, lipids, ribonucleic acid (RNA) including messenger RNA (mRNA), microRNA and DNA [140, 160]. The binding of EVs to its recipient cells requires specific receptors on both, vesicles and the target plasma membrane. This engagement is often mediated by adhesion molecules such as integrins present on EVs. Upon binding to target cells, vesicles can be internalised by different mechanisms including receptor mediated endocytosis [161, 162], fusion with the plasma membrane mediated by soluble N-ethylmaleimide-sensitive factor attachment protein receptor (SNARE) complexes [163], or dynamin-, phosphatidylinositol 3-kinase (PI3K)- and actin-polymerization dependent phagocytosis [140, 164, 165]. Upon internalisation, EVs may subsequently fuse with the endosomal delimiting membrane or be targeted to lysosomes for degradation [134, 166]. As a consequence, EVs are involved in maintenance of normal cell physiology, but also in tissue repair, immune surveillance and the prevention of infections [146, 167, 168].

Extracellular vesicles can, depending on the status of the particular immune cells, trigger adaptive immune responses or suppress inflammation in a tolerogenic manner and can transfer MHC molecules and antigens [144, 148, 169]. Thereby, they can confer immune suppression either by enhancing the function of regulatory T cells, suppression of NK and CD8<sup>+</sup> T cells, or by inhibiting monocyte differentiation into dendritic cells (DCs) [148, 149, 170]. In contrast, EVs can mediate immune activation by promoting proliferation and the activation of monocytes, B cells and NK cells [142, 171, 172].

Given the fact that EVs regulate a variety of fundamental biological processes, it is not surprising that they can also have influence in disease pathogenesis, for example in tumour progression.

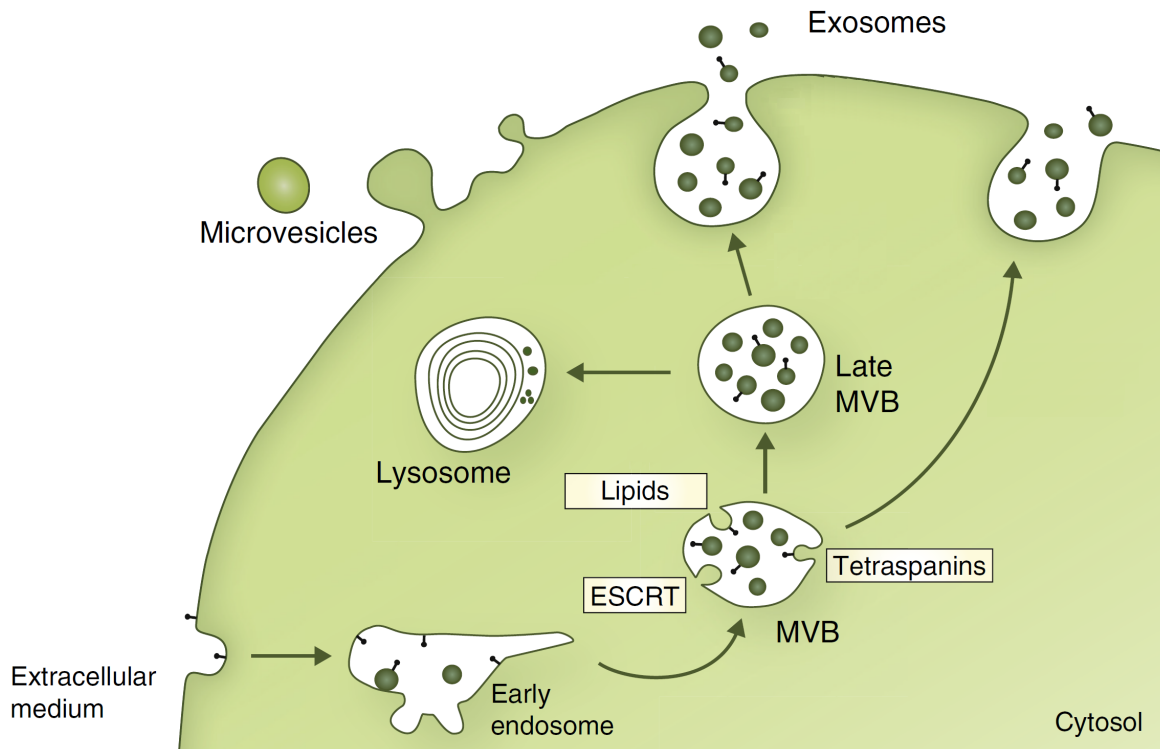


**Figure 2.4: Biogenesis and secretion of extracellular vesicles.**

Schematic representation of the origin and release of exosomes and microvesicles in eukaryotic cells. Exosomes are formed as ILVs via inward budding into early endosomes and MVBs. Several molecules are involved in the biogenesis of ILVs, such as the ESCRT-machinery, lipids and tetraspanins. MVBs can either fuse with the lysosome for degradation or with the plasma membrane, resulting in the extracellular release of exosomes. Microvesicles are generated by outward budding and fission of the plasma membrane. Adapted from [156].

### 2.5.1 EVs in cancer

Tumour derived EVs have been widely described as promoters of tumour progression and are associated with several hallmarks of cancer [11, 150]. EVs are present in many different biological fluids, so that tumour EVs have been exploited as circulating biomarkers for the detection of cancers and other malignancies [157]. Tumour EVs contain a unique composition of nucleic acids, especially miRNAs, that qualifies them as potential biomarkers or to monitor tumour progression in a variety of different cancers such as ovarian, lung, glioblastoma,

prostate and pancreas cancer [173–177]. DNA from EVs can furthermore provide information of cancer specific mutations and thus offer an opportunity for precise diagnosis and to prediction of therapeutic outcomes [157, 178]. Besides genomic informations, proteins within EVs reflect their cellular origin and are consequently useful for the detection of emerging cancer [157].

Tumour cells and cells in the TME secrete EVs that predefine recipient cells for the benefit of the tumour cell [179]. Consequently, EVs shed by cancer cells can stimulate tumour progression in different ways [142, 146, 179]. For example, tumour derived EVs can promote cancer immune evasion by suppressing NK cell proliferation and induce T cell apoptosis via FasL within the TME [157, 180].

Tumour EVs also play an important role in tumour angiogenesis. As a result of intratumoral hypoxia, endothelial cells increase the uptake of tumour derived EVs, which consequently stimulates angiogenesis by enhancing the release of VEGF. Increased VEGF release thus result in an increased endothelial infiltration in the ECM [181–183].

Tumour derived EVs are not restricted to the TME but even circulate to distant sites throughout the body where they can induce a favourable environment for the outgrowth of disseminated tumour cells. This process is also known as pre-metastatic niche (PMN)-formation [141, 157, 183, 184]. For example, melanoma-derived EVs may increase metastasis and the recruitment of bone marrow progenitor cells by upregulation of S100A8, S100A9 and TNF $\alpha$  [179, 183, 185].

EVs shed by tumour cells can also cause therapeutic resistance to various chemotherapeutic agents and antibodies. For example, tumour cells use EVs as genetic exchange vectors in the TME to hijack and to confer resistance to sensitive tumour cells [186, 187]. Additionally, it has been shown, that drug-resistance cancer cells manage to pack chemotherapeutic agents into EVs and export them from the tumour cell [186, 188].

Taken together, tumour derived EVs are an unique source of tumour markers, which were used here for the generation of novel tumour-specific mAbs.

### **2.6 Aim of this thesis**

Only a limited number of tumour specific antigens which can be targeted for the treatment of solid tumours are known today, so that there is a huge demand for new target molecules and new therapeutic regimens. This demand should be addressed during this thesis. For this, a technique that had been developed in our group was used for the identification of new tumour antigens and the generation of the corresponding monoclonal antibodies with therapeutic and diagnostic potential. In detail, tumour derived EVs isolated from cancer patients were used for the immunisation of animals. EVs consist of hundreds of known (and unexpected) proteins in their native conformation, so that these experiments resulted in hundreds of monoclonal antibodies targeting well-known and novel, unexpected antigens alike. The mAbs generated and characterised in detail within this thesis bind to peroxiredoxin 4 (PRDX4), a protein which has so far been described as localised in ER and the cytosol of cells. As our antibodies detect PRDX4 on the tumour cell surface it may emerge as a potential new tumour biomarker and target molecule.

## 3 Materials

### 3.1 General laboratory equipment

All devices and general equipment used during this thesis are listed in the following table (see table 3.1).

**Table 3.1: Devices and equipment used in this thesis.**

<b>Equipment / Device</b>	<b>Manufacturer / Distributor</b>
Bacteria incubator/ Innova 44/4400 Incubator Shaker	New Brunswick Scientific (Edison, USA)
Benchtop centrifuge / 5414R	Eppendorf SE (Hamburg, Germany)
Blotting instrument / trans-blot turbo transfer system	Bio-Rad (München, Germany)
Centrifuge / Avanti J-26 XP Centrifuge	Beckman Coulter (Krefeld, Germany)
Centrifuge / Pico 21 Centrifuge	Heraeus (Hanau, Germany)
Centrifuge / Rotanta 460R	Hettich Zentrifugen (Tuttlingen, Germany)
Centrifuge / Rotanta 46 RSC	Hettich Zentrifugen (Tuttlingen, Germany)
Counting chamber Neubauer Improved	Paul Marienfeld (Lauda-Königshofen, Germany)
Cytofluorometer Canto	BD Biosciences (Heidelberg, Germany)
Cytofluorometer LSR Fortessa	BD Biosciences (Heidelberg, Germany)
Electrophoresis power supply / PowerPac 200	Bio-Rad (München, Germany)
Electrophoresis system / Mighty Small Mini	Hoefer (Massachusetts, USA)
Freezer -20 °C	Bosch (Gerlingen, Germany)
Freezer -80 °C Igloo Green Line 830L	Telstar (Tarrassa, Spain)
Fridge 2-8 °C	Liebherr (Biberach an der Riss, Germany)
Gel dual casting chamber	Hoefer (Massachusetts, USA)
Gel Documentation / Quantum ST5	Vilber Lourmat (Eberhardzell, Germany)
Gel Electrophoresis chamber / PerfectBlue Gel System Mini & Midi L	Peqlab, Biotechnologie (Erlangen, Germany)

continued on next page

### 3 MATERIALS

**Table 3.1 Devices and equipment** – continued from previous page

<b>Device / Equipment</b>	<b>Manufacturer / Distributor</b>
Gel Electrophoresis chamber / XCell4 SureLock Midi-Cell	Thermo Fisher Scientific (Waltham, USA)
Heat block / Eppendorf Thermomixer compact	Eppendorf SE (Hamburg, Germany)
Ice Flaker AF206	Scotsman Ice systems (Suffolk, UK)
Incubator / Heraeus 150	Heraeus (Hanau, Germany)
Imaging system / Fusion FX6 Edge	Vilber Lourmat (Eberhardzell, Germany)
Laminar flow hoods	Prutscher Laboratory Systems (Neudörfel, Austria)
Magnetic stirrer	IKA-Werke (Staufen, Germany)
Microplate reader / CLARIOstar	BMG LABTECH (Ortenberg, Germany)
Microplate washer / Tecan hydroSPEED	Tecan (Männedorf, Switzerland)
Microscope (fluorescence) / Axiovert 200M	Zeiss (Jena, Germany)
Microscope (inverted) / Axiovert 25	Zeiss (Jena, Germany)
Microscope (confocal) / Leica DMI8 TCS SP8	Leica Camera (Wetzlar, Germany)
Microscope (confocal) / Leica SP5	Leica Camera (Wetzlar, Germany)
Multiobiologic Workbench	BDK, (Sonnenbühl-Genkingen, Germany)
NTA instrument (ZetaView)	BDK, (Sonnenbühl-Genkingen, Germany)
Oven /Heraeus UT 6060	Thermo Scientific Heraeus, (Waltham, USA)
pH-Meter pH 526	WTW, Xylem Analytics (Weilheim, Germany)
Pipetboy acu2	Integra Biosciences (Fernwald, Germany)
Pipette (multichannel) / Transferette-12 (20-200 µL)	Brand (Wertheim, Germany)
Pipette (multichannel) / Pipet-Lite Multi L12-200XLS+ & L8-300XLS+	Mettler Toledo (Ohio, USA)
Pipettes / Rainin Pipet-Lite XLS (0.1-2 µL, 0.5-10 µL, 2-20 µL, 20-200 µL, 100-1000 µL)	Mettler Toledo (Ohio, USA)
Precision scale / SPB55	Scaltec (Regau, Austria)
Repeat dispenser / AutoRep E	Mettler Toledo (Ohio, USA)
Rotor / JA-10, fixed angle, 17700 g	Beckman Coulter (Krefeld, Germany)
Rotor / SW32Ti swinging bucket	Beckman Coulter (Krefeld, Germany)
Rotor/ SW28Ti swinging bucket	Beckman Coulter (Krefeld, Germany)
Rotor / SW60Ti swinging bucket	Beckman Coulter (Krefeld, Germany)
Rotor/ S55A2, fixed angle, 201046 g	Thermo Scientific (Waltham, USA)

continued on next page

### 3.1 GENERAL LABORATORY EQUIPMENT

**Table 3.1 Devices and equipment** – continued from previous page

<b>Device / Equipment</b>	<b>Manufacturer / Distributor</b>
Rotor/ S52ST, swinging bucket 275458 g	Thermo Scientific (Waltham, USA)
Shaker / KA HS 260 b	IKA Works (Staufen, Germany)
Sonifier / Branson Digital Sonifier 250 cell disruptor	G. Heinemann Ultraschall- und Labortechnik (Schwäbisch-Gmünd, Germany)
Spectrophotometer / NanoDrop ND-1000	Peqlab Biotechnologie (Erlangen, Germany)
Thermocycler / T-Gradient ThermoBlock	Biometra (Göttingen, Germany)
Tumble roller mixer TRM-50	IDL (Nidderau, Germany)
Ultracentrifuge / Beckman Optima TL-100	Beckman Coulter (Krefeld, Germany)
Ultracentrifuge / Beckman Optima L60	Beckman Coulter (Krefeld, Germany)
Ultracentrifuge / Beckman Optima L70	Beckman Coulter (Krefeld, Germany)
Ultracentrifuge / Sorvall MTX 150	Thermo Scientific Sorvall (Waltham, USA)
Ultra pure water device	Aquintus membraPure (Hennigsdorf, Germany)
UV transilluminator / UVT 400-M	IBI Scientific (New Haven, USA)
UV/Vis photometer / Eppendorf BioPhotometer Plus	Eppendorf SE (Hamburg, Germany)
Vacuum pump	KNF Laboport (Freiburg, Germany)
Vortex mixer / Vortex-Genie 2	Fisher Scientific (Schwerte, Germany)
Water bath	GFL (Burgwedel, Germany)

### 3.2 General consumables

All utilized general consumables are listed in the table below (see table 3.2).

**Table 3.2: Consumables used during this thesis.**

Name	Brand name / size	Manufacturer
<b>Common consumables</b>		
Conical tubes, high clarity	Falcon / 15 mL, 50 mL	Corning Inc. (Corning, USA)
Dispenser tips	Combitips advanced 0.1 mL, 1 mL, 2.5 mL, 5 mL, 10 mL, 50 mL	Eppendorf SE (Hamburg, Germany)
DNA LoBind tubes	1.5 mL	Eppendorf SE (Hamburg, Germany)
Filter unit (CA)	0.8 $\mu$ m, sterile	Thermo Scientific (Waltham, USA)
Filter unit (SFCA)	0.2 $\mu$ m, sterile	Corning Inc. (Corning, USA)
Filter unit (Millex-HA, MCE)	0.45 $\mu$ m, sterile	Merck Millipore (Burlington, USA)
Nitril gloves	Nitril NextGen	Meditrade (Kiefersfelden, Germany)
Parafilm M Laborator film		Amcor (Zürich, Switzerland)
Pipette tips	Diamond TowerPac, 0.1-10 $\mu$ L, 2-200 $\mu$ L, 100-1000 $\mu$ L	Gilson Inc. (Middleton, USA)
Pipette tip	epT.I.P.S. reloads 0.1-10 $\mu$ L	Eppendorf SE (Hamburg, Germany)
Pipette filter tips	ART barrier Pipet Tip, 200 $\mu$ L, 1000 $\mu$ L	Thermo Scientific (Waltham, USA)
Plastic pipette, sterile	2 mL, 5 mL, 10 mL, 25 mL,	Greiner Bio-One (Kremsmünster, Austria)
Protein LoBind tubes	1.5 mL	Eppendorf SE (Hamburg, Germany)
Safe-lock reaction tubes	1.5 mL, 2 mL, 5 mL	Eppendorf SE (Hamburg, Germany)
Syringe without needle	1 mL, sterile	Caretechion (Düsseldorf, Germany)

continued on next page

**Table 3.2 Consumables** – continued from previous page

<b>Name</b>	<b>Brand name / size</b>	<b>Manufacturer</b>
<b>Cell culture</b>		
Cell culture flasks	25, 75, 175 cm <sup>2</sup>	Nunc A/S (Roskilde, Denmark)
Cell scraper	20 mm width, 30 cm length	TPP Techno Plastic Products (Trasadingen, Switzerland)
Cell strainer	Falcon / 40, 70, 100 µm	Corning Inc (Corning, USA)
Counting chamber	C-Chip Neubauer chamber improved	incyto (Nanoentek, Korea)
CryoTubes	Nunc / 1.6 mL	Thermo Scientific (Waltham, USA)
Culture delta surface dishes	15x60 mm	Thermo Scientific (Waltham, USA)
Multiwell plates, flat-bottom	Falcon / 6-well, 12-well, 24-well, 48-well, 96-well	Corning Inc. (Corning, USA)
Multiwell plate, V-bottom	96-well	Hartenstein, Würzburg, Germany
Pasteur pipette (sterile, single use)	3.2 mL	Carl Roth (Karlsruhe, Germany)
Pasteur pipette (glass)	230 mm	Thermo Scientific (Waltham, USA)
<b>Immunoblot</b>		
Cuvettes single use	10x10x48 mm	Sarstedt (Nümbrecht, Germany)
Disposable cuvettes, semi-micro, PS	12.5 x 12.5 x 45 mm	Brand (Wertheim, Germany)
Gel Blotting Paper (GB003)	Whatman / 10 x 10 cm	Schleicher & Schuell, (Dassel, Germany)
Gradient gels NuPAGE	mini and midi 4-12% Bis-Tris	Thermo Scientific (Waltham, USA)
Gradient gels Novex	Tricine gels, mini or midi, 10-20%, 16%	Thermo Scientific (Waltham, USA)
Needle	21G, 26G, 30G, 240 mm	Sarstedt (Nümbrecht, Germany)
Nitrocellulose blotting membrane	Amersham Protan Premium, 0.45 µm	GE Healthcare (München, Germany)
Surgical disposable scalpels		B. Braun (Melsungen, Germany)

continued on next page

### 3 MATERIALS

**Table 3.2 Consumables** – continued from previous page

<b>Name</b>	<b>Brand name / size</b>	<b>Manufacturer</b>
Transfer packs trans-blot turbo	mini or midi, 0.2 µm nitrocellulose	Bio-Rad (München, Germany)
<b>LSCM</b>		
Cover glasses	12 mm, 15 mm, 18 mm	Paul Marienfeld (Lauda-Königshofen, Germany)
Immersion Oil	Type F	Leica Microsystems (Wetzlar, USA)
Superfrost microscope slides, cut, white	76 x 26 mm	Thermo Scientific (Waltham, USA)
Whatman Lens Cleaning Tissue	100 x 150 mm	Cytiva (Marlborough, USA)
<b>Flow cytometry</b>		
multiwell plate, round-bottom	96-well	Nunc A/S (Roskilde, Denmark)
round-bottom tubes	Falcon, 5 mL, 12 x 75 mL	BD Biosciences (Heidelberg, Germany)
<b>ELISA</b>		
Cover foil easyseal	79 x 135 mm	Greiner Bio-One (Kremsmünster, Austria)
multiwell plate, flat bottom	MaxiSorp Immunoplate, 96-well	Nunc A/S (Roskilde, Denmark)
Reagent reservoir	Costar, 50 mL	Corning Inc. (Corning, USA)
<b>PCR, DNA- &amp; RNA- isolation</b>		
Pipette barrier tips, PCR clean and sterile	ep Dualfilter T.I.P. S. 0.1-10 µL, 2-100 µL, 50-1000 µL	Eppendorf SE (Hamburg, Germany)
RNaseZAP		Sigma Aldrich (St. Louis, USA)
Stripes of 8 PCR tubes with attached flat individual covers	0.2 mL	Brand (Wertheim, Germany)
<b>Ultracentrifugation</b>		
Microcentrifuge polypropylene tube	1.5 mL	Beckman Coulter (Krefeld, Germany)

continued on next page

**Table 3.2 Consumables** – continued from previous page

<b>Name</b>	<b>Brand name / size</b>	<b>Manufacturer</b>
Ultracentrifuge PA thin wall tube	38.5 mL	Kisker Biotech (Steinfurt, Germany)
Ultra clear centrifugation tubes	11 x 60 mm	Beckman Coulter (Krefeld, Germany)

### 3.3 Chemicals and Reagents

All used and required chemicals and reagents for this thesis are listed below (see table 3.3).

**Table 3.3: Chemicals and reagents used during this thesis.**

<b>Chemicals and reagents</b>	<b>Concentration/ Size/ Composition</b>	<b>Manufacturer/ Distributor</b>
<b>Common chemicals and reagents</b>		
Aqua ad iniectabilia	100 mL	B. Braun (Melsungen, Germany)
Dismozon plus		Paul Hartmann AG (Heidenheim ,Germany)
Mucocit T		Schülke & Mayr (Norderstedt, Germany)
<b>Cell culture &amp; transfection</b>		
EZ-Link NHS-PEG <sub>4</sub> - Biotin reagent	10 x 2 mg	Thermo Scientific (Waltham, USA)
Pancoll	1.077 g/L	PAN Biotech (Aidenach, Germany)

continued on next page

### 3 MATERIALS

**Table 3.3 Chemicals and reagents** – continued from previous page

<b>Chemicals and reagents</b>	<b>Concentration/ Size/ Composition</b>	<b>Manufacturer/ Distributor</b>
Transfection reagent metafectene Pro		Biontix Laboratories (München, Germany)
Transfection reagent Pei Max	(MW 40,000)	Polysciences, Inc. (Warrington, USA)
<b>ELISA</b>		
Sulfonic acid H <sub>2</sub> SO <sub>4</sub>	37.5 %	Carl Roth (Karlsruhe, Germany)
TMB substrate reagent set	BD OptEIA	BD Biosciences (Heidelberg, Germany)
Tween20		Carl Roth (Karlsruhe, Germany)
<b>Flow cytometry</b>		
FC Clean Solution		BD Biosciences (Heidelberg, Germany)
FC Rinse Solution		BD Biosciences (Heidelberg, Germany)
FC Sheath Fluid		BD Biosciences (Heidelberg, Germany)
<b>LSCM</b>		
BSA		Carl Roth (Karlsruhe, Germany)
DAPI		Thermo Scientific (Waltham, USA)
PFA	EM grade, 16 % solution	Electron Microscopy Sciences (Hatfield, USA)
ProLonge Diamond Antifade Mountant	10 mL	Thermo Scientific (Waltham, USA)
Triton X-100		Sigma Aldrich (St. Louis, USA)
Vectashield Antifade Mounting Medium	10 mL	Vector Laboratories (Burlingame, USA)

continued on next page

**Table 3.3 Chemicals and reagents** – continued from previous page

<b>Chemicals and reagents</b>	<b>Concentration/ Size/ Composition</b>	<b>Manufacturer/ Distributor</b>
<b>SDS-PAGE</b>		
APS		Merck Millipore (Burlington, USA)
Coomassie Brilliant blue G250		Thermo Scientific (Waltham, USA)
Detection reagent ECL select		GE Healthcare (München, Germany)
MOPS SDS Running Buffer	20 x concentrate	Thermo Scientific (Waltham, USA)
Recombinant PRDX4 protein	0.22 µg/mL	Abnova (Taipeh, Taiwan)
Recombinant CCDC47 protein		Sino Biological (Beijing, China)
Restore Western Blot stripping buffer	500 mL	Thermo Scientific (Waltham, USA)
Rotiphorese Gel 30	30 % Acrylamide	Carl Roth (Karlsruhe, Germany)
Powdered milk		Carl Roth (Karlsruhe, Germany)
Prestained Protein Ladder	Pageruler, 10 to 180 kDa	Thermo Scientific (Waltham, USA)
Prestained Protein Ladder	Pageruler, 10 to 260 kDa	Thermo Scientific (Waltham, USA)
Protein Assay Dye Reagent Concentrate		Bio-Rad (München, Germany)
Protease Inhibitor Cocktail Tablets	EDTA-free	Sigma Aldrich (St. Louis, USA)
TEMED		Carl Roth (Karlsruhe, Germany)
<b>Immunoprecipitation</b>		
CNBr-activated Sepharose 4 Fast Flow		GE Healthcare (Chicago, USA)
Laurylsarcosine		Carl Roth (Karlsruhe, Germany)
Sodium Desoxychlorate		Sigma Aldrich (St. Louis, USA)

continued on next page

### 3 MATERIALS

**Table 3.3 Chemicals and reagents** – continued from previous page

<b>Chemicals and reagents</b>	<b>Concentration/ Size/ Composition</b>	<b>Manufacturer/ Distributor</b>
<b>Protein purification</b>		
Imidazole		Merck Milipore (Burlington, USA)
Ni-NTA agarose	25 mL	Qiagen (Hilden, Germany)
Urea		Carl Roth (Karlsruhe, Germany)
<b>PCR, DNA- &amp; RNA- isolation</b>		
Agarose ultra pure		Thermo Scientific (Waltham, USA)
DMSO	100 %	NEB (Frankfurt, Germany)
DNA Gel Loading Dye	6 x concentrate	Thermo Scientific (Waltham, USA)
DNA Gel Loading Dye	6 x concentrate	NEB (Frankfurt, Germany)
DNA ladder	GeneRuler 100 bp Plus	Thermo Scientific (Waltham, USA)
DNA ladder	GeneRuler 1 kb Plus	Thermo Scientific (Waltham, USA)
DNA Stain Clear G		SERVA Electrophoresis (Heidelberg, Germany)
GoTaq G2 Flexi DNA Polymerase	5 U/ $\mu$ L	Promega Corporation (Madison, USA)
dNTP mix	2 nM each	Thermo Scientific (Waltham, USA)
Phusion High-Fidelity DNA Polymerase	2000 U/mL	NEB Frankfurt am Main, Germany
<b>Cloning</b>		
Agar-Agar	Kobe I	Carl Roth (Karlsruhe, Germany)
Ampicillin	1000 x stock (100 mg/mL)	Carl Roth (Karlsruhe, Germany)
Kanamycin	1000 x stock (50 mg/mL)	Carl Roth (Karlsruhe, Germany)

continued on next page

**Table 3.3 Chemicals and reagents** – continued from previous page

<b>Chemicals and reagents</b>	<b>Concentration/ Size/ Composition</b>	<b>Manufacturer/ Distributor</b>
KpnI	20,000 U/mL	NEB (Frankfurt, Germany)
LB-medium		Carl Roth (Karlsruhe, Germany)
XcmI	5,000 U/mL	NEB (Frankfurt, Germany)
<b>Ultracentrifugation &amp; nanoparticle tracking analysis (NTA)</b>		
Extra daily-check suspension	0.1 % concentration 102 nm polystyrene dispersion	Particle Metrix (Inning, Germany)
OptiPrep density gradient medium	60 % Iodixanole solution in H <sub>2</sub> O	Sigma Aldrich (St. Louis, USA)

### 3.4 General buffers and solutions

All prepared and used buffers and solutions are listed in table 3.4.

**Table 3.4: Prepared buffers and solutions.**

<b>Buffer</b>	<b>Composition</b>
<b>Buffers for Immunoblots</b>	
Biotinylation quenching buffer	100 mM glycine in PBS pH=8.0
Blocking solution I	5 % [w/v] powdered milk in TBS-T
Blocking solution II	3 % [w/v] BSA in TBS-T
ECL solution I	0.1 M TRIS/HCl, pH=8.8 200 mM p-Coumaric acid 1.25 mM luminol in H <sub>2</sub> O

continued on next page

### 3 MATERIALS

**Table 3.4 Buffers and solutions** – continued from previous page

<b>Buffer</b>	<b>Composition</b>
ECL solution II	3 % H <sub>2</sub> O <sub>2</sub>
Hypotonic buffer	5 mM TRIS/HCl, pH=7.4 25 mM NaF 5 mM MgCl <sub>2</sub> 1 mM EGTA in H <sub>2</sub> O
Non-reducing laemmli (2 x)	160 mM TRIS/HCl, pH=6.8 4 % [w/v] SDS 20 % [v/v] Glycerol 0.0625 % [w/v] Bromphenol blue in H <sub>2</sub> O
MOPS running buffer	MOPS buffer concentrate (20X) 5 mM NaHCO <sub>3</sub> in H <sub>2</sub> O
Reducing laemmli (2 x)	160 mM TRIS/HCl, pH=6.8 4 % [w/v] SDS 10 % [v/v] β -Mercaptoethanol 20 % [v/v] Glycerol 0.0625 % [w/v] Bromphenol blue in H <sub>2</sub> O
Reducing laemmli (5 x)	312.5 mM TRIS/HCl, pH=6.8 20 % [w/v] SDS 25 % [v/v] β-Mercaptoethanol 20 % [v/v] Glycerol 0.0625 % [w/v] Bromphenol blue in H <sub>2</sub> O
RIPA lysis buffer	50 mM TRIS/HCl, pH=7.4 150 mM NaCl 1 % Igepal CA-630 0.5 % Sodiumdesoxychlorate 1 tablet/10 mL Protease inhibitor cComplete in H <sub>2</sub> O

continued on next page

### 3.4 GENERAL BUFFERS AND SOLUTIONS

**Table 3.4 Buffers and solutions** – continued from previous page

Buffer	Composition
SDS-PAGE buffer I	1.5 M TRIS/HCl, pH=8.8 in H <sub>2</sub> O
SDS-PAGE buffer II	0.5 M TRIS/HCl, pH=6.8 in H <sub>2</sub> O
TBS (10x)	200 mM TRIS 1.5 M NaCl in 1 L H <sub>2</sub> O
TBS-T	0.05 % [v/v] Tween-20 in TBS
Transfer buffer (1 x)	25 mM TRIS (3.03 g/L) 200 mM glycine (15 g/L) 0.04 % [v/v] SDS 20 % Methanol in H <sub>2</sub> O
<b>Buffers for immunoprecipitation (IP)</b>	
Coupling buffer (1 x)	0.1 M NaHCO <sub>3</sub> 0.5 M NaCl in H <sub>2</sub> O, pH= 8.3
Coupling buffer (3 x)	0.3 M NaHCO <sub>3</sub> 1.5 M NaCl, in H <sub>2</sub> O, pH= 8.3
Laurylsarcosine wash buffer	0.5 % N-Laurylsarcosine 0.1 % SDS in PBS
NaAc buffer	0.1 M NaAc 0.5 M NaCl in H <sub>2</sub> O, pH= 4

continued on next page

### 3 MATERIALS

**Table 3.4 Buffers and solutions** – continued from previous page

<b>Buffer</b>	<b>Composition</b>
PBS buffer	137 mM NaCl (8 g/L) 2.7 mM KCl (0.2 g/L) 10 mM Na <sub>2</sub> HPO <sub>4</sub> (1.44 g/L) 1.8 mM KH <sub>2</sub> PO <sub>4</sub> (0.24 g/L) in H <sub>2</sub> O, pH=7.4
Wash buffer	0.1 M TRIS-HCl 0.5 M NaCl in H <sub>2</sub> O, pH= 8
<b>Buffers for LSCM</b>	
Blocking buffer	3 % [w/v] BSA in PBS
Fixation buffer	4 % [v/v] PFA in PBS
Permeabilisation buffer	0.3 % [v/v] Triton X-100 in PBS
Staining buffer	1 % [w/v] BSA 0.1 % [v/v] Triton X-100 in PBS
<b>Buffers for ELISA</b>	
Wash buffer	0.05 % [v/v] Tween-20 in PBS
Blocking buffer	2.5 % [w/v] milk powder in wash buffer
Stop solution	1 M H <sub>2</sub> SO <sub>4</sub> in H <sub>2</sub> O
<b>Buffer for flow cytometry</b>	
FC buffer	2 % [v/v] FCS 2 mM EDTA in PBS (Ca <sup>2+</sup> /Mg <sup>2+</sup> free)

continued on next page

### 3.4 GENERAL BUFFERS AND SOLUTIONS

**Table 3.4 Buffers and solutions** – continued from previous page

<b>Buffer</b>	<b>Composition</b>
<b>Buffer for agrose gels</b>	
TAE buffer (1x)	1 mM EDTA 20 mM acetic acid 40 mM TRIS in H <sub>2</sub> O
<b>Buffers for Coomassie staining</b>	
Coomassie destaining buffer	50 % methanol 10 % acetic acid 40 % H <sub>2</sub> O
Coomassie staining buffer	50 % methanol 10 % acetic acid 40 % H <sub>2</sub> O 0.05 % brilliant blue
<b>Buffers for protein purification</b>	
Urea lysis buffer	8 M Urea 0.1 M NaH <sub>2</sub> PO <sub>4</sub> 10 mM TRIS-HCl 0.05 % Tween20 20 mM imidazole in 1 L H <sub>2</sub> O, pH = 8.0
Elution buffer	0.5 M imidazole in urea lysis buffer, pH = 7.5
<b>Buffer for bacteria</b>	
LB media	1 % Tryptone 0.5 % yeast extract 0.5 % NaCl in H <sub>2</sub> O
LB agar plates	8 g Agar antibiotics of interest in 400 mL LB-media

## 3.5 Cell culture

### 3.5.1 Cell culture media and additives

All needed media and additives used for cell cultivation were listed in table 3.5.

**Table 3.5: Media and additives used for cell cultivation of cell lines.**

Name	Application	Manufacturer	Reference No./ Lot No.
Bambanker Serum-free Cell Freezing Media	Cryopreservation	Nippon Genetics Europe (Düren, Germany)	BB01 / various
DMEM (+) L-Glutamine, D-Glucose, Pyruvate	Cell culture medium for adherent cells	Gibco, Thermo Scientific Heraeus (Waltham, USA)	1195-065 / various
Fetal calf serum (FCS)	Nutritive substance	Sigma-Aldrich (St. Louis, USA)	FCS.SAM.0500 / various
Hygromycin B (50 mg/mL)	Antibiotics, selection of stable transfected cells	Gibco, Thermo Scientific Heraeus (Waltham, USA)	10687010 / H044-54US
DPBS without Ca <sup>2+</sup> and Mg <sup>2+</sup>	Buffer, to remove residual media	Sigma-Aldrich (St. Louis, USA)	D8535 / various
Pen Strep 10000 U/mL	Antibiotics, inhibition of bacterial growth	Gibco, Thermo Scientific Heraeus (Waltham, USA)	15140-122 / various
Opti-MEM Reduced Serum Medium	Cell culture medium for transfection	Gibco, Thermo Scientific Heraeus (Waltham, USA)	31985-047 / various
RPMI 1640 (+) L-Glutamine, D-Glucose, Pyruvate	standard cell culture medium	Gibco, Thermo Scientific Heraeus (Waltham, USA)	21875-034 / various
Trypan Blue Stain (0.4%)	1:10 diluted, cell counting and cell viability check	Thermo Fisher Scientific (Waltham, USA)	T10282 / 2000254

continued on next page

**Table 3.5 Cell culture media and additives** – continued from previous page

<b>Name</b>	<b>Application</b>	<b>Manufacturer</b>	<b>Reference No./ Lot No.</b>
Trypsin EDTA 0.05 %	Detachment of adherent cells	Gibco, Thermo Scientific Heraeus (Waltham, USA)	25300054 / various
TrypLE Select Enzyme	Detachment of adherent cells	Gibco, Thermo Scientific Heraeus (Waltham, USA)	12563-029 / 2301998

### 3.5.2 Cell lines

All cell lines cultured during this thesis were available at the Department of gene vectors (AGV) at the Helmholtz Zentrum München if not indicated otherwise and are listed in the following table 3.6 below.

**Table 3.6: Cell lines cultivated during this thesis.**

<b>Name</b>	<b>Description</b>
A549	human lung carcinoma cell line, epithelial-like
AsPC-1	human pancreas adenocarcinoma,
Capan-1	human pancreas adenocarcinoma, epithelial
Colo 320DM	human large intestine colon colorectal adenocarcinoma (Dukes' type C), rounded and refractile
DAN-G	human pancreas carcinoma, epithelial
Du 145	human prostate carcinoma, epithelial
ES-2	human ovary clear cell carcinoma, fibroblast
ExpiCHO-S	chinese hamster, ovaria, derived from a non-engineered subclone. Purchased from Thermo Fisher (Waltham, USA) [189]
G261	mouse glioblastoma (obtained from Prof. Glaß, LMU)
HCT116	human large intestine colorectal carcinoma, epithelial
HEK293T	human embryo kidney cell line, epithelial, the HEK293T cell line was generated by transformation with the adenovirus type 5 E1a and E1b genes into HEK293 cells [190]
HEK293T PRDX4-KO	HEK293T cell line with PRDX4-KO. Purchased from Abcam (Cambridge, UK)/ab266727
HepG2	human liver hepatocellular carcinoma, epithelial-like

continued on next page

### 3 MATERIALS

---

**Table 3.6 Cell lines** – continued from previous page

<b>Name</b>	<b>Description</b>
HeLa	human cervic adenocarcinoma, epithelial
HT29	human colon colorectal adenocarcinoma, epithelial
Huh7	human liver hepatocellular carcinoma, epithelial
Jurkat	human acute T cell leukemia, T lymphoblast
Kato III	human lung, fibroblast
LL8	mouse, fibroblast
MCF-7	human mammary gland adenocarcinoma, epithelial
MDA-MB-231	human mammary gland adenocarcinoma, epithelial
MIA PaCa-2	human pancreas carcinoma, epithelial
MRC-5	human lung, fibroblast
MSTO-211H	human lung biphasic mesothelioma, fibroblast
NCI-H2452	human lung mesothelioma, epithelial
NCI-H520	human lung squamous cell carcinoma, epithelial
NCI-H526	human lung small cell lung cancer (stage E), epithelial
NCI-H661	human lung carcinoma, epithelial
NIH: OVCAR-3	human ovary adenocarcinoma, epithelial
PaCa5061	human pancreatic ductal adenocarcinoma, epithelial
Panc-1	human pancreatic epithelioid carcinoma, epithelial
PCI-1	human squamous cell carcinoma of the larynx, epithelial
PCI-13	human squamous cell carcinoma of the oral cavity
RT112	human bladder carcinoma, epithelial
RC 124	human kidney, epithelial
SK-Mel-23	human cutaneous malignant melanoma, skin epithelial
SK-N-SH	human brain, neuroblastoma, epithelial
SKOV-3	human ovarian adenocarcinoma (ascites), epithelial
SK-BR-3	human mammary gland adenocarcinoma, epithelial
SW620	human large intestine colorectal adenocarcinoma, epithelial
T-47D	human mammary gland ductal carcinoma, epithelial
UWB1.289	human ovary carcinoma, epithelial-like
U-87 MG	human brain likely glioblastoma, epithelial
U-138 MG	human brain glioblastoma (Grade IV), polygonal
U-251 MG	human brain glioblastoma, fibroblastic pattern
U2-OS	human bone osteosarcoma, epithelial
Vero	african green monkey, kidney, epithelial
Wi-38	human lung, fibroblast
YCCEL-1	human gastric adenocarcinoma (ascites)
ZR-75-1	human mammary gland ductal carcinoma, epithelial

### 3.6 Antibodies

Most mAbs were produced by the Monoclonal antibody core facility (MAB) at the Helmholtz Munich. MAbs marked (\*) result from immunisation with EVs generated in the working group of Prof. Zeidler. All used directly labelled antibodies (ABs) are listed in table 3.7 and were utilized in the listed dilution if not indicated otherwise.

**Table 3.7: Directly labelled antibodies used in this thesis.**

Antigen	Immunisation/Clone	Species/ isotype	Conjugate	Dilution	Manufacturer/ Reference No.
<b>Fluorescently labelled antibodies</b>					
$\alpha$ -PRDX4*	OCA2E/ 5H5	Rat/ IgG2a	Alexa Fluor 647	1 $\mu$ g/mL	AG Zeidler, HMGU
$\alpha$ -PRDX4*	OCA2E/ 5H5	Rat/ IgG2a	Alexa Fluor 488	1 $\mu$ g/mL	AG Zeidler, HMGU
$\alpha$ -tPRDX4	PRDX/ 15C8	Rat/ IgG2a	Alexa Fluor 488	1 $\mu$ g/mL	AG Zeidler, HMGU
$\alpha$ -CD49c*	EXO/ 8F2	Rat/ IgG2a	Alexa Fluor 647	1 $\mu$ g/mL	AG Zeidler, HMGU
$\alpha$ -CD49c*	EXO/ 8F2	Rat/ IgG2a	Alexa Fluor 488	1 $\mu$ g/mL	AG Zeidler, HMGU
$\alpha$ -CD81	M38	Mouse/ IgG1	Alexa Fluor 647	2.5 $\mu$ g/mL	Novus Biological (Littleton, USA)/NBP1-44861AF647
$\alpha$ -CCDC47		Rabbit/ IgG1	Alexa Fluor 647	2 $\mu$ g/mL	Bioss AB (Woburn, USA)/ bs-6922R-A647
$\alpha$ -CD147*	OCAM/ 9G2	Rat/ IgG2a	Atto Fluor 488	1:500	AG Zeidler, HMGU

continued on next page

### 3 MATERIALS

**Table 3.7 Directly labelled antibodies** – continued from previous page

Antigen	Immunisation/Clone	Species/ isotype	Conjugate	Dilution	Manufacturer/ Reference No.
<b>HRP-conjugated antibodies</b>					
$\alpha$ -tubulin	GT112	Mouse/ IgG2a	HRP	0.1 $\mu$ g/mL (1:2,000)	GeneTex (Waltham, USA)/ GTX628802
$\alpha$ -His	3D5	Rat/ IgG2a	HRP	1 $\mu$ g/mL (1:3,000)	MAB at the HMGU
$\alpha$ -CD63*	EXO-M/ 12E12	Rat/ IgG1	HRP	1.5 $\mu$ g/mL (1:2,000)	AG Zeidler, HMGU
$\alpha$ -PRDX4*	OCA2E/ 5H5	Rat/ IgG2a	HRP	1 $\mu$ g/mL	AG Zeidler, HMGU
$\alpha$ -GFP	3H9	Rat/ IgG2a	HRP	1 $\mu$ g/mL (1:3,000)	MAB at the HMGU
$\alpha$ -biotin		Mouse	HRP	4 ng/mL (1:200,000)	Jackson ImmunoResearch Laboratories Inc. (West Grove, USA)/ 200-032-211

All used commercial and in-house produced primary ABs were listed in the following tables (commercial, see table 3.8 and in-house, see table 3.9).

**Table 3.8: Commercial primary antibodies.**

Antigen	Immunisation/Clone	Species/ isotype	Dilution	Manufacturer/ Reference No.
$\alpha$ -human CCDC47		Rabbit	0.05-0.2 $\mu$ g/mL (1:2,000)	Sigma-Aldrich (St. Louis, USA)/ HPA029674
$\alpha$ -human PRDX4	EPR15458	Rabbit	0.02 $\mu$ g/mL (1:50,000)	Abcam (Cambridge, UK)/ ab184167
$\alpha$ -human PRDX4		Rabbit	1:5,000	Thermo Scientific (Waltham, USA)/ PA3-753

continued on next page

**Table 3.8 Commercial primary antibodies** – continued from previous page

Antigen	Immunisation/Clone	Species/ isotype	Dilution	Manufacturer/ Reference No.
$\alpha$ -human PRDX1	EPR5433	Rabbit	0.1 $\mu\text{g}/\text{mL}$ (1:10,000)	Abcam (Cambridge, UK)/ ab109498
$\alpha$ -human HPRT1		Rabbit	0.2 $\mu\text{g}/\text{mL}$ (1:3,000)	Thermo Fisher (Waltham, USA)/ PA5-22281
$\alpha$ -human ATP1A1	EP1845Y	Rabbit	0.01 $\mu\text{g}/\text{mL}$ (1:50,000)	Abcam (Cambridge, UK)/ ab76020
$\alpha$ -human CD81	5A6	Mouse	0.5 $\mu\text{g}/\text{mL}$ (1:1,000)	BioLegend (San Diego USA)/ 349502

**Table 3.9: In-house produced primary antibodies.**

Antigen	Immunisation/Clone	Species/ iso-type	Dilution	Manufacturer
$\alpha$ -CD73	EXO/ 20A8	Rat/ IgG2a	supernatant (1:3)	MAB at the HMGU
$\alpha$ -GFP	3H9	Rat/ IgG2a	supernatant (1:20) purified (5 $\mu\text{g}/\text{mL}$ )	MAB at the HMGU
$\alpha$ -CD63*	EXOM/ 24F9	Rat/ IgG2b	supernatant (1:20) purified (1 $\mu\text{g}/\text{mL}$ )	AG Zeidler, HMGU
$\alpha$ -MBP	7G4	Rat/ IgG2a	supernatant (1:3) purified (1 $\mu\text{g}/\text{mL}$ )	MAB at the HMGU
$\alpha$ -GST	6G9	Rat/ IgG2a	supernatant (1:3) purified (1 $\mu\text{g}/\text{mL}$ )	MAB at the HMGU
$\alpha$ -FLAG	3H3	Rat/ IgG2b	supernatant (1:3) purified (1 $\mu\text{g}/\text{mL}$ )	MAB at the HMGU

continued on next page

### 3 MATERIALS

**Table 3.9 Primary antibodies** – continued from previous page

Antigen	Immunisation/Clone	Species/ iso-type	Dilution	Manufacturer
α-PRDX4 (OCA2E)*	2C1	Rat/ IgG2a	supernatant (1:3) purified (1 µg/mL)	AG Zeidler, HMGU
	2F9	Rat/ IgG2a	supernatant (1:3) purified (1 µg/mL)	AG Zeidler, HMGU
	5H5	Rat/ IgG2a	supernatant (1:3) purified (1 µg/mL)	AG Zeidler, HMGU
	8E10	Rat/ IgG2a	supernatant (1:3) purified (1 µg/mL)	AG Zeidler, HMGU
	10G7	Rat/ IgG2a	supernatant (1:3) purified (1 µg/mL)	AG Zeidler, HMGU
	11F2	Rat/ IgG2b	supernatant (1:3) purified (1 µg/mL)	AG Zeidler, HMGU
	13B2	Rat/ IgG2a	supernatant (1:3) purified (1 µg/mL)	AG Zeidler, HMGU
	15F11	Rat/ IgG2a	supernatant (1:3) purified (1 µg/mL)	AG Zeidler, HMGU
	17A10	Rat/ IgG2a	supernatant (1:3) purified (1 µg/mL)	AG Zeidler, HMGU
	18G8	Rat/ IgG2a	supernatant (1:3) purified (1 µg/mL)	AG Zeidler, HMGU
	19H9	Rat/ IgG2a	supernatant (1:3) purified (1 µg/mL)	AG Zeidler, HMGU
	24B7	Rat/ IgG2a	supernatant (1:3) purified (1 µg/mL)	AG Zeidler, HMGU

All used secondary antibodies are listed in table 3.10.

**Table 3.10: Secondary antibodies used in this thesis.**

Antigen	Species/ isotype	Conjugate	Dilution	Manufacturer/ Reference No.
<b>Fluorescently labelled antibodies</b>				
$\alpha$ -rabbit IgG (H+L)	Goat	Alexa Fluor Plus 555	4 $\mu$ g/mL	Invitrogen (Waltham, USA)/ A32732
$\alpha$ -rabbit IgG (H+L)	Goat	Alexa Fluor Plus 488	4 $\mu$ g/mL	Invitrogen (Waltham, USA)/ A32731
$\alpha$ -rabbit IgG (H+L)	Goat	Alexa Fluor Plus 647	4 $\mu$ g/mL	Invitrogen (Waltham, USA)/ A32733
$\alpha$ -rat IgG (H+L)	Goat	Alexa Fluor 568	4 $\mu$ g/mL	Invitrogen (Waltham, USA)/ A11077
$\alpha$ -rat IgG (H+L)	Donkey	Alexa Fluor 488	4 $\mu$ g/mL	Invitrogen (Waltham, USA)/ A21208
$\alpha$ -rat IgG (H+L)	Goat	Alexa Fluor 647	3 $\mu$ g/mL (1:500)	Jackson ImmunoResearch Laboratories Inc. (West Grove, USA)/ 112-605-062
$\alpha$ -rat IgG (H+L)	Goat	Alexa Fluor 647	3 $\mu$ g/mL (1:500)	Jackson ImmunoResearch Laboratories Inc. (West Grove, USA)/ 112-605-062
$\alpha$ -human IgG (H+L)	Donkey	Alexa Fluor 647	3 $\mu$ g/mL (1:500)	Jackson ImmunoResearch Laboratories Inc. (West Grove, USA)/ 709-605-149

continued on next page

### 3 MATERIALS

**Table 3.10 Secondary antibodies** – continued from previous page

Antigen	Species/ isotype	Conjugate	Dilution	Manufacturer/ Reference No.
<b>HRP-conjugated antibodies</b>				
$\alpha$ -mouse IgG (H+L)	Goat	HRP	0.04 $\mu$ g/mL (1:20,000)	Jackson ImmunoResearch Laboratories Inc. (West Grove, USA / 115-035-003
$\alpha$ -rat IgG (H+L)	Goat	HRP	0.04 $\mu$ g/mL (1:20,000)	Jackson ImmunoResearch Laboratories Inc. (West Grove, USA)/ 112-035-062
$\alpha$ -rabbit IgG (HC)	Donkey	HRP	4 $\mu$ g/mL	Invitrogen (Waltham, USA)/ A27036
$\alpha$ -human IgG (H+L)	Donkey	HRP	0.04 $\mu$ g/mL (1:5,000)	Jackson ImmunoResearch Laboratories Inc. (West Grove, USA)/ 709-035-149

## 3.7 Oligonucleotides

### 3.7.1 Oligonucleotides for PRDX4 plasmid cloning

Primers used for cloning of the different His- and GFP-tagged PRDX4 and tPRDX4 plasmid constructs are listed in table 3.11.

**Table 3.11: Oligonucleotides used for the generation of PRDX4 plasmid constructs.**

Name	Direction	Sequence (5' $\rightarrow$ 3')
PRDX4 GFP	fwd	p-GGT GGT GGA GGC TCT GTG A
PRDX4 prom ex1	rev	CTT CGC TTT GCT TAG GTG CA
PRDX4 ex2-7	fwd	GTT TCT AAG CCA GCG CC
PRDX4 ex2-7	rev	p-CAT GGT ACC AAG CTT GGT GG

continued on next page

**Table 3.11 Oligonucleotides for PRDX4 constructs** – continued from previous page

Name	Direction	Sequence (5' → 3')
tPRDX4 tex1	rev	CAT AAC ATT ATC TGG CAG CTC TT
PRDX4 His	fwd	CAT CAC CAT CAT TAA ACT CGA GTC TAG AGC G
PRDX4 His ex1	rev	p-ATG ATG AGA GCC TCC ACC CCC CTT C
PRDX4 His ex7	rev	p-ATG ATG AGA GCC TCC ACC CCC ATT CA

### 3.7.2 Oligonucleotides for tPRDX4 detection in human cell lines

Oligonucleotides for detection of tPRDX4 in the human cell lines are listed in the following table 3.12.

**Table 3.12: Oligonucleotides used for the detection of tPRDX4 in human cell lines.**

Name	Direction	Sequence (5' → 3')
PRDX4	fwd	CTA GCC GCG ACA ACT CC
tPRDX4 ex1 (a)	fwd	ATG GAT CAC CGA AGC CGA
tPRDX4 ex1 (b)	fwd	ACA GGC CTG AAC CGA ATC
tPRDX4 prom	fwd	GAC ATA ACG CTT TCC TCA AGC T
PRDX4 ex2 (a)	rev	GTT AAC TTC AGC TCC TTA AA <sub>t</sub> TCT C
PRDX4 ex2 (b)	rev	GGT AGA AGA AGA AAA CCA AGT ATT
PRDX4 ex3	rev	TCT GAA TTC TTC AAG TCT GTC G
PRDX4 ex4	rev	CCT GAG TCC TCT AGG TAT AC

### 3.7.3 Oligonucleotides for 5' RACE-PCR

Oligonucleotides used for the identification of AB sequences are listed in the following table 3.13. All oligonucleotides which were used for subsequent validation of the received AB sequences are listed in table 3.14.

### 3 MATERIALS

**Table 3.13: Oligonucleotides for 5' RACE-PCR.**

Name	Species/ type	Iso-	Antibody chain	Sequence (5' → 3')
<b>cDNA oligonucleotides for HC and LC (priming in hinge region)</b>				
1634	rat/IgG2a		HC	ACA AGG ATT GCA TTC CCT TGG
1635	rat/IgG2b		HC	GCA TTT GTG TCC AAT GCC GCC
1639	rat/IgGκ		LC	CTC ATT CCT GTTT GAA GCT CTT GAC GAC
<b>Primer for PCR with dC-tailed HC and LC</b>				
1642	rat		HC	CTA CTA GCA TGC TCG AGC TCA ATT TTC TTG TCC ACC TTG GTG C
1647	mouse & rat κ		LC	CTA CTA GCA TGC TCG AGC TCA TTC CTG TTG AAG C TC TTG ACG ACG GG

**Table 3.14: Oligonucleotides for 5' RACE-PCR antibody sequence validation.**

Name	Antibody chain	Direction	Sequence (5' → 3')
2C1	HC	rev	GTC ACT GAG CTG GTG AGA GTG
	LC	fwd	AGA CAG GAC ACA GGT CAG TCA
5H5	HC	rev	GGT GAC TGG CTC AGG GAA ATA
	LC	fwd	AGA CAG GAC ACA GGT CAG TCA
13B2	HC	rev	GAA ATA GCC CTT GAC CAG
	LC	fwd	CAG TCA TGA TGG CTC CAG TCC
15F11	HC	fwd	TCC CCT GAA CAC AAT GAC GAT
	LC	rev	TTC ACT GCC ATC AAT CTT CCA CTT G
17A10	HC	rev	TGA CTG GCT CAG GGA AAT AGC
	LC	fwd	CAG ACA GGA CAC AGG TCA GT
1H1	HC	rev	GTC ACT GAG CTG GTG AGA G
	LC	rev	GTC CAG GAC ACC ATC TCG TTG
19A4	HC	rev	GCA GGA CAG CTG GGA AGG TGT
	LC	rev	CCA TCA ATC TTC CAC TTG ACA C
15C8	HC	rev	GCT GGG CCA GGT CCT GGA GGT
	LC	rev	AGT TGT TCA CGA AGC ACA CGA C

### 3.8 Plasmids

All plasmids purchased or generated during this study are shown in table 3.15 and table 3.16. The expression of the PRDX4 protein variant was under control of the immediate-early enhancer and the promoter of human cytomegalovirus (HCMV). Plasmids for humanisation of one PRDX4 antibody (OCA2E 5H5) were all purchased from GenScript Biotech (Piscataway, USA).

**Table 3.15: Generated plasmids.**

Plasmid	Description	Manufacturer
p1925	GFP	AGV
pCMV-PRDX4 -C-GFPspark	full length PRDX4 gene with C-terminal GFPspark tag under CMV promoter.	Sino Biological (Beijing, China)
pCMV-PRDX4 -C-His	full length PRDX4 gene with C-terminal His6 tag under CMV promoter.	generated from pCMV-PRDX4 -C-GFPspark plasmid
pCMV-ex1-GFPspark	PRDX4 exon1 with C-terminal GFPspark tag under CMV promoter.	generated from pCMV-PRDX4 -C-GFPspark plasmid
pCMV-ex1-His	PRDX4 exon1 with C-terminal His6 tag under CMV promoter.	generated from pCMV-ex1 -C-GFPspark plasmid
tPRDX4-ex1a	PRDX4 exon1 sequence	Purchased from Genscript
pCMV-tPRDX4-GFPspark	full length tPRDX4 gene with C-terminal GFPspark tag under CMV promoter.	generated from pCMV-PRDX4 -C-GFPspark plasmid
pCMV-tPRDX4-His	full length tPRDX4 gene with C-terminal His6 tag under CMV promoter.	generated from pCMV-PRDX4 -C-His plasmid
pCMV-ex2-7-C-GFPspark	PRDX4 exon2-7 with C-terminal GFPspark tag under CMV promoter.	generated from pCMV-PRDX4 -C-GFPspark plasmid
pCMV-ex2-7-C-His	PRDX4 exon2-7 with C-terminal His6 tag under CMV promoter.	generated from pCMV-PRDX4 -C-His plasmid

### 3 MATERIALS

**Table 3.16: Plasmids purchased for PRDX4 antibody (OCA2E 5H5) humanisation.**

Plasmid humanisation	Description
<b>5H5 HC plasmids</b>	
5H5 HC chim	5H5 AB sequence, rat variable HC and human constant HC regions under CMV promoter, cerulean under AmpR promoter
5H5 HC graft	5H5 AB sequence, humanised variable HC and human constant HC regions under CMV promoter, cerulean under AmpR promoter
5H5 HC set1a	
5H5 HC set1a mutS	
5H5 HC set1a mutV	
5H5 HC set1a mutSV	
5H5 HC set1b	
5H5 HC set1b mutS	
5H5 HC set1b mutV	
5H5 HC set1b mutSV	5H5 AB sequence of humanised variable HC sequence with several different backmutations and constant human HC regions under CMV promoter,
5H5 HC set2a	cerulean under AmpR promoter
5H5 HC set2a mutS	
5H5 HC set2a mutV	
5H5 HC set2a mutSV	
5H5 HC set2b	
5H5 HC set2b mutS	
5H5 HC set2b mutV	
5H5 HC set2b mutSV	
<b>5H5 LC plasmids</b>	
5H5 LC chim	5H5 AB sequence, rat variable LC and human constant LC regions under CMV promoter, mCherry under AmpR promoter
5H5 LC graft	5H5 AB sequence, humanised variable LC and human constant LC regions under CMV promoter, mCherry under AmpR promoter

continued on next page

**Table 3.16 Plasmids for humanisation** – continued from previous page

Plasmid humanisation	Description
5H5 LC set 1	
5H5 LC set 2	5H5 AB sequence, humanised variable LC with several different
5H5 LC graft mutT	backmutations and human constant LC regions under CMV
5H5 LC graft mutY	promoter,
5H5 LC graft mutQ	mCherry under AmpR promoter
5H5 LC graft mutTYQ	

### 3.9 Bacteria strain

For preparation of plasmid DNA, the following bacteria strain was utilized (see table 3.17).

**Table 3.17: Bacteria strain used in this thesis.**

Name	Description	Manufacturer
E. coli DH5 $\alpha$	F-endA1 glnV44 thi-1 recA1 relA1 gyrA96 deoR nupG $\Phi$ 80dlacZ $\Delta$ M15 $\Delta$ (acZYA-largF) U169, hsdR17(rK-mK+), $\lambda$ - [191]	Invitrogen life technologies, Karlsruhe, Germany

### 3.10 Commercial Kits

All kits used for this thesis are listed in table 3.18.

**Table 3.18: Kits used during this thesis.**

<b>Kit name</b>	<b>Supplier</b>	<b>Reference No.</b>
EndoFree Plasmid Maxi Kit	Qiagen GmbH (Hilden, Germany)	12362
Monarch Total RNA Miniprep Kit	NEB (Frankfurt, Germany)	T2010S
Monarch PCR & DNA Cleanup Kit	NEB (Frankfurt, Germany)	T1030S
Monarch Plasmid DNA Miniprep Kit	NEB (Frankfurt, Germany)	T1010L
Mycoalert, mycoplasma detection kit	Lonza (Basel, Switzerland)	LT07-218
NucleoSpin Gel and PCR Clean-up Kit	Macherey-Nagel (Düren, Germany)	740609.50
Pierce BCA protein assay Kit	Thermo Scientific (Waltham, USA)	23225
Rapid DNA Dephos & Ligation Kit	Roche (Basel, Switzerland)	04898117001
5' RACE System for Rapid Amplification of cDNA Ends, Version 2.0	Invitrogen life technologies (Karlsruhe, Germany)	18374058
SuperScript III First-Strand Synthesis System	Thermo Scientific (Waltham, USA)	18080051

## 3.11 Software

All software used in this study for data acquisition and analysis is shown in table 3.19.

**Table 3.19: Software used during this thesis.**

Name	Version	Application	Producer
Bio-1D	15.08	WB image quantification and analysis	Vilber Lourmat Deutschland GmbH (Eberhardzell, Germany)
CLARIOStar	5.40.R2	ELISA data acquisition	BMG LABTECH (Ortenberg, Germany)
Diva	8.0.1	FC data acquisition and compensation	BD Biosciences (Heidelberg, Germany)
Evolution Capt-Edge	15.08	WB image acquisition	Vilber Lourmat Deutschland GmbH (Eberhardzell, Germany)
Excel 2016	16.56	Data analysis	Microsoft (Redmond, USA)
Fiji	2.3.0/1.53f	LSCM image analysis	[192]
FlowJo	10.8.1	FC data analysis and compensation	TreeStar Inc. (Ashland, USA)
LAS X	3.5.7.23225	LSCM image acquisition	Leica Microsystems (Wetzlar, Germany)
MacVector	17.0.10	Plasmid design, DNA sequencing analysis	MacVector Inc. (Cary, USA)
Mars	3.31	ELISA data analysis	BMG LABTECH (Ortenberg, Germany)
PowerPoint 2016	16.57	Illustration and Presentation	Microsoft (Redmond, USA)
Prism 9	9.3.1	Data analysis, statistics and visualisation	GraphPad Software (La Jolla, USA)
TexMaker	5.0.4	Thesis writing	GNU General Public Licence,
Word 2016	16.57		Microsoft (Redmond, USA)
ZetaView	8.04.02	EV analysis	Particle Metrix GmbH (Inning am Ammersee, Germany)

### 3.12 Services and databases

- **AB annotation** was done by the online tool **abYsis** [193].
- **abDesign**-tool was used to humanise AB sequences, the tool was established by Benjamin Schubert at the Helmholtz Munich, Institute of Computational Biology (ICB).
- **Oligonucleotides** were synthesized by Metabion (Martinsried, Germany).
- **Sanger DNA sequencing** of purified PCR products was done by Eurofins Genomics (Ebersberg, Germany).
- **Mass spectrometry** of immunoprecipitation (IP) samples was conducted at the Research unit Protein Science (PROT) at the Helmholtz Munich by Dr Stefanie Hauck.
- **Antibody generation and purification** was performed at the MAB at the Helmholtz Munich.
- **Primary human hepatocytes** isolated and purchased from human tissue and cell research Services GmbH (Martinsried, Germany).

f



## 4 Methods

### 4.1 Cell biological methods

#### 4.1.1 Cell culture conditions

Eukaryotic cell lines and human primary cells were handled under sterile conditions in a laminar airflow according to the current S1- and S2- guidelines of the genetic engineering safety regulations (GenTSV). All cells used during this study were cultivated in their respective media at 37 °C, 5 % CO<sub>2</sub> in a humidified atmosphere in an incubator. For hypoxic conditions cells were cultivated in a separate incubator at 37 °C, 5% CO<sub>2</sub> and 1% O<sub>2</sub>. Adherent cell lines (see table 3.6) were passaged by default twice a week or at 70-100 % confluency. Cell culture media were removed, cells washed once with PBS and detached by adding TrypLE select enzyme detachment reagent (see table 3.5). Detached cells were resuspended in PBS and seeded in fresh culture media in the desired cell density.

Suspension cells were regularly split 1:3 to 1:10. The composition of the culture media used are listed in the following table 4.1. Cells were consequently tested for contaminations with mycoplasma (see table 3.18).

**Table 4.1: Composition of standard media used for mammalian cell culture.**

Component	DMEM	RPMI
DMEM	500 mL	-
RPMI	-	500 mL
FCS	40 mL (8 %)	40 mL (8 %)
Pen Strep	5 mL (1%)	5 mL (1 %)

### 4.1.2 Cryopreservation of cells

For long term storage,  $5 \cdot 10^6$  cells were pelleted by centrifugation and resuspended in 1 mL cold freezing medium (Bambanker Cell Freezing medium, see table 3.5). The cell suspension was transferred into pre-cooled cryotubes and frozen at  $-80^\circ\text{C}$ . For long-term storage, cells were transferred into liquid nitrogen and stored in the vapor phase. For thawing, frozen cells were resuspended smoothly in pre-warmed ( $37^\circ\text{C}$ ) culture medium (see table 4.1) and pelleted by centrifugation. Afterwards, cells were seeded in their respective standard cell culture media and cultured under standard conditions.

### 4.1.3 Cell counting

The cell number of a respective cell line was determined by means of a Neubauer counting chamber. Therefore, the cell suspension was diluted 1:1 with trypan blue cell counting solution (see table 3.5). Cells within the four big squares were counted under the microscope and the cell number was calculated according to the following equation 4.1.

$$\frac{\text{live cells}}{\text{mL}} = \sqrt{\frac{\text{counted cell number}}{4}} \cdot \text{dilution factor} \cdot \frac{10^4}{\text{mL}} \quad (4.1)$$

**Equation 4.1:** Calculation of the cell number.

### 4.1.4 Isolation of peripheral blood mononuclear cells (PBMCs)

PBMCs were isolated by density gradient centrifugation using Pancoll (see table 3.3). The blood was diluted 1:1 with PBS and 12 mL Pancoll were carefully underlayered. After centrifugation at  $1.000 \times g$  for 25 min, the interphase directly above the Pancoll phase containing the PBMCs was carefully isolated with a pipette and washed four times with PBS (10 min,  $300 \times g$ ) to remove remaining Pancoll.

### 4.1.5 Transfection of cells

For transient transfections, a suitable number of cells was seeded into multi-well or 15 cm dishes in standard medium and incubated over night at 37 °C. For transfection Opti-MEM (see table 3.5) and the transfection reagent Pei Max (see table 3.3) were used according to the manufacturer's protocol. Successful transfection was checked either via flow cytometry, or fluorescence microscopy 24 to 72 h post transfection.

For the generation of stable cell lines, cells were transfected as already described followed by selection with appropriate antibiotics [194].

## 4.2 Flow cytometry

$2 \cdot 10^5$  cells per sample in 100  $\mu$ L FC-buffer were stained with a directly labelled primary antibody or with unlabelled antibody for 30 min at room temperature (see tables 3.7 and 3.9), followed by staining with fluorescently labelled secondary antibody (see Table 3.10). Finally, cells were washed twice with FC-buffer and analysed.

### 4.2.1 Epitope blocking assay

Different amounts of purified antibodies (0.5  $\mu$ g - 25  $\mu$ g, table 3.9) were given for an initial incubation step (1 hour) to a single cell suspension ( $2 \cdot 10^5$  cells per sample). Afterwards, cells were washed, incubated with fluorescently labelled OCA2E 5H5 antibody (5H5 Alexa Fluor 647, see table 3.7) and finally analysed by FC.

### 4.2.2 Analysis of antibody $K_D$

To analyse the dissociation constant ( $K_D$ ) of an antibody, a FC based assay was performed. Therefore,  $2 \cdot 10^5$  cells per sample were used and every staining was performed in triplicates. Cells were incubated with a serial dilution of a purified antibody of a given stock concentration for 1 h. Upon washing twice with FC-buffer, a secondary antibody ( $\alpha$ -rat-Alexa Fluor 647, see table 3.10) was added for another 30 min. After washing, cells were analysed by flow

cytometry. From the measured mean fluorescence intensity (MFI) at a defined concentration, the  $K_D$  could be back calculated (equation 4.2).

$$\text{MFI} = \frac{B_{\text{max}} \cdot \text{Antibody molarity}}{K_D + \text{Antibody molarity}} \quad (4.2)$$

**Equation 4.2:** Calculation of the antibody  $K_D$

### 4.3 Laser scanning confocal microscopy (LSCM)

For LSCM cells were seeded one day prior to staining. Therefore, cells were washed with DPBS, counted and a defined cell number seeded on 15 mm cover slips in 12-well plates. All following steps were performed with 1 mL buffer/well at room temperature and all buffers were listed in table 3.4. On the next day, cells were carefully washed with PBS and incubated for 10 min in fixation buffer (4% PFA). Upon fixation, cells were permeabilised with 0.3% Triton X-100 in PBS for 10 min, blocked with 3% BSA for 40 min and stained with first antibody (1 h, room temperature, 400  $\mu$ L/well in staining buffer). Samples were washed four times with staining buffer (5 min shaking in between) and secondary antibody mix also including DAPI was added for one hour in the dark (400  $\mu$ L/well in staining buffer). Samples were washed three times with staining buffer and another three times with PBS. After the last washing step, cover slips were carefully taken out of the 12-well plates and placed upside down on microscope slides with a drop of mounting medium avoiding air bubbles (Vectashield Antifade Mounting medium or ProLonge Diamond Antifade Mountant, 7  $\mu$ L, see table 3.3). Samples were sealed with nail-polish to prevent them from drying out and stored at 4 °C. Imaging of samples was conducted with the Leica DMI8 TCS SP8 confocal microscope.

### 4.4 Microbiological methods - Transformation of bacteria

Transformation was conducted using the heat-shock method [191]. Therefore, 100  $\mu$ L of chemical competent bacteria *e. coli* DH5 $\alpha$  were thawed on ice. Afterwards, bacteria suspension was mixed with up to 1  $\mu$ g plasmid DNA and incubated for 5-10 min on ice. Thereupon, a heat-shock was performed for 2 min at 42 °C and afterwards, bacteria suspension was cooled

down to room temperature and 1 mL of LB-media without antibiotics was added and bacteria grown for 1 h at 37 °C under constant agitation. 20 or 200 µL of the bacteria suspension were distributed on antibiotic containing LB-Agar plates and incubated at 37 °C overnight. Single colonies were picked on the next day and used for further propagation. Therefore, bacteria were cultured over night in LB-media (see table 3.4) at 37 °C with additional antibiotics for selection (ampicillin (100 µg/mL) or kanamycin (50 µg/mL)) under constant agitation at 200 rounds per minute (rpm). For long-term storage, 800 µL bacteria suspension were mixed with 200 µL glycerol and stored at -80 °C.

## 4.5 Molecular biological methods

### 4.5.1 Plasmid DNA purification from *E. coli*

For small scale purification, single bacteria colonies from transformation (see paragraph 4.4) were transferred into 4 mL LB-medium containing antibiotics and grown under constant agitation at 37 °C over night. Afterwards, 1.5 mL were taken and centrifuged at 7000 x g for 2 min. The plasmid DNA was purified using the Monarch Total DNA Miniprep Kit (see table 3.18) according to the manufacturers protocol by alkalic lysis. The success of the plasmid construction was examined by test digestion resulting in pDNA fragments of characteristic size for the respective plasmid, followed by validation via agarose gel electrophoresis (see paragraph 4.5.4.2).

For large scale purification, 400 mL LB-media supplemented with antibiotics were inoculated with bacteria from a single colony (see paragraph 4.4) for over night culture and the DNA was extracted from the received pellet by using the EndoFree Plasmid Maxi Kit (see table 3.18) following the manufacturer's protocol. The final DNA pellet was dissolved in 300 µL TE-buffer and stored at -20 °C. Concentration and purity of the preparation determined by absorbency measurement at 260 and 280 nm using the Nanodrop spectrophotometer (see table 3.1).

### 4.5.2 Isolation of RNA

RNA was isolated from frozen or fresh harvested cells using the Monarch Total RNA Miniprep Kit following the manufacturer's instructions (see table 3.18). Concentration and purity of

the RNA preparation was determined by absorbency measurement at 230 and 260 nm using the Nanodrop spectrophotometer (see table 3.1) and samples were stored short-term at -20 °C or -80 °C for long-term.

#### 4.5.3 5' RACE-PCR to resolve antibody sequences

5' RACE-PCR was performed to amplify immunoglobulin HC and LC sequences using the 5' RACE kit (see table 3.18) according to the manufacturer's instructions. Steps of the 5' RACE-PCR procedure are depicted in the following scheme 4.1 [195].

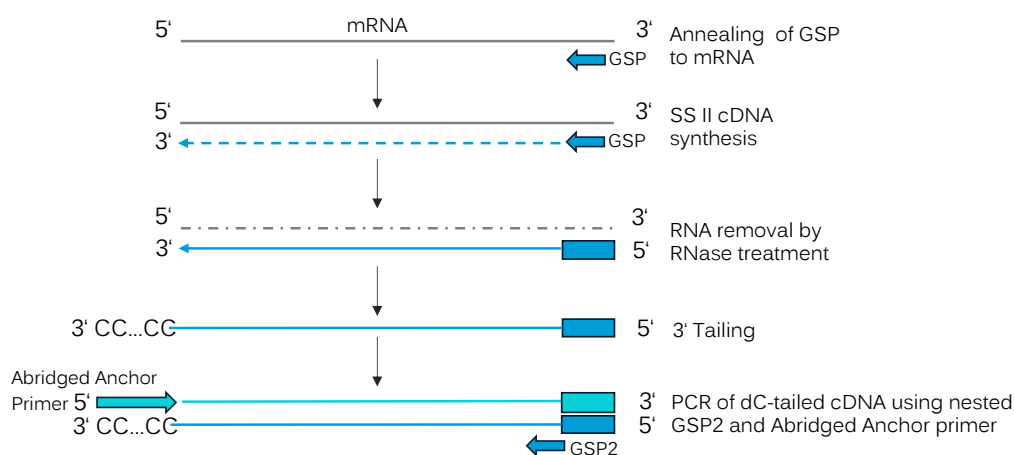


**Figure 4.1: Scheme of 5' RACE-PCR reaction steps.**

RNA was reverse transcribed into cDNA, purified, 3' dC-tail added. Tailed DNA was amplified by PCR using an abridged anchor primer and a gene specific primer (GSP). Adapted from Invitrogen [195].

Isolated RNA (described in paragraph 4.5.2) was used for first strand cDNA synthesis using GSP (see table 3.13) and SuperScript II reverse transcriptase. Afterwards, the original RNA template was removed by RNase H treatment. In a next step, single cDNA was purified using S.N.A.P columns. Upon purification a homopolymeric tail was added to the 3' end of the cDNA-strand using terminal deoxynucleotidyl transferase (TdT) and deoxycytidine triphosphate (dCTP). The dC-tailed DNA was then subsequently used for another PCR-reaction using another GSP and an anchored primer (see table 3.13). The PCR reaction steps are listed in table 4.2.

**Table 4.2: 5' RACE-PCR program steps.**

<b>Program</b>	<b>Cycle</b>	<b>Temperature</b> °C	<b>Time</b> s
initial denaturation	1	94	90
amplification	35	denaturation	94
		annealing	55
		elongation	72
elongation	1	72	360
hold	1	10	∞

The substances used for the PCR reaction mix are listed in table 4.3. The used primers (1642 and 1647) are listed in table 3.13. The success of the PCR was checked by agarose gel electrophoresis (see paragraph 4.5.4.2) and purified samples were sent for sequencing to Eurofins genomics. In case of vague sequencing results for some nucleotide positions, sequencing was repeated using specially designed oligonucleotides (see table 3.14).

**Table 4.3: Substances for 5' RACE-PCR preparation.**

<b>Volume</b> μL	<b>Reagent</b>	<b>Final concentration</b>
5	5' RACE-PCR template	variable
10	5 x GoTaq flexi buffer	1 x
1	dNTP (10 mM)	200 μM
2	gene specific primer (HC or LC) (10 μM)	0.5 μM
2	anchor primer (10 μM)	0.5 μM
3	MgCl <sub>2</sub> (25 mM)	1.5 mM
1	GoTaq Flexi DNA Polymerase (5U/μL)	0.1U/μL
26	Nuclease-free H <sub>2</sub> O	

#### 4.5.4 Cloning of PRDX4 deletion constructs

##### 4.5.4.1 PCR for cloning of PRDX4 constructs

Different plasmid constructs bearing only parts of the PRDX4 gene and different tags (GFP or His) were designed. Therefore the purchased pCMV-PRDX4-C-GFPspark plasmid (see table 3.15) was used as template. Using different primer pair combinations for PCR-reaction (see table 3.11), parts of the PRDX4 gene were excluded or the existent GFP-tag replaced by a His-tag. The different primer pair combinations and the resulting plasmid constructs are listed in table 4.4.

**Table 4.4: Primer pair combinations for the generation of different PRDX4-deletion constructs.**

Plasmid template	Primer fwd	Primer rev	Plasmid product
pCMV-PRDX4 -C-GFPspark	PRDX4-GFP	PRDX4 prom ex1	pCMV-ex1-GFPspark
pCMV-PRDX4 -C-GFPspark	PRDX4 ex2-7	PRDX4 ex2-7	pCMV-ex2-7GFPspark
pCMV-PRDX4 -C-GFPspark	PRDX4-His	PRDX4-ex7	pCMV-PRDX4-His
pCMV-PRDX4-His	PRDX4-His	PRDX4-ex1-His	pCMV-ex1-His
pCMV-PRDX4-His	PRDX4-His	PRDX4-ex7	pCMV-ex2-7-His

The PCR-reactions for either GFP or His-tagged PRDX4-constructs are depicted in table 4.5. Elongation time was set up to around 3 minute/cycle since the Phusion HF polymerase synthesizes around 1 kb in 15-30 seconds to ensure that the complete product is synthesized [196]. The PCR reaction components are listed in table 4.6.

**Table 4.5: PCR program steps for the generation of PRDX4 deletion constructs.**

<b>Program</b>	<b>Cycle</b>	<b>Temperature</b> °C	<b>Time</b> s
<b>Program for GFP-tagged constructs</b>			
initial denaturation	1	98	120
amplification	denaturation	98	10
	annealing	67	30
	elongation	72	210
elongation	1	72	360
hold	1	4	∞
<b>Program for His-tagged constructs</b>			
initial denaturation	1	98	120
amplification	denaturation	98	10
	annealing	50	30
	elongation	72	210
amplification	denaturation	98	10
	annealing	65	30
	elongation	72	210
elongation	1	72	360
hold	1	4	∞

**Table 4.6: PCR reagents for the generation of PRDX4 deletion constructs.**

<b>Volume</b> μL	<b>Reagent</b>	<b>Final concentration</b>
0.5	Plasmid DNA template	5 ng
4	5 x Phusion HF buffer	1 x
2	dNTP (2 mM)	200 μM
1	primer fwd (10 μM)	0.5 μM
1	primer rev (10 μM)	0.5 μM
1	MgCl <sub>2</sub> (25 mM)	25 mM
0.5	DMSO	2.5 %
0.5	Phusion HF DNA Polymerase (2U/μL)	0.1U/μL
9.5	Nuclease-free H <sub>2</sub> O	

### 4.5.4.2 Agarose gel electrophoresis

For gel electrophoresis 500 mg of agarose were dissolved in 50 mL 1 x TAE-buffer (see table 3.4) and heated until the agarose was completely dissolved. After shortly cooling down, 3  $\mu$ L of Serva DNA Stain Clear G (see table 3.3) was added and the agarose poured into a gel cassette and let dry for 20-30 min. All samples were diluted 1:6 with 6 x gel loading dye (see table 3.3), loaded onto the gel and run at 90 V in 1 x TAE-buffer. Afterwards, the DNA-fragments were visualised under UV-light at 254 nm (Quantum ST5 Gel documentation, table 3.1).

To extract DNA from agarose gel, the DNA fragments were made visible under UV light (400-M ultra violet transluminator, table 3.1) and the correct fragments were cut out. The DNA was isolated from the agarose slice by using the Monarch PCR & DNA Clean-up Kit (see table 3.18) following the manufacturer's instructions. The DNA concentration and purity was determined by absorbance measurement as already described in paragraph 4.5.1.

### 4.5.4.3 Ligation

For re-ligation of the prepared DNA parts of the Rapid DNA Dephos & Ligation Kit was used following the manufacturer's protocol (see table 3.18). 200 ng of purified DNA were taken, mixed in 5 x DNA dilution buffer, T4 DNA-ligase (5U) was added and incubated over night at room temperature. The ligation mix was then subsequently used for transformation (see paragraph 4.4).

## 4.5.5 tPRDX4 plasmid construction

### 4.5.5.1 Vector and insert digestion and ligation

The tPRDX4-specific exon 1 was cloned into the PRDX4-GFP plasmid to generate a tPRDX4 expression plasmid. Therefore, the PRDX4-GFP vector as well as the purchased tPRDX4-ex1a plasmid (see table 3.15) were digested with two restriction enzymes KpnI and XcmI (see table 4.7, 120 min at 37 °C). The reaction was stopped by heating 15 min to 65 °C. Samples were checked by agarose gel electrophoresis, purified from the gel (see paragraph 4.5.4.2) and the DNA-concentrations were measured.

**Table 4.7: Restriction digestion of vector and insert for the generation of a tPRDX4-GFP construct.**

Reagent	Vector (4 $\mu$ g DNA)	Insert (4 $\mu$ g DNA)
	$\mu$ L	$\mu$ L
PRDX4-GFP plasmid	1.45	-
tPRDX4-ex1a insert	-	3.33
10 x NEBuffer r2.1	2	2
KpnI (20.000 U/mL)	1	1
XcmI (5.000 U/mL)	1	1
H <sub>2</sub> O	14.5	12.6

Dephosphorylation of the vector DNA and ligation of the vector and insert were performed with the rAPid Dephos and Ligation kit (see table 3.18) following the manufacturer's instructions.

**Table 4.8: Reaction mix for dephosphorylation of vector DNA.**

Reagent	Volume	Final concentration
x $\mu$ L	vector DNA	500 ng
4 $\mu$ L	10 x Phosphatase buffer	1 x
2 $\mu$ L	rAPid Alkaline Phosphatase	1 U
add	sterile H <sub>2</sub> O to 40 $\mu$ L	

For the ligation reaction, a molar ratio of vector-to-insert of 1:3 was used. Therefore, the molarity of the respective DNA fragment was calculated based on the estimated DNA concentration and its size according to the following (equation 4.3) and prepared following the manufacturer's instructions (see paragraph 4.5.4.3 and table 3.18). Additionally, two negative controls were prepared, one control containing only the vector DNA and no ligase to test whether the vector re-ligates by itself, and one control containing the vector DNA and the ligase to check if the ligase religates the vector without the insert. The ligation reactions were incubated for 1 h at room temperature, followed by transformation (see paragraph 4.4).

$$\mu\text{g DNA} \cdot \frac{\text{pmol}}{6.60 \text{ pg}} \cdot \frac{10^6 \text{ pg}}{1 \mu\text{g}} \cdot \frac{1}{\text{Number of nucleotides}} = \text{pmol DNA} \quad (4.3)$$

**Equation 4.3:** Conversion of DNA concentration into molarity for the calculation of ligation reactions.

#### 4.5.6 PCR for tPRDX4 verification in human cell lines

##### RNA isolation

RNA was isolated following the Monarch Total RNA Miniprep Kit instructions as described in paragraph 4.5.2.

##### Reverse transcriptase PCR (RT-PCR)

First strand cDNA was synthesized using the SuperScript III First-Strand Synthesis System (see table 3.18) following the manufacturer's instructions. In brief, 2  $\mu\text{g}$  total RNA were heated 5 min to 65 °C and cooled on ice for at least 1 min. Upon adding cDNA synthesis mix to the RNA, the reaction was incubated for 50 min at 50 °C and then stopped by heating 5 min at 85 °C. Finally, 1  $\mu\text{L}$  RNase H was added and incubated for 20 min at 37 °C to remove remaining RNA. cDNA concentrations were measured and stored at -20 °C for further PCR reactions.

**Table 4.9: RT-PCR components.**

Volume	Component
<b>poly(A) RNA mix</b>	
2 $\mu\text{g}$	RNA
2 $\mu\text{L}$	Primer Oligo (dT) <sub>20</sub> (50 $\mu\text{M}$ )
1 $\mu\text{L}$	dNTP mix (10 mM)
to 10 $\mu\text{L}$	DEPC-treated H <sub>2</sub> O
<b>cDNA Synthesis mix</b>	
2 $\mu\text{L}$	10 x RT buffer
4 $\mu\text{L}$	MgCl <sub>2</sub> (25 mM)
2 $\mu\text{L}$	DTT (0.1 M)
1 $\mu\text{L}$	SuperScript III (200U/ $\mu\text{L}$ )

**PCR for tPRDX4 detection in human cell lines**

Synthesized cDNA was further used for tPRDX4-specific PCR. The components for the PCR-reaction mix are listed in table 4.10 and the program steps are shown in table 4.11. Synthesized PCR-products were checked by agarose gel electrophoresis (see paragraph 4.5.4.2), purified and sent for sequencing to Eurofins genomics.

**Table 4.10: PCR-reagents for the detection of tPRDX4.**

<u>Volume</u> $\mu\text{L}$	<u>Reagent</u>	<u>Final concentration</u>
0.5	DNA template	200 ng
10	5x Phusion HF buffer	1x
1	dNTP (2 mM)	200 $\mu\text{M}$
2.5	primer fwd (10 $\mu\text{M}$ )	0.5 $\mu\text{M}$
2.5	primer rev (10 $\mu\text{M}$ )	0.5 $\mu\text{M}$
1	$\text{MgCl}_2$ (25 mM)	0.5 mM
0.5	Phusion HF DNA Polymerase (2U/ $\mu\text{L}$ )	0.02U/ $\mu\text{L}$
to 50	Nuclease-free $\text{H}_2\text{O}$	

**Table 4.11: PCR program for the amplification of tPRDX4.**

<u>Program</u>	<u>Cycle</u>	<u>Temperature</u> $^{\circ}\text{C}$	<u>Time</u> s
initial denaturation	1	98	30
amplification	denaturation	98	10
	annealing	55	30
	elongation	72	60
elongation	1	72	360
hold	1	10	$\infty$

### 4.6 Protein biochemical methods

#### 4.6.1 Preparation of cell lysates

For the generation of lysates, the cells were pelleted by centrifugation, washed once with DPBS and the supernatant discarded. Afterwards, approximately  $1 \cdot 10^6$  cells were lysed in 50  $\mu$ L RIPA-buffer (see table 3.4) by incubating 30 min on ice. The cell suspension was sonified once (amplitude: 40 %, time: 1 ms) and centrifuged at 4 °C, 16,000 x g for 30 min. Afterwards, the protein concentration was evaluated via Bradford- or bicinchoninic acid (BCA) assay (see paragraph 4.6.2). The lysates were stored at -20 °C until further use.

#### 4.6.2 Determination of protein concentration

Protein concentrations of lysates were measured with either Bradford- or BCA-assays (see table 3.3 and 3.18). All steps were performed according to the manufacturer's protocols and the absorbances were measured using the Clariostar Microplate reader (see table 3.1).

#### 4.6.3 Subcellular fractionation of cell lysates

Around  $5 \cdot 10^7$  cells were washed with PBS and resuspended in 500  $\mu$ L hypotonic buffer (see table 3.4). Upon incubation for 20 min on ice, the cell suspension was homogenized by soaking multiple times through a 26G needle. Trypan blue staining was used to determine the content of still intact cells. When more than 90 % of all cells were disrupted, the suspension was pelleted (1,000 x g, 5 min). This pellet contains the nuclear fraction. The supernatant was taken and centrifuged at 10,000 x g for 10 min, 4 °C. This pellet contains the mitochondrial and organelle fraction. The remaining supernatant was centrifuged at 100,000 x g for 1 h at 4 °C (Sorvall MTX 150, table 3.1). This pellet contains the remaining membrane fraction, and the remaining supernatant contains cytosolic proteins. The pellet was washed once with hypotonic buffer (100,000 x g, 1 h, 4 °C). Cell pellets were resuspended in RIPA-buffer and processed as described in paragraph 4.6.1.

#### **4.6.4 Identification of antigen specificity of antibodies via IP**

IP experiments were conducted to identify the specificity of different antibody clones. Thereby the antibodies from hybridoma supernatants were coupled via subclass specific antibodies to beads whereby the specificity of the IP-reaction is increased. All used buffers are listed in table 3.4.

##### **Activation and coupling of subclass-specific antibodies**

All centrifugation steps were performed at 4 °C and 3,000 rpm, 1 min. 1 g CNBr beads were solved in 10 mL of 1 mM HCl, incubated for 20 min and washed 15 x with 10 mL of 1 mM HCl. Next, the coupling of the anti-subclass specific antibodies to the activated beads was performed. Therefore, 1 mL beads were washed once in cold 1 x coupling buffer. 2 mg of anti-subclass specific antibody were solved in 3 x coupling buffer, filled to 1400 µL with PBS and mixed with the washed and activated beads. Upon incubation for 1 h at room temperature, beads were washed in 5 mL 1 x coupling buffer. To block the remaining active groups, beads were incubated for 2 h in 5 mL 25 M ethanolamine, pH=8 at room temperature. Finally, beads were washed 3 x in wash buffer, 3 x in NaAc buffer, 3 x in wash buffer, 3 x in NaAc buffer, 3 x in PBS and stored at 4 °C.

##### **IP with hybridoma supernatant**

All centrifugation steps were performed at 4 °C, 1,000 x g for 5 min. 250 µL hybridoma supernatant were mixed with 50 µL anti-subclass coupled beads and incubated for 2 h at room temperature or over night at 4 °C on a tumble roller. Upon washing three times with cold PBS, usually 500-1,000 µg cell lysate were added and incubated for 2 h at room temperature or over night at 4 °C. Afterwards, beads were washed once in RIPA-buffer, two times with laurylsarcosine wash buffer and two times in PBS. The last supernatant was removed and the beads resuspended in 2 x Laemmli buffer (30 µL). Samples were incubated for 5 min at room temperature and for 10 min at 70 °C. Samples were spun down and the supernatant carefully transferred to a new reaction tube. Samples were stored at -20 °C for further analysis by western blot or mass spectrometry.

### 4.6.5 Purification of His-tagged protein

Recombinant proteins were purified by their His-tag from HEK293T cells previously transfected (see paragraph 4.1.5). Therefore cells were washed once with PBS, the cell pellet solved in 50 mL urea lysis buffer (see table 3.4) and centrifuged for 30 min at 4,600 rpm. To remove DNA, the solution was filtered through gaze into a fresh falcon and 300  $\mu$ L Ni-NTA agarose beads were added. In this step the Histidine residues (His-tag) bind with high affinity to the vacant positions in coordination sphere of the Ni-ions [197]. The mixture was shaken over night and centrifuged (2,000 rpm, 5 min) on the next day. Upon washing once with urea lysis buffer, the His-bound proteins were eluted from the beads by adding an imidazole containing buffer (elution buffer, see table 3.4). Imidazole binds with higher affinity to the Ni-NTA beads and leads to an elution of the His-tagged proteins. The elution was repeated 3x with 300  $\mu$ L elution buffer. The protein was stored at  $-20^{\circ}\text{C}$ , quantified and analysed by Coomassie staining (see paragraph 4.6.8).

### 4.6.6 Biotinylation of cell surface

NHS-PEG<sub>4</sub>-biotin reagent (see table 3.3) was used for labelling of cell surface proteins. The membrane-impermeable reagent reacts with primary amino groups ( $-\text{NH}_2$ ) by nucleophilic attack, forming an amide bond and releasing the NHS-linker. Proteins have naturally many sites for labelling, i.e. in the side chain of lysine residues. Cells were harvested, washed once with PBS to remove amine-containing media and resuspended in PBS at  $2.5 \cdot 10^7$  cells/mL. 2 mg biotin were resuspended in 170  $\mu$ L H<sub>2</sub>O to prepare the 20 mM stock solution. 100  $\mu$ L of the stock solution were added to 1 mL cell suspension and incubated for 45 min on ice (final concentration = 2 mM). Afterwards, cells were washed three times with biotinylation quenching buffer (see table 3.4) to remove excess biotin reagent. Finally, cell lysates were prepared from the labelled cells as described in paragraph 4.6.1.

### 4.6.7 SDS-PAGE

For protein analysis, polyacrylamide (PAA)-gels were poured. Therefore, the gel cassettes were assembled and first a 12% separating gel was poured and let dry, followed by a 4% separating stacking gel (gel composition, see table 4.12). Otherwise purchased gels were also used (Nupage, see table 3.2). The prepared lysates were supplemented either with reducing or non-reducing Laemmli buffer (see table 3.4) to a final concentration of 1 x Laemmli and heated for 10 min to 70 °C. A defined volume of lysate was then loaded together with a pre-stained marker (see table 3.3) onto the PAA-gels and electrophoresis was performed at 20/40 mA for 1.5-2 h in 1 x MOPS buffer (see table 3.4).

**Table 4.12: Composition of separating and stacking gel.**

Solutions	12 % Separating gel mL	4 % Stacking gel mL
1.5 M TRIS/HCl (pH=8.8)	2	-
0.5 M TRIS/HCl (pH=6.8)	-	1.25
30 % PAA	3.2	0.67
ddH <sub>2</sub> O	2.6	3
10 % APS	0.08	0.05
10 % SDS	0.08	0.05
TEMED	8 µL	5 µL

### 4.6.8 Coomassie staining of PAA-gels

Upon PAA gel electrophoresis, gels were incubated in Coomassie staining solution for 2 h under constant agitation (see table 3.4). Proteins were visualised by adding destaining solution over night at room temperature under constant agitation. Pictures were recorded with the Fusion FX6 Western Blot imaging system (see table 3.1).

### 4.6.9 Immunoblotting

To transfer proteins from the separating gel onto a nitrocellulose membrane, a semi-dry transfer was performed. The nitrocellulose membrane as well as filter papers were incubated shortly in transfer buffer (see table 3.4). Upon gel electrophoresis, the stacking gel was removed and the separating gel was also incubated shortly in transfer buffer. The proteins were transferred onto the membrane by putting the separating gel onto the membrane in between of filter papers and blotting for 35 min at 18 V. For purchased gels, trans-blot turbo sheets were used (see table 3.2) in combination with the trans-blot turbo transfer system (see table 3.1). Afterwards, the membrane was cut into pieces and blocked for 1-1.5 h in blocking solution (see table 3.4) under constant agitation. The membrane was incubated with primary antibody at 4 °C over night (diluted in blocking solution, shaking, see table 3.8 and 3.9). The membrane was washed three times (10 min each step) with TBS-T and incubated with secondary antibody (HRP-conjugated, table 3.10) for 2 h at room temperature under constant agitation. Afterwards, the membrane was again washed with TBS-T (four times, 15 min). For detection of the protein bands, the membrane incubated for with a mixture of ECL solution I and II (1 mL ECL solution I and 3  $\mu$ L ECL solution II, table 3.4). Apart from that also purchased detection reagent ECL select (see table 3.3) was used and the blot developed with the Fusion FX6 Western Blot imaging system (see table 3.1).

### 4.6.10 Dot blot

To perform dot blots, 1  $\mu$ L sample was pipetted onto a nitrocellulose membrane. The membrane was dried, blocked with 5% blocking solution for 1 h under constant agitation and incubated with first antibody, diluted in blocking solution (4 °C, shaking, see table 3.8 and 3.9). After washing with PBS the secondary antibody (see table 3.10) was added for 2 h at room temperature under constant agitation. After washing again several times, the membrane was developed with the Fusion FX6 Western Blot imaging system as described for immunoblotting (see paragraph 4.6.9).

### 4.6.11 ELISA for PRDX4 antibody clone testing

An ELISA was conducted to evaluate the binding site of the different PRDX4 antibody clones. Between all steps, washing four times with 300  $\mu$ L washing buffer per well was performed (see table 3.4).

96-well Maxisorp plates were coated with 50  $\mu$ L/well of the different PRDX4-His protein constructs (1  $\mu$ g/mL, see paragraph 4.6.5) and incubated at 4 °C over night. Afterwards, blocking for 1 h at 37 °C was performed (300  $\mu$ L/well blocking buffer, table 3.4) and antibody samples were added (1  $\mu$ g/mL, 50  $\mu$ L per well, see table 3.9) and incubated 1 h at room temperature. In a last step HRP-coupled secondary antibody  $\alpha$ -rat-HRP (1:5,000 in wash buffer, table 3.10) was added and incubated for another hour at room temperature. Finally, TMB-substrate (see table 3.3) was added (100  $\mu$ L/well, previously mixed 1:1) to develop the ELISA. The reaction was stopped by adding 100  $\mu$ L stop solution (see table 3.4) and OD at 450 nm was measured using the Clariostar Microplate reader (see table 3.1).

## 4.7 Purification and characterisation of EVs

### 4.7.1 Isolation via serial centrifugation

EVs were isolated from ascites or cell culture supernatants by several serial centrifugation steps. To remove cells and cell debris, the supernatant was first centrifuged at 300 x g for 10 min followed by another centrifugation step of 20 min at 2,000 x g. Afterwards, the supernatant was filtered through either a 0.45  $\mu$ m or 0.8  $\mu$ m pore filter.

The EVs were pelleted by ultracentrifugation at 4 °C, 100,000 x g for 2 h using the SW 32 Ti or the SW 28 swinging-bucket rotor (see table 3.1). The supernatant was carefully removed except for 1 mL, which was subsequently supplemented with 100  $\mu$ L of protease inhibitor cocktail (10x cOmplete Protease Inhibitor, see table 3.3). To detach the concentrated EVs from the tubes, those were shaken for at least 1 h on ice. The EVs were washed with PBS by another ultra centrifugation step (4 °C, 100,000 x g, 2 h) and resuspended in 1-2 mL. Finally, the EVs were concentrated by ultracentrifugation using the TL-100.3 fixed angle rotor (see table 3.1) for 1.5 h at 100,000 x g and 4 °C short term or -20 °C. The whole supernatant was discarded except of 50  $\mu$ L, the EVs were pooled in 300  $\mu$ L and stored at 4, °C or -20 °C.

### 4.7.2 Isolation and purification via iodixanol density gradient

Optionally, EVs were further purified via discontinuous bottom-up iodixanol gradients. EVs were mixed with 60 % Optiprep stock solution (see table 3.3) at a ratio of 1:1.36 resulting in a final Optiprep concentration of 44 %. 900  $\mu$ L of premixed EVs were given into a 4 mL centrifugation tube and carefully overlaid with 30 % Optiprep solution up to 3.4 mL. Finally, 600  $\mu$ L PBS were added on top and centrifugation at 160,000 x g at 4 °C in SW60Ti swinging bucket rotor was conducted over night. On the next day eight 500  $\mu$ L fractions were collected from top to bottom. Each fraction was subsequently analysed by dot blot (see paragraph 4.6.10) for vesicle markers like CD63. EV-containing fractions were pooled and the number of EVs was determined by NTA (see paragraph 4.7.3).

### 4.7.3 Quantification via nanoparticle tracking analysis (NTA)

NTA is a technology that allows to measure the number of dissolved nano-particles [198]. By the combination of a scattered light microscope and a video camera, the Brownian motion, which is dependent of the particles size could be evaluated and thereby the particles concentration could be determined. For the calibration, 102 nm polystyrol standard beads (see table 3.3) were utilized. All steps were performed according to the manufactures protocol and for the measurement the parameters listed in table 4.13 were applied.

**Table 4.13: Zetaview settings for the measurement of EV concentration.**

Parameter	Setting
Shutter	65
Sensitivity	75
Minimal/Maximal Particle size	20/500
Minimal Brightness	20
Cycles	3
Positions	11

### 4.7.4 ELISA for detection of EVs in patient samples

To examine whether EVs isolated from ascites samples express PRDX4 on their surface, ELISA experiments were performed. Between all steps, washing four times with 300  $\mu$ L wash buffer per well was performed (see table 3.4).

96-well Maxisorp plates were coated with 5  $\mu$ g/mL, 50  $\mu$ L/well purified antibodies (5H5 PRDX4, 24F9 CD63 (positive control), 7G4 MBP (isotype control), see table 3.9) and incubated at 4 °C over night. After blocking for 2 h at 37 °C with 300  $\mu$ L blocking buffer (see table 3.4) purified EV-samples (see paragraph 4.7.2) diluted 1:10 in 1 % milk in PBS were added and incubated for 2 h at 37 °C. Afterwards detection antibody 12E12-HRP (1:1,000 in PBS, 50  $\mu$ L/well, table 3.7) and incubated for 21 h at 37 °C. Finally, TMB-substrate (see table 3.3) was added (100  $\mu$ L/well, previously mixed 1:1) to develop the ELISA. The reaction was stopped by adding 100  $\mu$ L stop solution (see table 3.4) and OD at 450 nm was measured using the Clariostar Microplate reader (see table 3.1).



## 5 Results

### 5.1 Generation and characterisation of novel monoclonal antibodies

#### 5.1.1 Generation and selection of new mAbs targeting potential novel tumour antigens

Classically, mAbs are being generated by immunising animals with a specific purified protein or peptide. Logically, the outcome are mAbs against a single defined antigen. This conventional type of immunisation is, without doubt, a powerful technology but does not allow for the identification of new tumour specific targets and the generation of cognate mAbs. To identify novel specific targets for the development of new therapeutic and diagnostic applications, our group has developed a new immunisation platform based on EVs derived from permanent cancer cell lines. This led to the identification of a series of new antibodies throughout the last years [199, 200]. Because permanent cell lines are of clonal origin and normally have a long history of growth under artificial cell culture conditions, they do not necessarily represent ‘real’ tumours as they develop in patients and thus are not optimally suited for the identification of new targets on primary cancer cells. To use more authentic material to immunise animals, we used here EVs isolated and purified from ascites of patients as described in paragraph 4.7. Tumour derived EVs are a heterogeneous population shed by tumour cells and have been described to sustain tumour development and progression by regulating important biological functions, such as tumour growth, metastasis, angiogenesis and resistance to therapy [11, 146, 183, 201]. Those tumour derived EVs are thus a rich source of tumour-associated proteins and an attractive tool for the generation of mAbs against hitherto unknown antigens [146, 157]. This way, more than 800 new mAbs have been generated, and a fraction of them has been characterised in more detail. For an initial screening step, all mAbs were analysed by flow cytometry for their binding to a mixture of four different ovarian cancer cell lines. This resulted in the identification of 236 binding ABs, which were still way too many to be characterised in detail.

## 5 RESULTS

To further reduce their number, we decided to compare their binding to cell lines kept under normoxic and hypoxic conditions. We concentrated on those ABs that recognised antigens that were expressed at higher levels under hypoxia, because hypoxia is known as a relevant trigger of an aggressive tumour phenotype, resistance to treatment and an overall poor clinical prognosis [39, 202].

To analyse the antigen specificity of the remaining AB clones, IP experiments were conducted. For this, ABs were coupled to beads, incubated with whole cell lysates and the eluates were sent for mass spectrometric analysis (to the core facility PROT of the HMGU). All described steps for AB generation and characterisation are depicted in Figure 5.1.

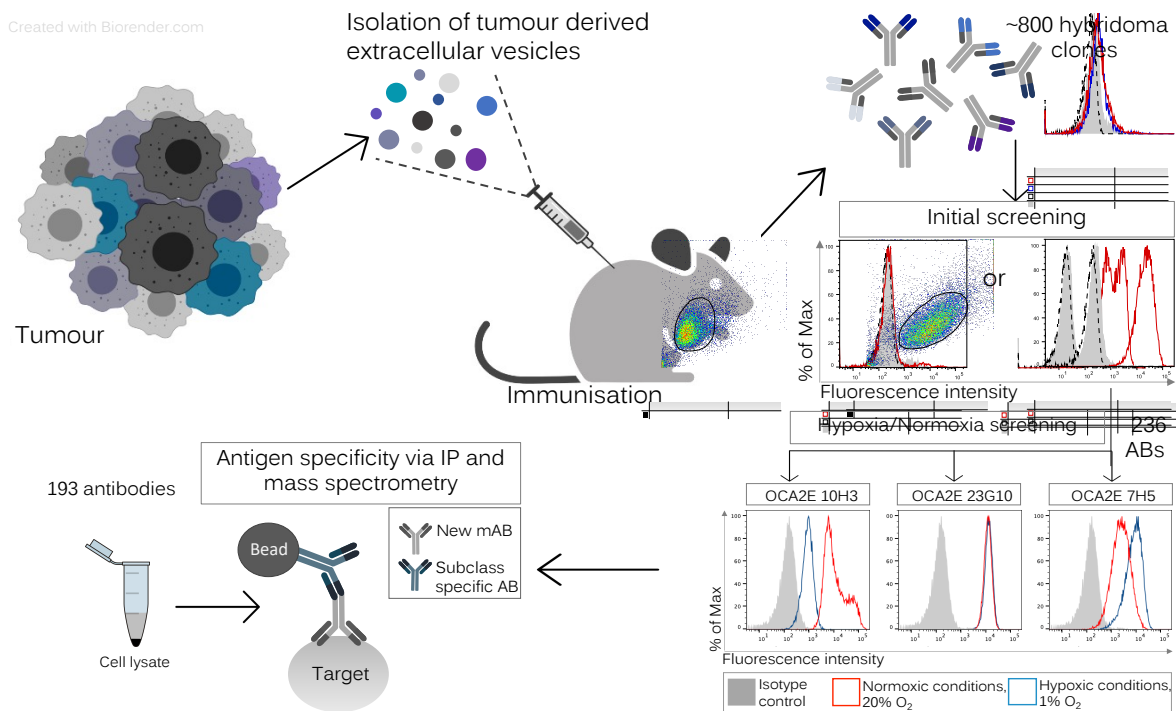


**Figure 5.1: Strategy for the generation and characterisation of new mAbs.**

EVs isolated from human ascites samples via differential centrifugation (see paragraph 4.7.1) were used to immunise animals. FC screening on four different tumour cell lines was performed as a first step towards the obtained antibodies. Antibody clones tested positive on at least one tumour cell line were re-analysed for antigen expression levels on cell lines kept under hypoxic or normoxic conditions. The specificities of antibodies recognizing hypoxia-induced target proteins were determined in IP experiments followed by mass spectrometric analysis. The Figure was created using BioRender [107].

## 5.1 GENERATION AND CHARACTERISATION OF NOVEL MONOCLONAL ANTIBODIES

The results from the screening described above are summarised in Figure 5.2. Among the remaining 236 mAbs, the majority, around 60%, were of a rat IgG2a subclass and around 25% of a rat IgG2b subclass. The remaining 15% were either rat IgG2c or IgG1 antibodies or a mixture of two or even three subclasses due to oligoclonality (depicted in the left pie chart of Figure 5.2). Around 80% of them were further analysed in IP experiments and sent for mass spectrometric analysis to identify their specificities. Antibodies that stained negative in FC analysis were not further analysed, also a number of clones became unstable (pie chart in the middle). The right pie chart illustrates the mass spectrometry results, highlighting the top results obtained upon IP experiments.

### 5.1.2 Identification of antibody specificity by mass spectrometry

Almost 12% of the antibodies that gave a clear mass spectrometry (MS) result and precipitated peroxiredoxin 4 (PRDX4). This came to a surprise, because PRDX4 has so far been described to be localised in the ER, the cytosol or the extracellular space, but not on the cell surface [113, 115, 120, 121]. This surprising finding promoted further analysis of the PRDX4 specific antibodies.

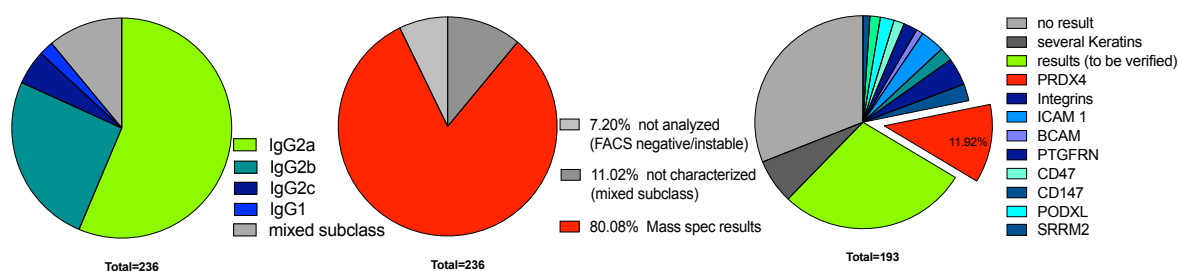


**Figure 5.2: PRDX4 is the most prominent target after immunisation with EVs from malignant ascites.**

Results from antibody characterisation by mass spectrometry. The left pie chart shows the different isotype subclasses of the analysed antibody clones. Around 80% of all antibodies were sent for mass spectrometry analysis (pie chart in the middle) and the results thereof are depicted in the right chart.

### 5.1.3 Discovery of PRDX4 as a new potential tumour antigen

To confirm the specificities obtained from mass spectrometry, the potential PRDX4 antibodies were again coupled to beads and incubated with whole cell lysates as described in paragraph 4.6.4. The precipitated proteins were eluted from the beads, separated by PAGE and transferred to a nitrocellulose membrane, which then was incubated with a commercial PRDX4 antibody. Except of three clones (Figure 5.3 A: 19E4, 14H9, 15B1) all mAbs investigated were confirmed as PRDX4 specific (see table 5.1).

PRDX4 is around 27 kDa in size and thus almost the same size as an IgG light chain. To unambiguously exclude that the signals obtained were derived from precipitated PRDX4 rather than from co-precipitated IgG light chains, HEK293T cells were transfected with an expression plasmid encoding a PRDX4-GFP fusion protein, and lysates were subsequently used for IP experiments followed by immunoblotting. These blots were incubated either with a PRDX4 (PA3-753, 1:5,000 table 3.8) or with a GFP antibody (clone 3H9-HRP, 1:2,000, table 3.7).

An additional specific signal at around 60 kDa, corresponding to the calculated size of the PRDX4-GFP fusion protein, was visible in the lysates from transfected HEK293T cells, but not in non-transfected cells (Figure 5.3 B). All supposed PRDX4 AB clones also precipitated the PRDX4-GFP, thus confirming their specificity.

## 5.1 GENERATION AND CHARACTERISATION OF NOVEL MONOCLONAL ANTIBODIES

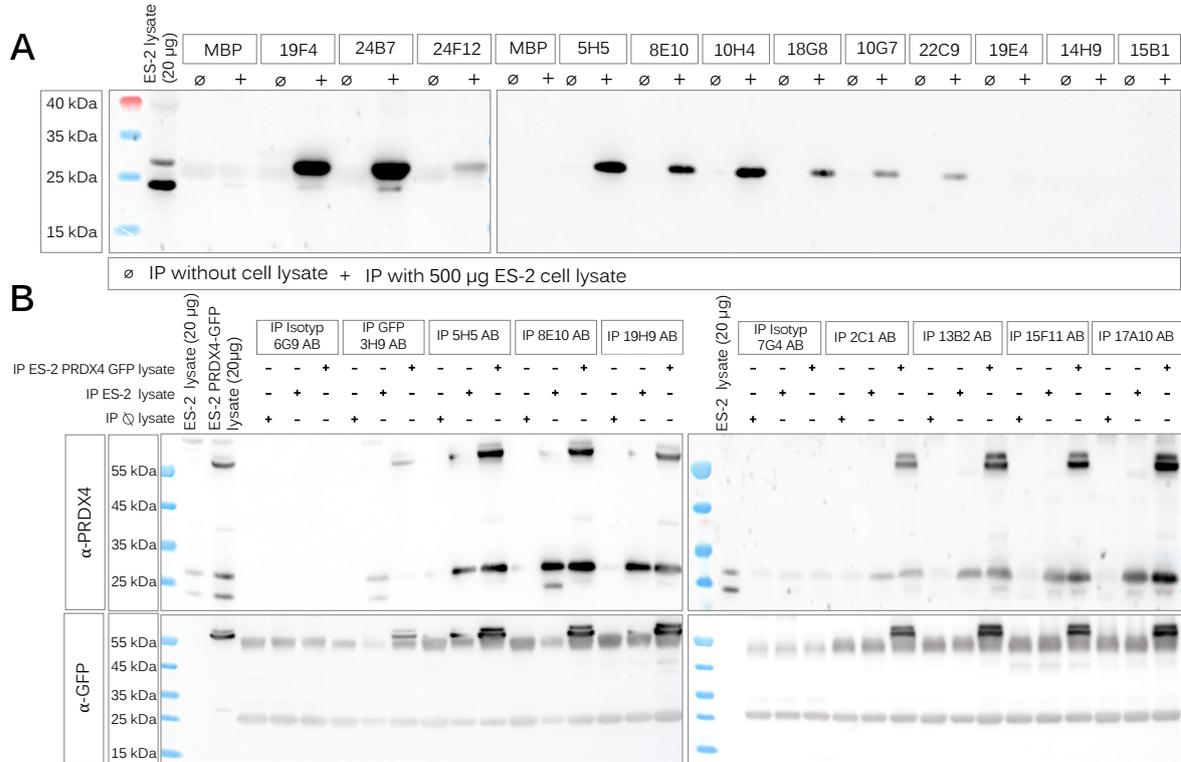


**Figure 5.3: Confirmation of PRDX4 antibody specificity by IP experiments.**

**A:** PRDX4 AB clones or an isotype control (MBP antibody) were coupled to beads and incubated with ES-2 whole cell lysate followed by immunoblot analysis. The blots were incubated with a commercial PRDX4 antibody (PA3-753, 1:5,000, table 3.8).

**B:** PRDX4 antibody clones were coupled to beads and incubated with cell lysates from ES-2 cells or from ES-2 cells transiently transfected with an expression plasmid encoding for PRDX4-GFP (see paragraph 4.1.5). Immunoblots were incubated with a PRDX4 antibody (see **A**) or a GFP antibody (3H9-HRP, 1:1,000, table 3.7).

To further confirm the specificity of the PRDX4 ABs, IP experiments were performed using a PRDX4-KO cell line to exclude a potential cross reactivity with PRDX1, which is highly homologous to PRDX4. Therefore, PRDX4 specific antibody clone 5H5 or an isotype control (MBP AB 7G4) was coupled to beads and incubated with either HEK293T, HEK293T PRDX4 KO cell lysate (750 µg) or purified PRDX4-His protein (1 µg).

## 5 RESULTS

The subsequent immunoblots were incubated with PRDX4 (ab184167, 1:10,000, table 3.8) or PRDX1 antibodies (ab109598, 1:10,000, table 3.8). IPs with wtHEK293T lysate or recombinant PRDX4 protein confirmed the binding of the 5H5 antibody. In contrast, lysate from PRDX4 KO cells did not show a signal with the commercial antibody. Thus, antibody 5H5 does not cross-react with PRDX1.

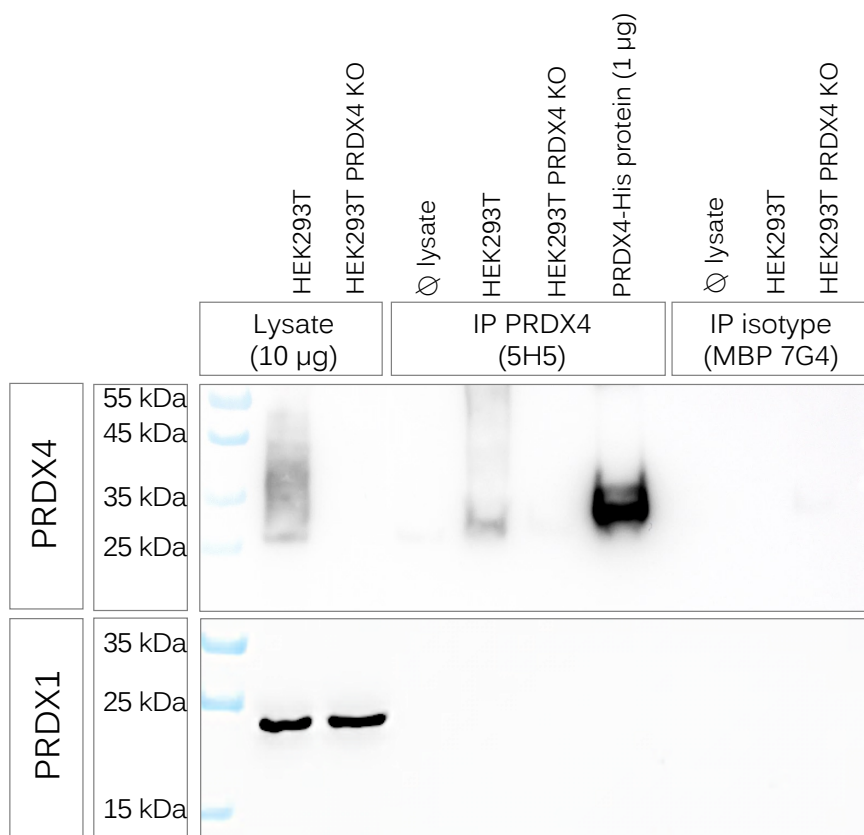


**Figure 5.4: IP experiments with HEK293T PRDX4-KO cell line also confirm PRDX4 antibody specificity.**

5H5 antibody or isotype control (MBP 7G4) were coupled to beads and incubated with HEK293T, HEK293T PRDX4-KO whole cell lysate or purified PRDX4-His protein (see paragraph 4.6.5) followed by immunoblot analysis. The blots were incubated either with PRDX4 antibody (ab184167, 1:10,000, table 3.8) or PRDX1 antibody (ab109598, 1:10,000, table 3.8).

## 5.1 GENERATION AND CHARACTERISATION OF NOVEL MONOCLONAL ANTIBODIES

All confirmed PRDX4 AB clones listed in table 5.1 were analysed by FC. ES-2 cells were stained with the hybridoma supernatant of the respective antibody clone (see table 3.9) and with  $\alpha$ -rat-IgG (H + L) Alexa Fluor 647 antibody (see table 3.10) as described elsewhere (see paragraph 4.2). All potential PRDX4 antibody clones showed similar signal intensities (see Figure 5.5).

**Table 5.1: Overview of all potential PRDX4 antibody clones.**

All potential PRDX4 antibody clones received from immunisation are listed with their respective subclass. The corresponding antibody sequences of the most prominent clones are listed in table 5.2.

PRDX4 AB clone name	Isotype	Specificity confirmed	Antibody sequence
2C1		✓	✓
2F9		✓	
5H5		✓	✓
8E10		✓	
10G7		✓	✓
10H4		✓	✓
13B2		✓	✓
14H9			
15B1	Rat IgG2a		
15F11		✓	✓
17A10		✓	✓
18G8		✓	✓
19E4			
19F4		✓	
19H9		✓	✓
22C9		✓	
24B7		✓	✓
24F12		✓	
11F2	Rat IgG2b	✓	✓

## 5 RESULTS

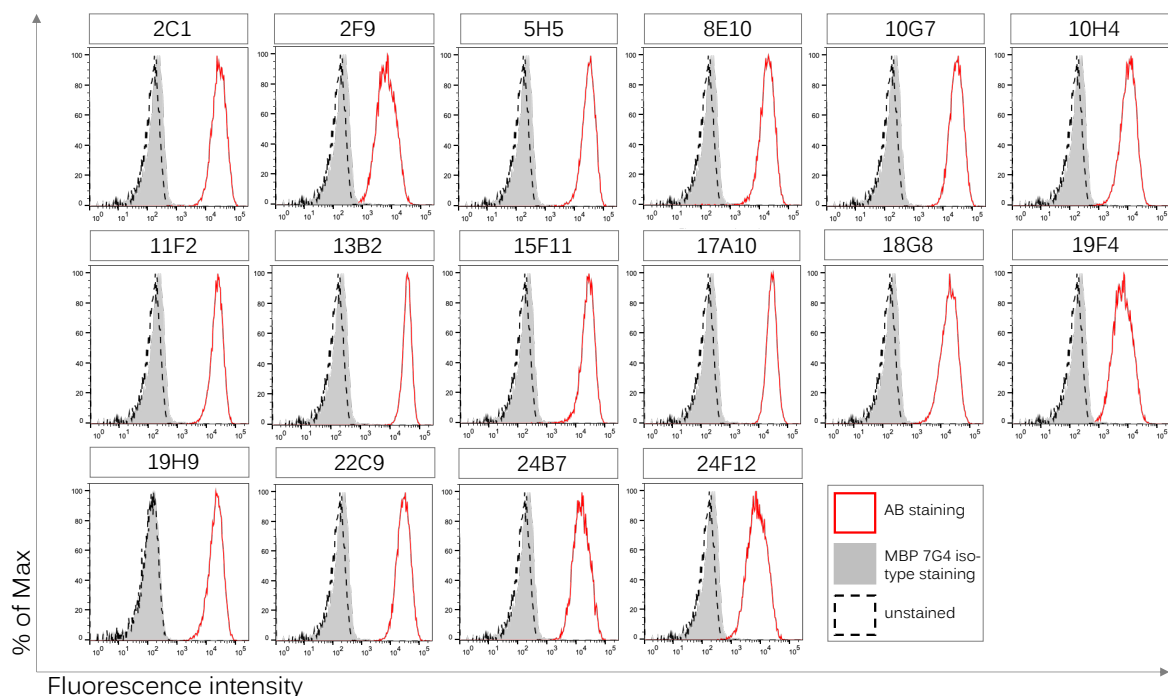


**Figure 5.5: All PRDX4 AB clones show similar surface staining on ES-2 cells in FC analysis.**

The different PRDX4 mAb clones were analysed by FC (see paragraph 4.2) in combination with an  $\alpha$ -rat-IgG (H + L) Alexa Fluor 647 antibody (see table 3.10).

In order to substantiate surface PRDX4 expression on tumour cells even further, A549 cells were labelled with membrane-impermeable biotin as described in paragraph 4.6.6. Then, cell lysates were prepared and used for IP experiments (see paragraph 4.6.4) with PRDX4 antibody 5H5, the CD73 specific antibody 20A8 as a positive control, or with the MBP-specific antibody 7G4 as an isotype control (all listed in table 3.9). Eluates were separated by PAGE, transferred to a nitrocellulose membrane, and immunoblots were incubated with antibodies specific for PRDX4 (PA3-753, 1:5,000, table 3.8) or biotin (1:200,000, table 3.7). Both blots showed a distinct signal at 27 kDa, corresponding to the size of PRDX4. Taken together, PRDX4 was biotinylated and thus present on the cell surface.

## 5.2 PRDX4 IS EXPRESSED ON THE SURFACE OF VARIOUS TUMOUR CELL LINES

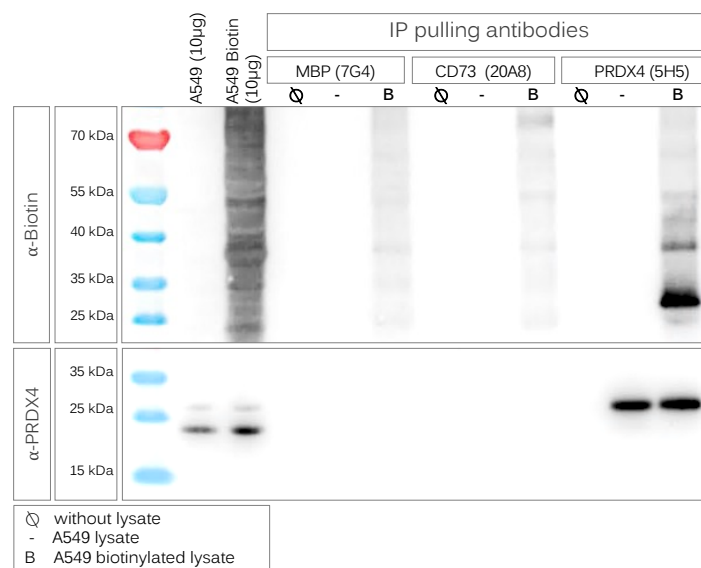


**Figure 5.6: Immunoblots of IP experiments performed with surface labelled cell lysates reveal PRDX4 surface expression.**

Antibodies for MBP (7G4, isotype control), CD73 (20A8, positive control) and PRDX4 (5H5) were coupled to beads and subsequently incubated with lysates prepared from A549 cells previously labelled with biotin as described in paragraph 4.6.6. The eluate was separated by PAGE, transferred to a nitrocellulose membrane and the immunoblots were incubated with antibodies for PRDX4 (PA3-753, 1:5,000 table 3.8) or biotin (1:200,000, table 3.7). CD73 is approximately 75 kDa in size.

## 5.2 PRDX4 is expressed on the surface of various tumour cell lines

PRDX4 is ubiquitously expressed and described as localised in the ER or secreted into the extracellular milieu. Its main function - lessening oxidative stress by reducing  $H_2O_2$  to water - has well been analysed [114, 203]. In contrast, surface expression on cells has not been described so far. Therefore, FC analysis was performed, which revealed enormous differences in PRDX4 surface expression levels. While surface PRDX4 was clearly detectable on many tumour cell lines derived from different tumour entities, some tumour cell lines showed no or only a weak surface expression. The measured MFI values of the cell lines are depicted in Figure 5.7 B. Exemplary histograms for two breast cancer cell lines, MDA MB-231 and T-47D, are depicted in Figure 5.7 C. An overview of all tested cell lines is given in Figure 5.7 D. To investigate, whether surface localisation correlates with the total PRDX4 expression amount, various cell lines were first evaluated by immunoblotting. All tested cell lines showed more or

5 RESULTS

less similar PRDX4 expression levels (see Figure 5.7 A). Therefore, the underlying mechanism that drives relocation of PRDX4 to the cell surface remained non understood and is subject to ongoing investigations in our group. Histograms of all cell lines analysed by FC are depicted in the appendix (see Figure 8.2).

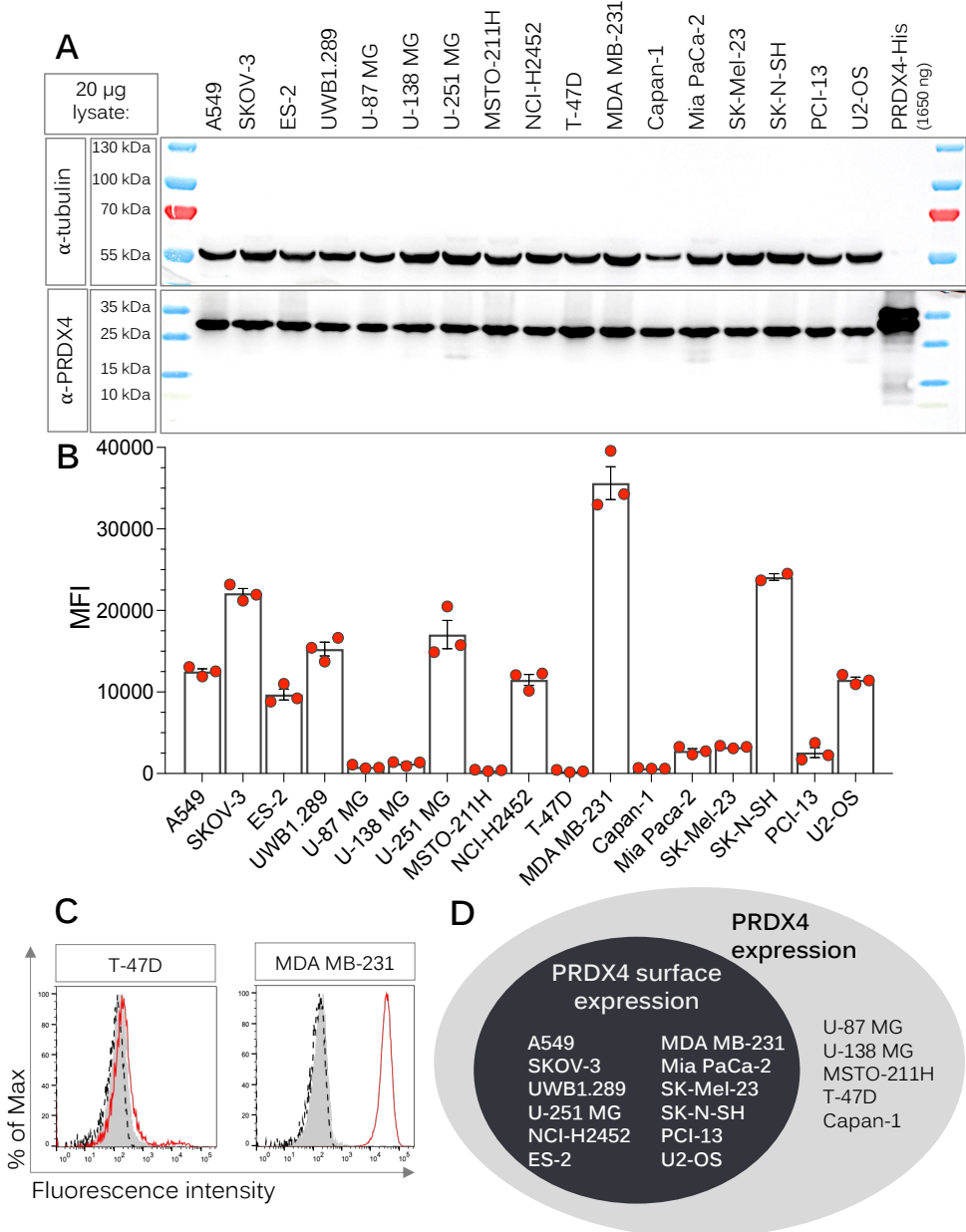


Figure 5.7: Total PRDX4 levels are comparable among cell lines, but cell surface localization differs significantly.

## 5.2 PRDX4 IS EXPRESSED ON THE SURFACE OF VARIOUS TUMOUR CELL LINES

---

**Figure 5.7: Total PRDX4 levels are comparable among cell lines, but cell surface localisation differs significantly.**

**A:** Immunoblots with different cell lysates were incubated either with antibodies for PRDX4 (ab184167, 1:20,000, table 3.8) or tubulin (GTX628802, 1:10,000, table 3.7).

**B, C & D:** FC analysis revealed heterogenous surface expression of PRDX4 among different tumour cell lines. Cells were stained with hybridoma supernatant (OCA2E 5H5, table 3.9) followed by an incubation step with  $\alpha$ -rat-IgG (H + L) Alexa Fluor 647 antibody (see table 3.10). MFI-values depicted in Figure **B** were calculated from three independent experiments and are shown as median + standard error of the mean (SEM). Histograms for a surface positive and negative staining are shown in **C** and the results are summarised in chart **D**.

The different surface expression levels of PRDX4 among different tumour cell lines were also evident in LSCM experiments, for which tumour cell lines were seeded and processed as described in paragraph 4.3. Cells were then stained for integrin  $\alpha$ 3 (CD49c, EXO 8F2 Alexa Fluor 488, table 3.7, green), to identify the cell membrane, DAPI (1:5,000, shown in cyan) to stain cell nuclei, and PRDX4 (OCA2E 5H5 Alexa Fluor 647, table 3.7, shown in purple). In line with the previous FC results, the cell lines tested positive for surface PRDX4 in FC analysis (A549, UWB1.289, MDA MB-231 and U-251 MG) also revealed surface staining in LSCM, while FC-negative cell lines (MSTO-211H and Capan-1) showed only intracellular PRDX4 staining (see Figure 5.8).

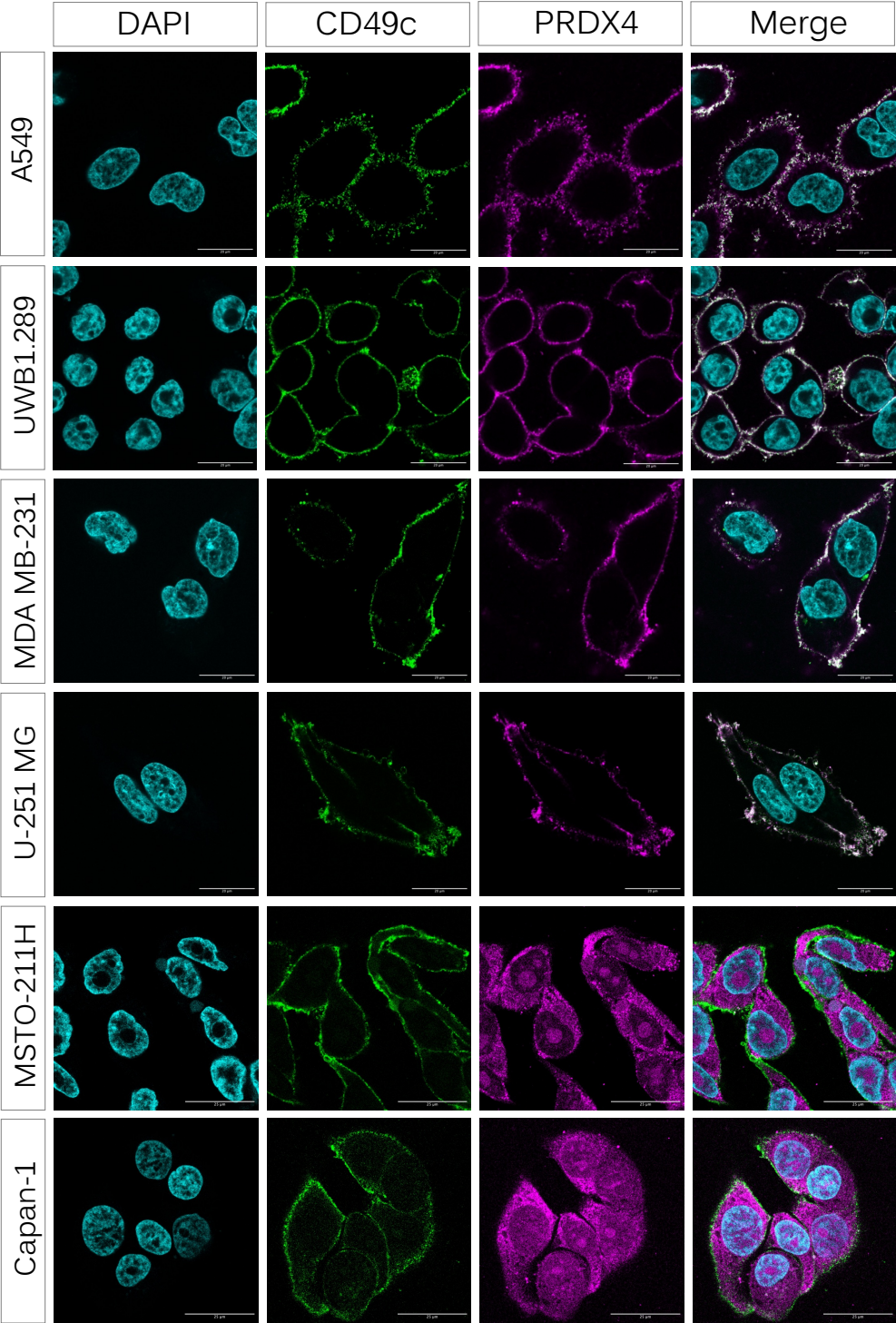


**Figure 5.8: Heterogenous surface PRDX4 expression among different tumour cell lines as observed in LSCM.**

Cells were fixed, permeabilized and stained for PRDX4 (OCA2E 5H5-Alexa Fluor 647, table 3.7), for CD49c (EXO 8F2 Alexa Fluor 488, table 3.7). Nuclei were stained with DAPI (1:5,000) as described in paragraph 4.3.

## 5.2 PRDX4 IS EXPRESSED ON THE SURFACE OF VARIOUS TUMOUR CELL LINES

To get an insight into the intracellular localisation of PRDX4, a separation of cellular components was performed by differential centrifugation as described in paragraph 4.6.3. This resulted in membrane fraction 1 (MF1) containing the nuclei, MF2 with organelles, MF3 containing the plasma membrane and intracellular membranes, and a supernatant with cytosolic proteins. For this experiment different cell lines, which had previously been tested either positive or negative for surface PRDX4 (see Figure 5.7 and 5.8), were used. Immunoblot analysis was performed with 20 µg lysate of each fraction and the blots were stained for PRDX4 (ab184167, 1:50,000, table 3.8) or for Na<sup>+</sup>/K<sup>+</sup>ATPase (ab76020, 1:20,000, table 3.8), an enzyme expressed on the plasma membrane [204–206]. Interestingly, fraction MF3, which is enriched for plasma membrane proteins, revealed stronger PRDX4 signals for those cell lines stated surface-PRDX4 positive by FC (i.e. U-251 MG, MDA MB-231 and NCI-H2452) as compared to the surface-PRDX4 negative cell lines (i.e. U-87 MG, T-47D and MSTO-211H). The summarised data are shown in Figure 5.9 A, C and E.

A normalisation of the PRDX4 signals from the immunoblots against Na<sup>+</sup>/K<sup>+</sup>ATPase corroborated higher amounts of PRDX4 in the plasma membrane-enriched fractions MF3 of the surface-PRDX4 positive cell lines (Figure 5.9 B, D and F).

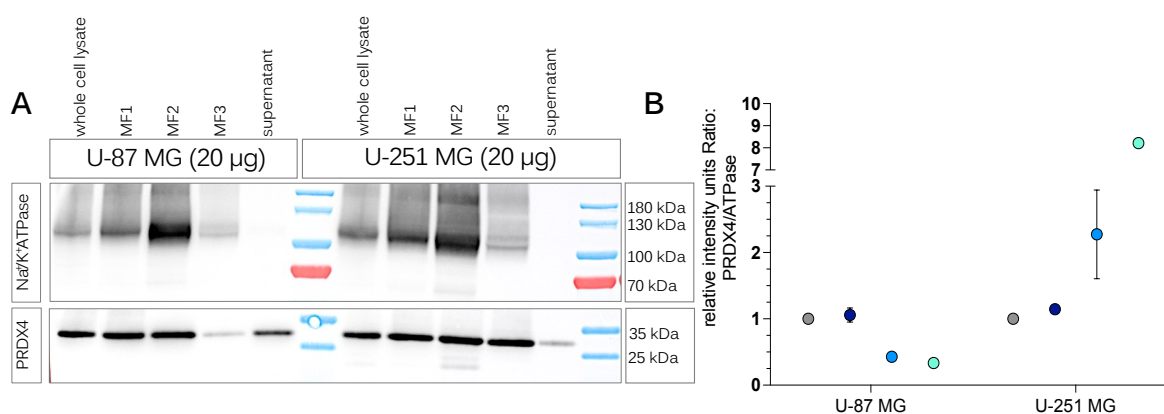


**Figure 5.9: Subcellular fractionation revealed PRDX4 enrichment in the plasma membrane fraction of surface PRDX4 positive cell lines.**

## 5 RESULTS

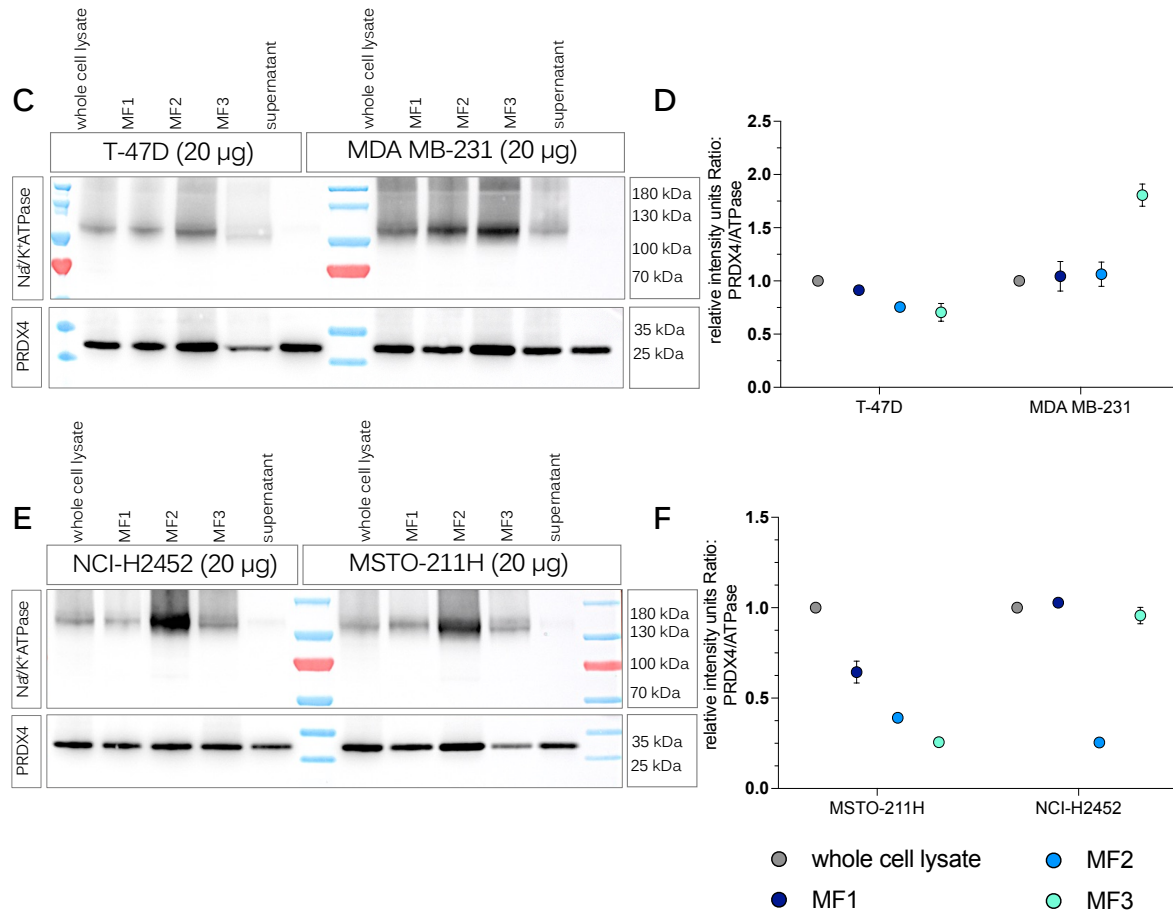


**Figure 5.9: Subcellular fractionation revealed PRDX4 enrichment in the plasma membrane fraction of surface PRDX4 positive cell lines.**

**A, C, E:** Immunoblot results of subcellular fractionations of different tumour cell lines (see paragraph 4.6.3). MF1 show lysates from enriched nuclei, MF2 from mitochondrial and organelle-derived proteins, MF3 is enriched for plasma membrane proteins and the supernatant mainly harbours residual cytosolic proteins. Each blot shows a pair of tumour cell lines from the same tumour entity, which have either high or low PRDX4 surface expression levels in FC analysis (see Figure 5.7). Blots were incubated with antibodies for PRDX4 (ab184167, 1:50,000, table 3.8) or with an antibody for Na<sup>+</sup>/K<sup>+</sup>ATPase (ab76020, 1:50,000, table 3.8).

**B, D, F:** Quantification of the immunoblot results. Relative intensity units were measured using Bio-ID software and a ratio between PRDX4 and Na<sup>+</sup>/K<sup>+</sup>ATPase was calculated.

## 5.2 PRDX4 IS EXPRESSED ON THE SURFACE OF VARIOUS TUMOUR CELL LINES

Because it could not be excluded that cell culture conditions induced surface-PRDX4 on permanent cell lines, primary cells isolated from malignant ascites samples were also tested by FC analysis using the OCA2E 5H5 antibody. All ascites-derived tumour cells, clearly stained surface-PRDX4 positive (see Figure 5.10), while no surface-PRDX4 was detectable on PBMCs, primary hepatocytes (purchased from HTCR, see section 3.12) and follicular dendritic cells (FDCs), isolated from adenoids. Thus, translocation of PRDX4 to the cell surface is obviously a phenomenon that takes place in many cancer cells, but not in normal cells.

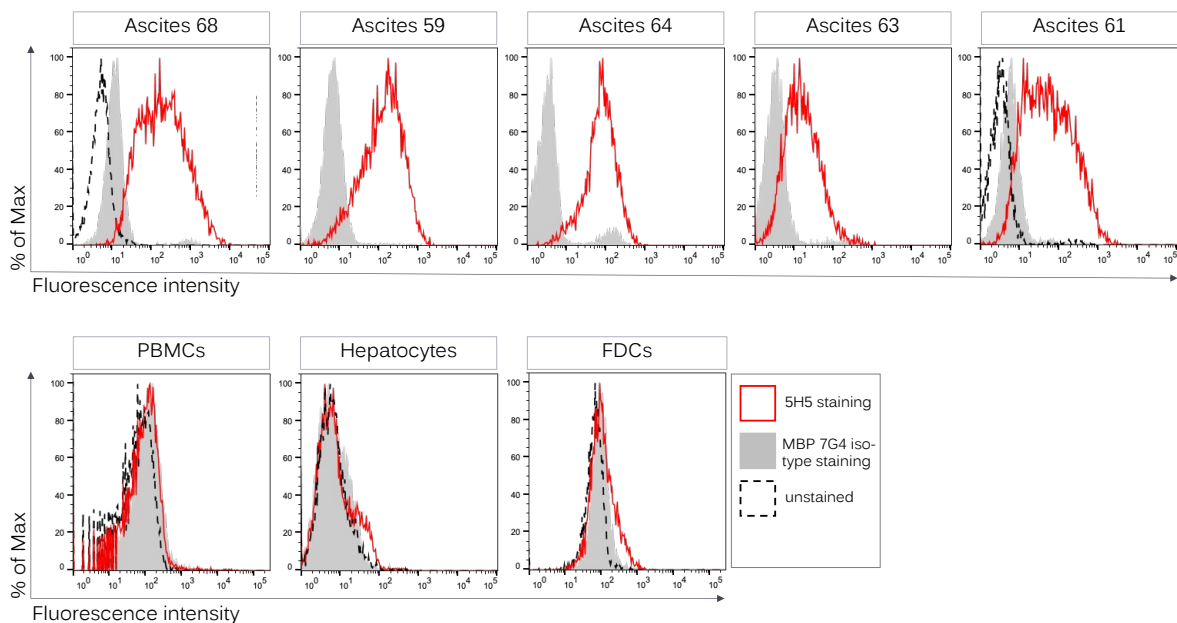


**Figure 5.10: PRDX4 is present on the surface of primary tumour cells isolated from ascites samples.**

FC analysis of cells isolated from primary samples. Cells were stained for PRDX4 (OCA2E 5H5, table 3.9 and  $\alpha$ -rat IgG Alexa Fluor 647, table 3.10) as described in paragraph 4.2.

Taken together, we could convincingly demonstrate for the first time, that PRDX4 is exposed on the surface of many human cancer cell lines and on primary cancer cells, while normal cells reveal no surface PRDX4 expression.

### 5.3 PRDX4 is expressed on EVs

EVs constitute a mixture of different types of vesicles, including exosomes that are released from MVBs, and microvesicles that bud from the plasma membrane [146]. The fact that we obtained PRDX4 specific antibodies from our immunisation is a proof that the protein was present on EVs from this particular patient. To investigate the presence of PRDX4 in tumour derived EVs, we tested a total of 15 EV preparations from malignant ascites samples by immunoblots. 10  $\mu$ L of each EV-preparation (see paragraph 4.7) were separated by PAGE, transferred onto a nitrocellulose membrane and incubated with antibodies either for CD63, a tetraspanin and universal biomarker for EVs (EXO-M 12E12-HRP, 1:2,000, table 3.7), or for PRDX4 (ab1484167, 1:20,000, table 3.8). Not surprisingly, CD63 levels varied among the different samples tested, but PRDX4 was clearly detected in 14 out of 15 EV preparations with only ascites 63 showing no signal (see Figure 5.11).

Results from immunoblots were further validated by ELISA experiments (see paragraph 4.7.4). Plates were coated with purified antibodies against PRDX4 (OCA2E 5H5), CD63 (EXOM 24F9) or MBP (7G4) (5  $\mu$ g/mL, table 3.9), blocked with 5% milk in PBS and subsequently incubated with the same EV preparations as above. After washing and incubation with a HRP-coupled CD63 antibody (EXO-M 12E12-HRP, 1:2,000, table 3.7) TMB-substrate was added and the optical density (OD) at 450 nm was measured (see Figure 5.11 B). Except for a single sample (ascites 59), all preparations showed signals for CD63 and PRDX4. As above, levels for CD63 and PRDX4 varied considerable among the different samples, however there was a clear correlation between the immunoblot and ELISA results. In summary, one can conclude that PRDX4 is present in primary tumour derived EVs from almost all patients with ovarian cancer.

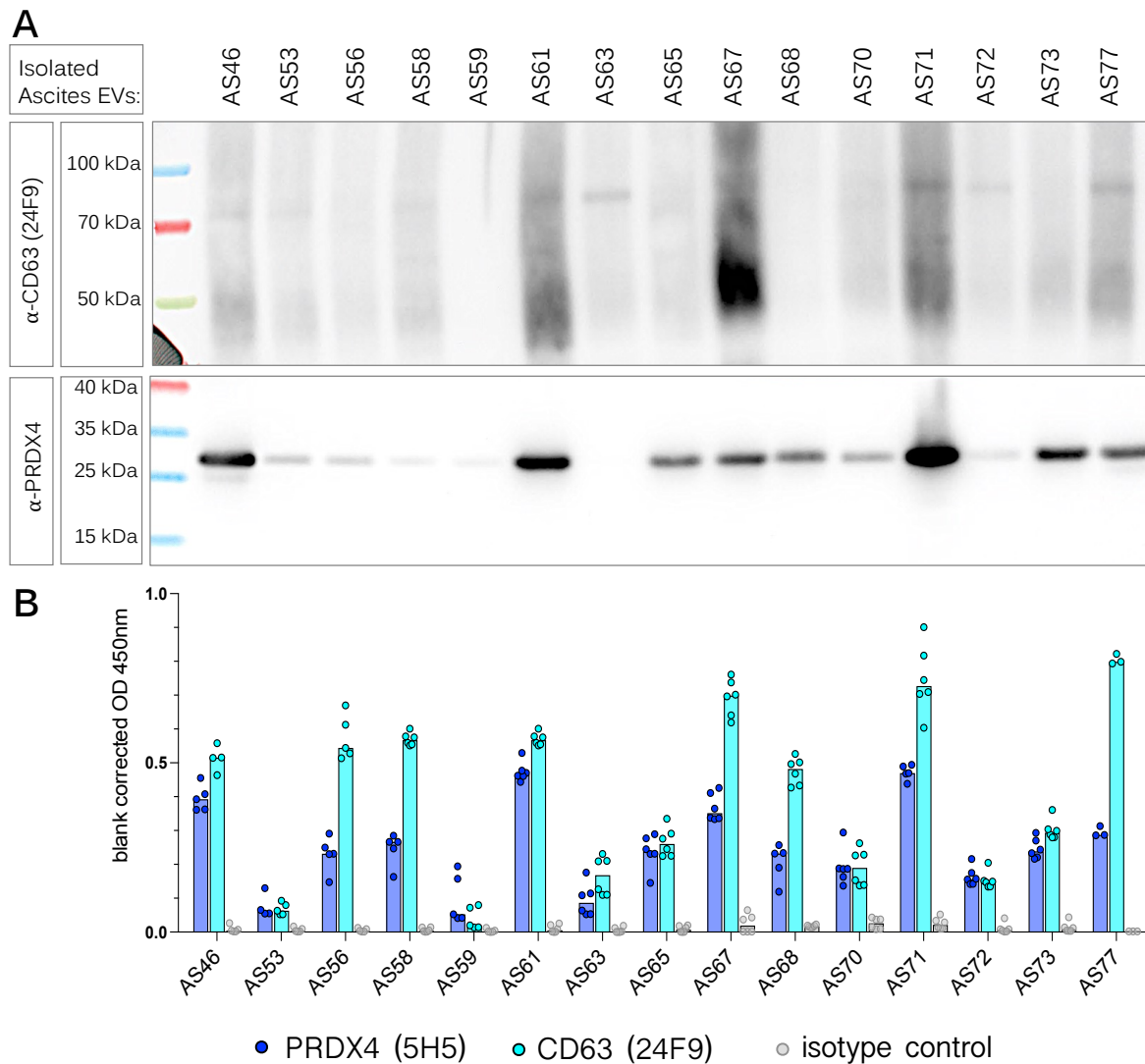


**Figure 5.11: PRDX4 is present on EVs isolated from ascites samples.**

**A:** EVs isolated from malignant ascites (AS) were analysed by immunoblots for CD63 (EXOM 12E12-HRP, 1:2,000, table 3.7) and PRDX4 (ab1484167, 1:20,000, table 3.8).

**B:** ELISA experiments evaluating the presence of PRDX4 in EVs from ascites samples. Plates were coated with 5 µg/mL purified antibodies against PRDX4 (OCA2E 5H5), CD63 (EXOM 24F9) or MBP (7G4), incubated with EVs followed by incubation step with a CD63-HRP antibody (EXO-M 12E12-HRP, 1:2,000, table 3.7, see paragraph 4.7.4). ODs were measured at 450 nm. All experiments were performed in triplicates (n=5).

## 5.4 PRDX4 antibodies are present in primary tumour samples

Immune responses against cancer [207] and the concomitant production of antibodies against tumour-associated antigens have been described [208, 209]. As PRDX4 is ectopically expressed on tumour cells and released via tumour derived EVs, the presence of PRDX4-specific autoantibodies was investigated. Such autoantibodies are promising potential diagnostic and/or prognostic biomarkers and may even be useful to monitor responses to treatment [208, 210]. For the first experiment, ascites samples derived from patients with ovarian cancer were tested for the presence of PRDX4 autoantibodies.

Therefore, purified PRDX4-His protein (750 ng, see paragraph 4.6.5) and a control protein (750 ng, trans-aldolase, a protein mainly located in the cytoplasm, kindly provided by Dr. Josef Mautner) were separated by PAGE, transferred onto nitrocellulose membranes and incubated with primary ascites samples, an  $\alpha$ -His antibody (3D5-HRP 1:2,000, table 3.7) or a PRDX4-specific antibody (PA3-753, 1:5,000, table 3.8 and  $\alpha$ -rat IgG (H+L)-HRP, 1:10,000, table 3.10). A suitable secondary antibody ( $\alpha$ -human IgG (H + L)-HRP, 1:2,000, table 3.10) was used for detection. As shown in Figure 5.12, PRDX4-specific autoantibodies were detected in all ascites samples tested, while no signal for trans-aldolase (around 40 kDa) was detected. Next, we repeated this experiment with sera derived from cancer patients and healthy donors, but were unable to detect such antibodies (not shown).

Taken together, PRDX4 autoantibodies are present in patients with ovarian cancer. Whereas they could be clearly detected in ascites, their concentration in peripheral blood is probably too low to be identified with the technologies used. This project is currently pursued by another member of our group.

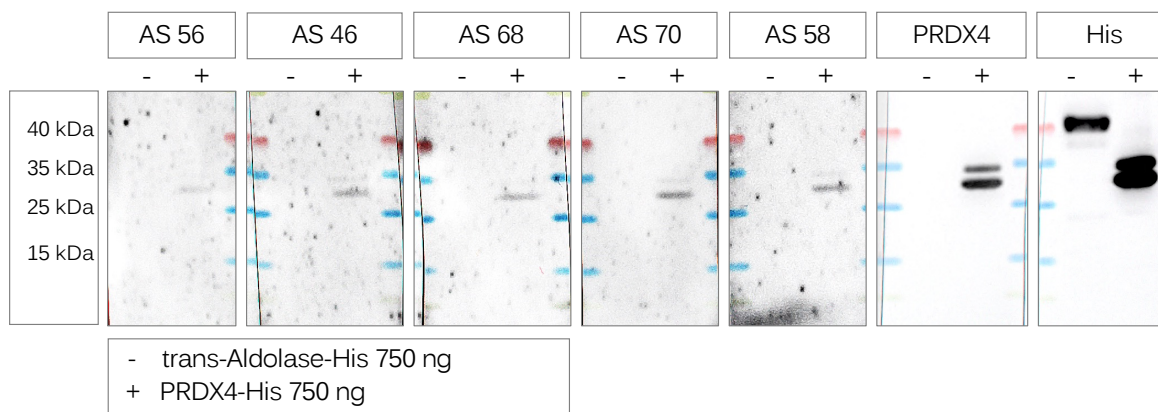


**Figure 5.12: PRDX4-specific antibodies are present in malignant ascites samples.**

Immunoblot analysis using ascites from patients with ovarian cancer as primary antibodies. 750 ng recombinant PRDX4-His protein or aldolase-His (negative control) were separated by PAGE (see paragraph 4.6.9). Blots were incubated in ascites samples (diluted 1:10 in blocking buffer) followed by incubation with an  $\alpha$ -human-HRP antibody (table 3.10).

## 5.5 CCDC47 is a novel interaction partner of PRDX4

As PRDX4 turned out as extremely interesting new target for cancer therapy, while the reason for the relocation of the protein remained unclear, we took a closer look onto the initial MS data to possibly unravel potential so far unidentified new interaction partners of PRDX4. These MS data (depicted in paragraph 5.1.2) revealed regular co-precipitation of known interaction partners like thioredoxin domain-containing protein 5 (TXNDC5) and protein disulfide isomerase 6 (PDIA6) but also a protein called coiled-coil domain containing 47 (CCDC47), also known as Calumin. Like PRDX4, CCDC47 is normally located in the ER, where it most probably functions as a chaperone and is involved in the regulation of  $\text{Ca}^{2+}$  homeostasis in the ER [211, 212].

To prove whether CCDC47 is a novel interaction partner of PRDX4, the 5H5 antibody was coupled to beads, incubated with lysates from different cell lines (750  $\mu\text{g}$  each) and the precipitates were analysed on immunoblots stained for either PRDX4 or CCDC47 (ab184167, 1:50,000 and HPA029674, 1:2,000, table 3.8). CCDC47 clearly co-precipitated with PRDX4 from all cell lysates tested, confirming the physical interaction of the two proteins.

## 5 RESULTS

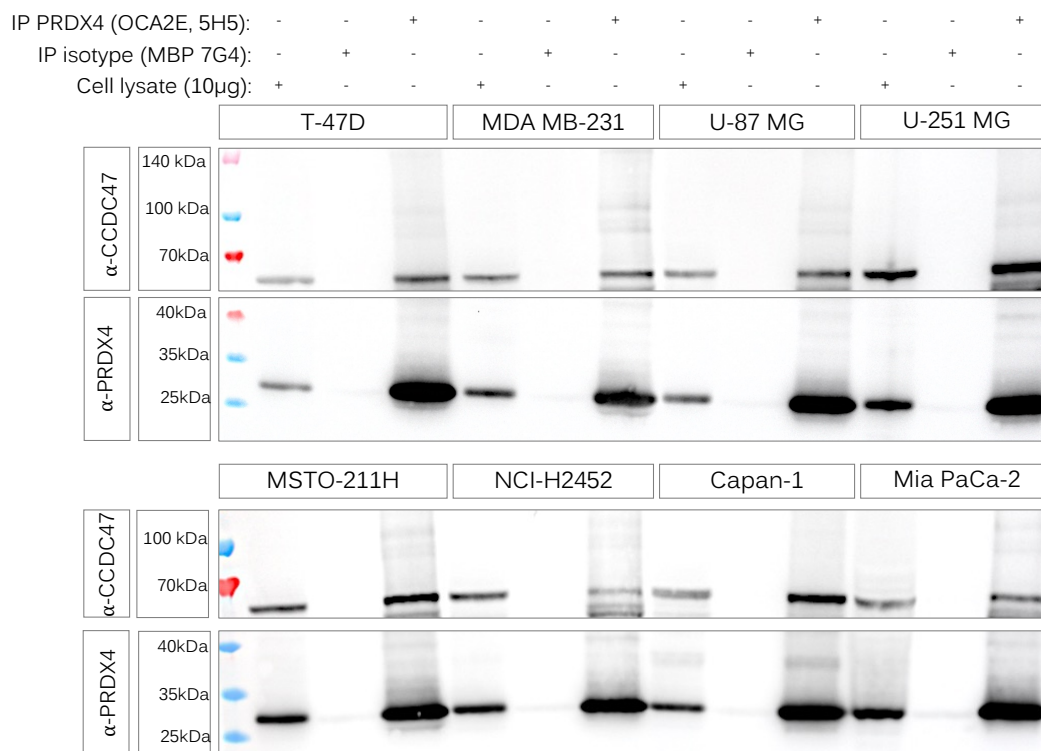


**Figure 5.13: IP experiments revealing interaction between CCDC47 and PRDX4.**

PRDX4 5H5 antibody or the isotype control MBP 7G4 antibody, were coupled to beads and incubated with different tumour cell lysates. The precipitates were analysed by immunoblots incubated with antibodies either for PRDX4 or for CCDC47.

Furthermore, different cell lines were analysed by LSCM for co-localisation of PRDX4 and CCDC47 (see Figure 5.14). For this, cells were processed as described in paragraph 4.3 and then stained for PRDX4 (5H5 Alexa Fluor 647, shown in purple), CCDC47 (HPA029674, and  $\alpha$ -rabbit IgG (H + L) Alexa Fluor Plus 555, shown in orange), CD49c for membrane staining (EXO 8F2 Alexa Fluor 488, shown in green) and DAPI for a staining of the nuclei (1:5,000, shown in cyan). All cell lines showed intracellular staining for CCDC47, while PRDX4 localisation is cell line dependent. MDA MB-231, NCI-H2452 and Mia PaCa 2 cell lines showed mainly a surface staining, while T-47D, MSTO-211H and Capan-1 cells showed an intracellular localisation of PRDX4, confirming the FC and LSCM data described above (see Figure 5.7 and 5.8). Taken together, IP experiments revealed physical interaction of CCDC47 and PRDX4. It remains unclear whether the protein is involved in the translocation of PRDX4 to the cell surface.

## 5.5 CCDC47 IS A NOVEL INTERACTION PARTNER OF PRDX4

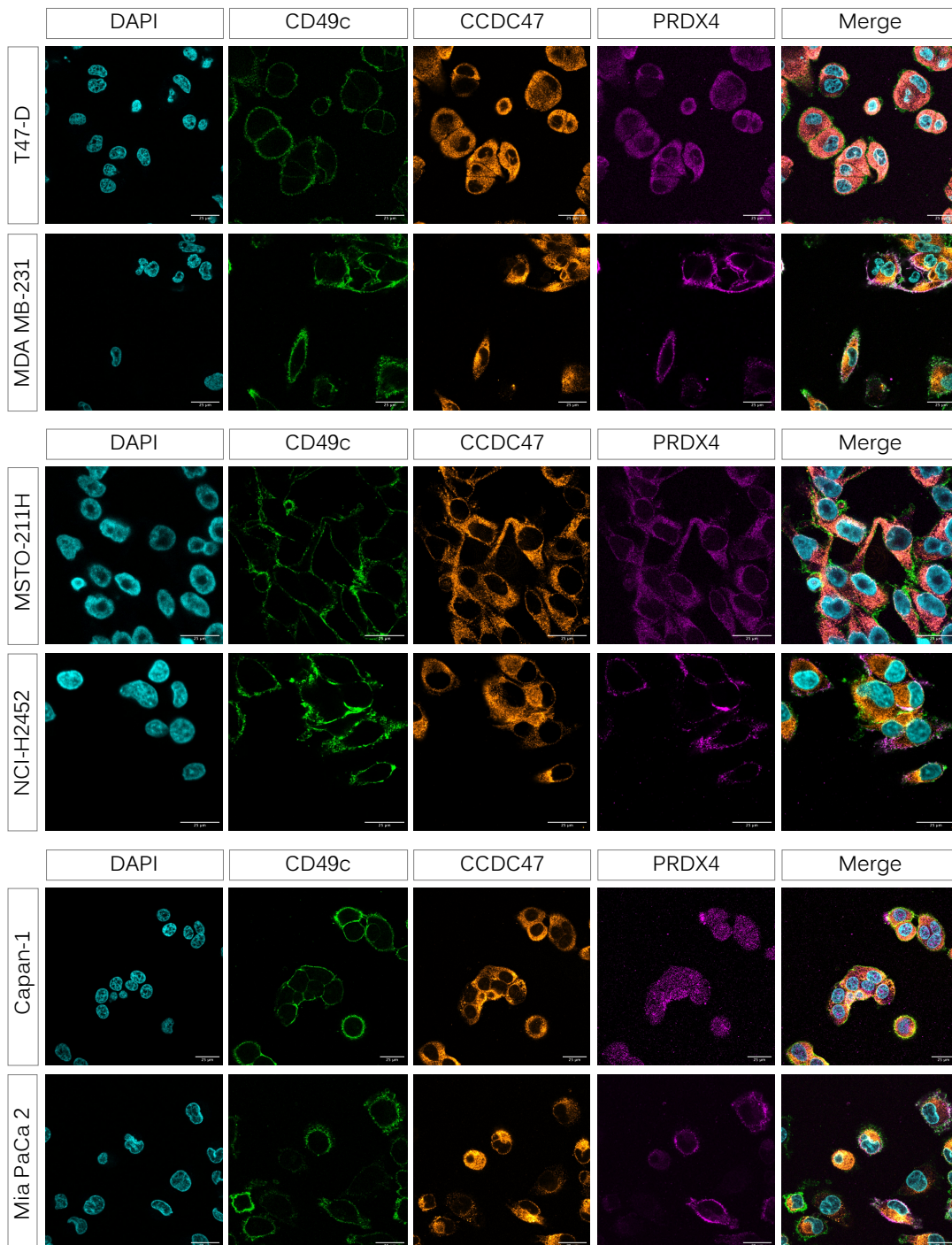


**Figure 5.14: LSCM images show intracellular CCDC47 staining and heterogeneous PRDX4 expression in different tumour cell lines.**

Cells were fixed, permeabilized and stained for PRDX4 (5H5 Alexa Fluor 647, table 3.7), CCDC47 (HPA029674, table 3.8 and  $\alpha$ -rabbit IgG (H + L) Alexa Fluor Plus 555, table 3.10), CD49c (EXO 8F2 Alexa Fluor 488, table 3.7) and DAPI (1:5,000, see paragraph 4.3).

## 5.6 Characterisation of PRDX4 antibodies

### 5.6.1 Analysis of the PRDX4 antibody sequences by 5' RACE-PCR

In the next set of experiments, the sequences of the PRDX4 antibodies were identified. This is a prerequisite for the generation of recombinant antibodies and derivatives. In order to obtain their sequences a 5' RACE-PCR on total RNA isolated from hybridoma cells was performed as described in paragraph 4.5.3. The successful amplification was checked by agarose gel electrophoresis, as exemplarily shown in Figure 5.15 for the 13B2 AB clone. PCR products were purified and sent for sequencing.

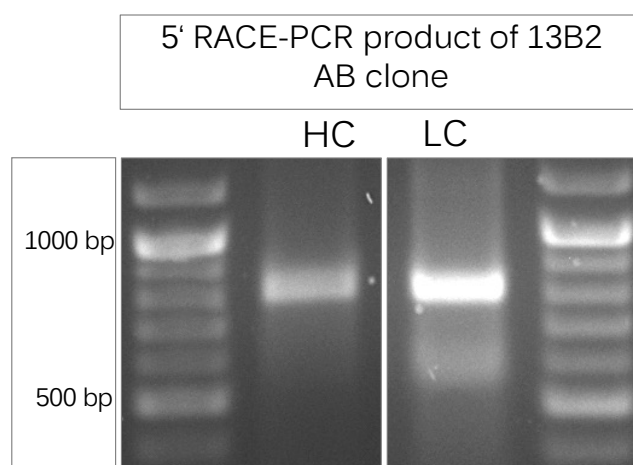


**Figure 5.15: Product of a successful 5' RACE-PCR of a PRDX4 antibody clone.**

Agarose gel image of generated 5' RACE-PCR product showing the expected DNA product at around 700 bp for the antibody light and heavy chain.

The heavy and light chain sequences of all eleven PRDX4 mAbs analysed are listed in table 5.2. All light and heavy chain sequences show high similarities with only single amino acids divergence from the sequence of AB 5H5, which was considered as the prototypic sequence (depicted in blue). CDRs were annotated following the Kabat definition using the abYsis online tool [193]. For all analysed mAbs the highly variable CDR-H3 is identical. Which amino acid (AA) provide specific antigen binding and which are involved in shaping the conformation of the CDR-loops needs further evaluation.

**Table 5.2: Identified protein sequences of PRDX4 antibody clones.**

Immunoglobulin light and heavy chain sequences of eleven PRDX4-specific antibodies. CDRs are marked in red and amino acids that differ from the '5H5 consensus sequence' are marked in blue.

AB clone	Protein Sequence
<b>Heavy chain</b>	
2C1	QVQLQQSGAELV <b>K</b> PGTSVKLSCKASGYTFT <b>SNHM</b> NWIK <b>Q</b> TTGQGLEWIG <b>I</b> <b>INSGNGG</b> <b>TKYNVKFKG</b> KATLTVDKSS <b>S</b> TAFMQLSSLTPEDSAVYYCARG <b>NPASFDY</b> WGQGVMTVSS
5H5	QVQLQQSGAELV <b>R</b> PGTSVKLSCKASGYTFT <b>SNHM</b> HWIK <b>E</b> TTGQGLEWIG <b>I</b> <b>INPGNGGSRFNVKFKG</b> KATLTVDKS <b>S</b> TA <b>F</b> MQLSSLTPEDSAVYYCARG <b>NPASFDY</b> WGQGVMTVSS
10G7	QVQLQQSGAELV <b>K</b> PGTSVKLSCKASGYTFT <b>SNHM</b> NWIK <b>Q</b> TTGQGLEWIG <b>I</b> <b>INPVNGG</b> <b>TRYNVKFKG</b> KATLTVDKSS <b>S</b> TAFMQLSSLTPEDSAVYYCARG <b>NPASFDY</b> WGQGVMTVSS
10H4	QVQLQQSG <b>V</b> ELVRPGTX <b>V</b> RLSCKASGYTFT <b>SNHM</b> HWIK <b>E</b> TTGQGLEWIG <b>I</b> <b>INPGNGGSRFNVKFKG</b> KATLTVDKS <b>S</b> TA <b>F</b> MQL <b>N</b> SLTPEDSAVYYCARG <b>NPASFDY</b> WGQGVMTVSS
11F2	QVQLQQSGAELV <b>K</b> PGTSVKLSCKASGYTFT <b>STH</b> HM <b>N</b> WIK <b>E</b> TTGQGLEWIG <b>I</b> <b>INPGNGG</b> <b>TKYNVKFKG</b> KATLTVD <b>S</b> SS <b>S</b> TAFMQL <b>G</b> SLTPEDSAVYYCARG <b>NPASFDY</b> WGQGVMTVSS
13B2	QVQLQQSGAELV <b>R</b> PGTSVKLSCKASGYTFT <b>SNHM</b> NWIK <b>E</b> TTGQGLEWIG <b>I</b> <b>INPGNGGSRFNVKFKG</b> KATLTVDKS <b>S</b> TA <b>F</b> MQLSSLTPEDSAVYYCARG <b>NPASFDY</b> WGQGVMTVSS
15F11	QVQLQQSGAELV <b>R</b> PGTSVKLSCKASGYTFT <b>SNHM</b> HWIK <b>E</b> TTGQGLEWIG <b>I</b> <b>INPGNGGSRFNVKFKG</b> KATLTVDKS <b>S</b> TA <b>F</b> MQLSSLTPEDSAVYYCARG <b>NPASFDY</b> WGQGVMTVSS
17A10	QVQLQQSGAELV <b>R</b> PGTSVKLSCKASGYTFT <b>SNHM</b> HWIK <b>E</b> TTGQGLEWIG <b>I</b> <b>INPGNGGSRFNVKFKG</b> KATLTVDKS <b>Y</b> TA <b>F</b> MQLSSLTPEDSAVYYCARG <b>NPASFDY</b> W <b>R</b> GVMTVSS
18G8	QVQLQQSGAELV <b>E</b> PGTSV <b>R</b> LSCKASGYTFT <b>NH</b> I <b>N</b> WIK <b>Q</b> AT <b>G</b> ALEWIG <b>I</b> <b>INSGNGG</b> <b>TKYDVKFKG</b> KATLTVDKSS <b>N</b> TAFMQLSSLTPEDSAVYYCARG <b>NPASFDY</b> WGQ <b>V</b> LTVTSS
19H9	QVQLQQSG <b>V</b> ELVRPGTSV <b>R</b> LSCKASGYTFT <b>SNHM</b> HWIK <b>E</b> TTGQGLEWIG <b>I</b> <b>INPGNGGSRFNVKFKG</b> KATLTVDKS <b>S</b> TA <b>F</b> MQL <b>N</b> SLTPEDSAVYYCARG <b>NPASFDY</b> WGQGVMTVSS
24B7	QVQLQQSGAELV <b>R</b> PGTSVKLSCKASGYTFT <b>SNHM</b> HWIK <b>E</b> TTGQGLEWIG <b>I</b> <b>INPGNGGSRFNVKFKG</b> KATLTVDKS <b>S</b> TA <b>F</b> MQLSSLTPEDSAVYYCARG <b>NPASFDY</b> W <b>R</b> GVMTVSS
<b>Light chain</b>	
2C1	DIQMTQSPSFLSASV <b>G</b> DRVTIN <b>C</b> AS <b>Q</b> N <b>I</b> NKYLNWY <b>Q</b> H <b>K</b> LGEAPKRLI <b>Y</b> <b>NTDNL</b> Q <b>T</b> GIPSRFSGSGSGTD <b>Y</b> LTIS <b>G</b> LQPEDFATYF <b>CLQHSNFP</b> PFTFGSGTKLEI <b>ARAD</b>
5H5	DIQMTQSPSFLSASV <b>G</b> DRVTIN <b>C</b> RA <b>S</b> E <b>N</b> I <b>Y</b> KYLNWY <b>Q</b> Q <b>K</b> FGEAPKRLI <b>Y</b> <b>NTNTLET</b> GIPSRFSGSGSGTD <b>F</b> LTIS <b>S</b> LQPEDFATYF <b>CLQHSNFP</b> PFTFGSGTKLEI <b>KRA</b>
10G7	DIQMTQSPSFLSASV <b>G</b> DRVTIN <b>C</b> AS <b>Q</b> <b>N</b> I <b>H</b> KYLNWY <b>Q</b> H <b>K</b> LGEAPKRLI <b>Y</b> <b>NTNNLQ</b> <b>T</b> D <b>I</b> PS <b>N</b> FSGSGSGTD <b>Y</b> LTIS <b>S</b> LQPEDFATYF <b>CLQHS</b> <b>S</b> <b>F</b> P <b>P</b> FTFGSGTKLEI <b>KRA</b>
10H4	DIQMTQSPSFLSASV <b>G</b> DRVTIN <b>Y</b> RA <b>S</b> E <b>N</b> I <b>Y</b> N <b>Y</b> LNWY <b>Q</b> Q <b>K</b> FGE <b>G</b> PKRLI <b>Y</b> <b>NTNTLET</b> GIPSRFSGSGSGTD <b>F</b> LTIN <b>S</b> LQPEDFATYF <b>CLQHSNFP</b> PFTFGSGTKLEI <b>KRA</b>
11F2	DIQMTQSPSFLSASV <b>G</b> DRVTIN <b>C</b> AS <b>Q</b> <b>N</b> I <b>Y</b> KYLNWY <b>Q</b> Q <b>K</b> LGEAPKRLI <b>Y</b> <b>NTNNLET</b> D <b>I</b> PS <b>R</b> FSGSGSGTD <b>Y</b> <b>T</b> F <b>I</b> SS <b>L</b> QPEDFATYF <b>CLQHSNFP</b> PFTFGSGTKLEI <b>KRA</b>
13B2	DIQMTQSPSFLSASV <b>G</b> DRVTIN <b>C</b> RA <b>S</b> E <b>N</b> I <b>Y</b> KYLNWY <b>Q</b> Q <b>K</b> LGEAPKRLI <b>Y</b> <b>NTNTLET</b> GIPSRFSGSGSGTD <b>F</b> LTIS <b>S</b> LQPEDFATYF <b>CLQHSNFP</b> PFTFGSGTKLEI <b>KRA</b>
15F11	DIQMTQSPSFLSASV <b>G</b> DRVT <b>F</b> <b>N</b> CRA <b>S</b> E <b>N</b> I <b>Y</b> N <b>Y</b> LNWY <b>Q</b> R <b>K</b> FGEAPKRLI <b>S</b> <b>NTNTLET</b> GIPSRFSGSGSGTD <b>F</b> LTIS <b>S</b> LQPEDFATYF <b>CLQHSNFP</b> PFTFGSGTKLEI <b>KRA</b>
17A10	DIQMTQSPSFLSASV <b>G</b> DRVTIN <b>C</b> RA <b>S</b> E <b>N</b> I <b>Y</b> N <b>Y</b> LNWY <b>Q</b> Q <b>K</b> FGEAPKRLI <b>Y</b> <b>NTNTLET</b> GIPSRFSGSGSGTD <b>F</b> LTIS <b>S</b> LQPEDFATYF <b>CLQHSNFP</b> PFTFGSGTKLEI <b>KRA</b>
18G8	DIQMTQSPSFLSASV <b>G</b> D <b>R</b> L <b>T</b> IN <b>C</b> AS <b>Q</b> <b>N</b> I <b>Y</b> KYLNWY <b>Q</b> Q <b>K</b> LGEAPKRLI <b>Y</b> <b>D</b> <b>TNNLQ</b> <b>T</b> GIPSRFSGSGSGTD <b>Y</b> LTIS <b>S</b> LQPEDFATYF <b>CLQHSNFP</b> PFTFGSGTKLEI <b>KRA</b>
19H9	DIQMTQSPSFLSASV <b>G</b> DRVTIN <b>C</b> RA <b>S</b> E <b>N</b> I <b>Y</b> N <b>Y</b> LNWY <b>Q</b> Q <b>K</b> FGE <b>G</b> PKRLI <b>Y</b> <b>NTNTLET</b> GIPSRFSGSGSGTD <b>F</b> LTIN <b>S</b> LQPEDFATYF <b>CLQHSNFP</b> PFTFGSGTKLEI <b>KRA</b>
24B7	DIQMTQSPSFLSASV <b>G</b> DRVTIN <b>C</b> RA <b>S</b> E <b>N</b> I <b>Y</b> N <b>Y</b> LNWY <b>Q</b> Q <b>K</b> FGEAPKRLI <b>Y</b> <b>NTNTLET</b> GIPSRFSGSGSGTD <b>F</b> LTIS <b>S</b> LQPEDFATYF <b>CLQHSNFP</b> PFTFGSGTKLEI <b>KRA</b>

### 5.6.2 Evaluation of the PRDX4 antibodies binding site

Besides identifying the antibody's sequences, the determination of the exact epitope binding site is a crucial part of antibody characterisation. To investigate whether PRDX4 AB clones recognise the same or close-by epitope, a FC-based assay was performed (see paragraph 4.2.1). For this, MDA MB-231 cells were pre-incubated with serial dilutions (1-250 µg/mL) of the different PRDX4 AB clones, washed, and then incubated with 5H5 antibody labelled with Alexa Fluor 647 (table 3.7). Binding of an AB to the same or to a close-by epitope will result in reduced 5H5 binding thus in lower fluorescence signal intensity. As a benchmark, unlabelled 5H5 as the first antibody was included in the assay, and a MBP-specific antibody was used as a negative control. The normalised results from this FC experiment are depicted in Figure 5.16.

One class of antibodies showed a signal reduction similar to the 5H5 antibody (around 95 % reduction of the MFI, C-F). These antibodies presumably bind to the same epitope as 5H5. A second set of antibodies reduced the 5H5 fluorescence signal intensity by only up to 75 % (A and B) indicative for binding of the antibodies to a nearby or partially overlapping epitope resulting in steric interference with 5H5 binding.

## 5.6 CHARACTERISATION OF PRDX4 ANTIBODIES

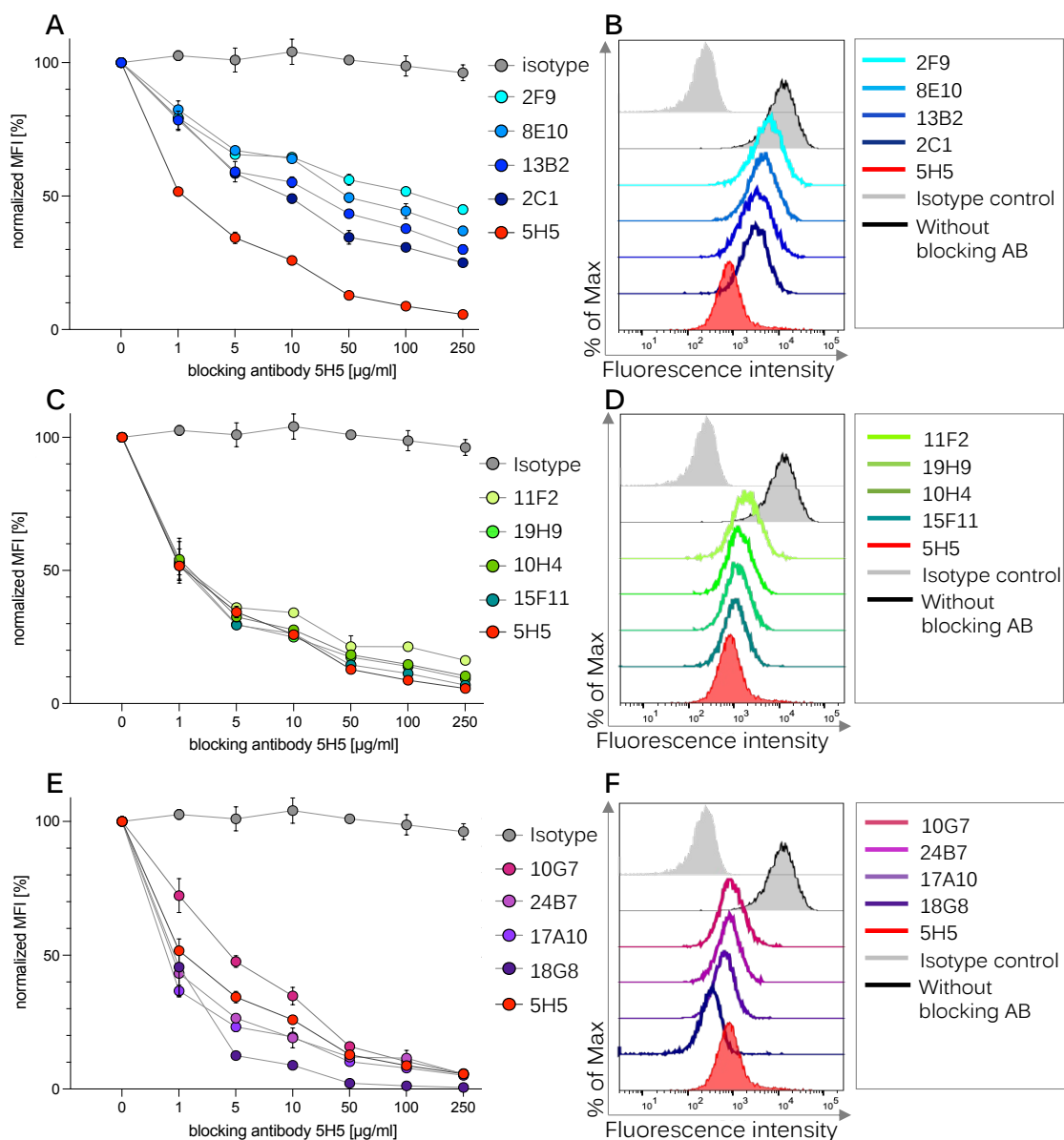


**Figure 5.16: PRDX4 antibody bind to the same or near-by epitope.**

MDA MB-231 cells were pre-incubated with 1-250  $\mu\text{g}/\text{mL}$  purified PRDX4 AB (see paragraph 4.2.1) and then stained with 5H5-Alexa Fluor 647 antibody (see table 3.7). A reduction of the signal intensity indicates binding of the respective AB alone to the same epitope as 5H5 or to an epitope in close vicinity. All MFI values were acquired in triplicates from three independent experiments and are shown as mean + SEM.

Graphs **A**, **C** and **E** show normalised MFI values of the different antibody clones. Histograms **B**, **D** and **F** show 5H5 fluorescence signal intensities upon pre-incubation with the highest AB concentrations of the different PRDX4 AB clones (250  $\mu\text{g}/\text{mL}$ ).

To gain further insight into the localisation of the epitope, IP experiments were performed. Exon 1, spanning nucleotides 1-241 of the PRDX4-gene encodes for a signal sequence and a unique hydrophobic domain followed by a hydrophilic stretch with a theoretical surface probability (see appendix 8.1) [115, 121]. To tackle the question whether the newly identified PRDX4-specific antibodies bind to this hydrophobic domain, deletion mutants of PRDX4 consisting only of exon 1 (ex1GFP, ex1His) or lacking exon 1 (ex2-7GFP, ex2-7His) were generated as described in section 4.5.4.

These mutants were then used for IP experiments. Therefore, cells were transfected with the respective expression plasmids (paragraph 4.1.5 and table 3.15). Lysates (750 µg/sample) were generated and incubated with PRDX4-, GFP- or MBP-specific antibodies coupled to beads. Upon precipitation and elution, the samples were analysed by immunoblotting for GFP (3H9-HRP, 1:2,000, table 3.7), PRDX4 (ab1484167, 1:20,000, table 3.8) or CCDC47 (HPA029674, 1:2,000, table 3.8). These results are depicted in Figure 5.17.

IPs with a GFP-specific antibody followed by an immunoblot with another GFP antibody revealed that all fusion proteins were efficiently expressed (ex1GFP at around 35 kDa, ex2-7GFP at around 53 kDa, and wtPRDX4-GFP at around 60 kDa). It should be noted, that the GFP antibody used for immunoblotting also revealed unspecific signals for immunoglobulin light chains (around 25 kDa) and heavy chains (around 50 kDa). An IP performed with the 5H5 antibody and subsequent immunoblot analysis with a GFP antibody only gave signals for ex2-7GFP and full-length PRDX4-GFP, indicating that the 5H5 epitope is located within the region encompassing exons 2-7 of PRDX4. An immunoblot with a CCDC47-antibody showed signals for all IPs with the PRDX4 5H5 antibody, i.e. also with a lysate from non-transfected cells. This is presumably due to the fact that 5H5 also precipitates endogenous PRDX4 and thus co-precipitates CCDC47. Finally, the immunoblots performed with the commercial PRDX4 antibody following IPs with the 5H5 or a GFP specific antibody gave signals for ex2-7GFP and wtPRDX4-GFP, but not for ex1GFP. The commercial PRDX4 antibody also recognised endogenous PRDX4 at 27 kDa.

5.6 CHARACTERISATION OF PRDX4 ANTIBODIES

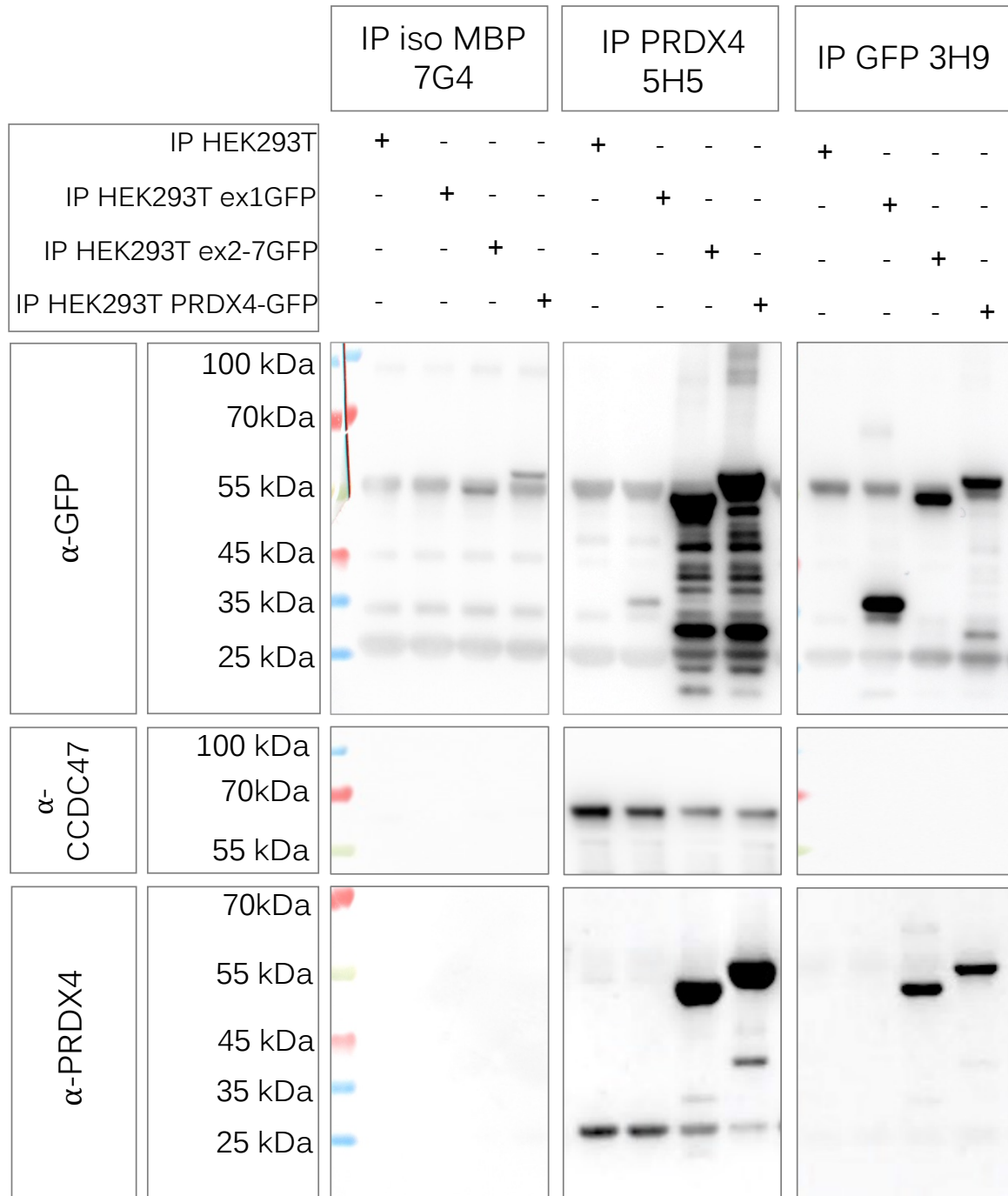


**Figure 5.17: The epitope of the PRDX4 antibody is located within exons2-7.**

Beads coupled to antibodies against PRDX4 (OC2E 5H5), GFP (3H9) or MBP (7G4, isotype control) were incubated with lysates of HEK293T cells transiently transfected with either ex1GFP, ex2-7GFP or PRDX4-GFP (see paragraph 4.1.5). Then, immunoblots were performed and incubated with antibodies specific for either GFP (3H9-HRP, 1:2,000), for PRDX4 (ab1484167, 1:50,000) or for CCDC47 (HPA029674, 1:2,000).

## 5 RESULTS

The results above were further confirmed by ELISA experiments. For these, HEK293T cells were transfected with the His-tagged deletion constructs as described in paragraph 4.1.5. The His-fusion proteins were then purified with Ni-NTA-beads (see paragraph 4.6.5) and analysed by PAGE followed by Coomassie staining. Their concentrations were determined by comparison to commercial PRDX4 protein of a given concentration (see Figure 5.18 A). The purified wtPRDX4-His and PRDX4-His deletion mutants were consequently used for ELISA experiments as described in paragraph 4.6.11. Upon coating with the different PRDX4-His proteins (1  $\mu\text{g}/\text{mL}$ ) and blocking, the different PRDX4 AB clones were added for 2 hours. The plate was then washed and incubated with an  $\alpha$ -rat IgG (H + L) antibody coupled to HRP (1:5,000, table 3.10). The assay was developed with TMB-substrate and the ODs at 450 nm were measured, blank corrected and normalised.

All tested antibodies bound to the full length PRDX4 protein and to the ex2-7His construct. Even though equal amounts of the different PRDX4 antibodies were used, their binding efficiency varied considerably for unknown reasons. Among all candidates tested, the 5H5 antibody clone showed the strongest binding to recombinant PRDX4 protein.

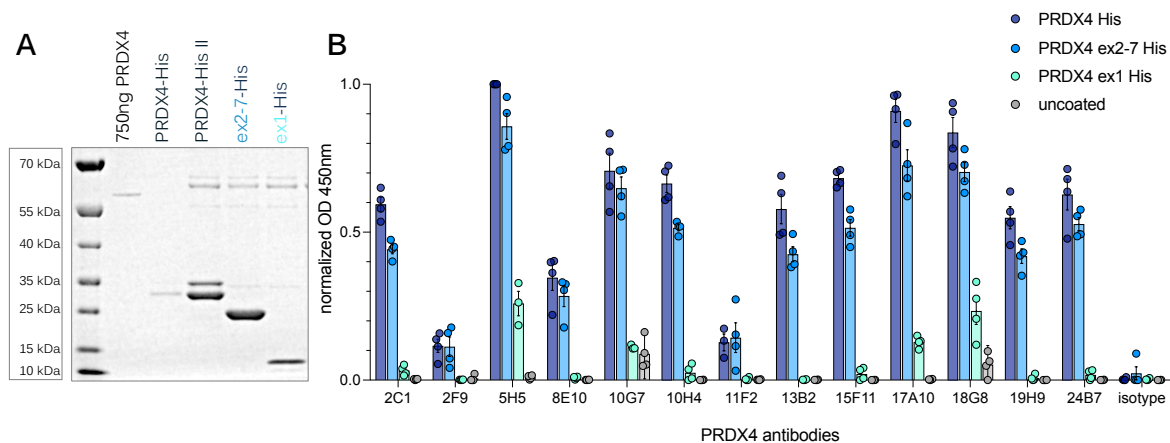


**Figure 5.18: PRDX4 ABs recognise an epitope within exons2-7 of PRDX4.**

**A:** Coomassie staining of different PRDX4-His constructs (ex1-His, ex2-7His and PRDX4-His), which were generated and purified as described in paragraph 4.6.5.

**B:** ELISA experiments using different purified proteins (1  $\mu\text{g}/\text{mL}$ ) for coating followed by incubation with the PRDX4-AB clones (see paragraph 4.6.11). All OD values were blank corrected, normalised and shown as mean  $\pm$  SEM. All experiments were conducted in triplicates (n=5).

## 5.7 Humanisation of a PRDX4 antibody

Because non-human antibodies regularly induce immune responses in humans and thus limit their applicability, humanisation of an animal-derived antibody is mandatory for a (repeated) *in vivo* use in patients. ‘Humanisation’ means that the CDRs of an antibody are grafted into a suitable human antibody framework region (FR). The challenge is to preserve as much as possible of the specificity, affinity, and stability of the original rodent-derived antibody. Therefore, the human FR that is the most homologous to that of the original sequence is selected from a database. The human CDRs are replaced by the original CDRs and the construct is synthesized and cloned into a suitable expression plasmid. In case the antibody’s functionality is not fully restored, backmutations of sensible amino acids are introduced until the humanised antibody fully regains the original antibody’s properties [102, 103, 213].

In this project the PRDX4-specific antibody OCA2E 5H5 was humanised. This antibody clone was selected as it showed the highest affinity to PRDX4 in ELISA experiments (see Figure 5.18). With the help of a dedicated online tool (abDesign) that has been designed by and co-developed with Dr. Benjamin Schubert from the Department of Computational Biology at Helmholtz Munich (see section 3.12), the correct FR was chosen and different sets of backmutations were introduced, taking into account the rules listed below. The thereby generated plasmids with the various antibody sequence including the specific backmutations are listed in the appendix (see table 8.1).

As a first rule, backmutations were induced at positions, where the AA from the original rat sequence is more abundant across human IgG sequences compared to the AA of the used grafted human sequence. This resulted in a set of plasmids named ‘set1’. As a second criterion backmutations were induced where an AA originating from the rat sequence is present in more than 15% of human IgG sequence, even if the AA in the selected human framework is more frequent across human IgG sequences. This resulted in ‘set2’ of backmutations. Theoretically, as a third rule, backmutations are induced at positions where amino acids present in the original rat sequence as well as in the selected human framework, are very rare ( $\leq 1\%$  abundance, ‘set3’). This rule three did not apply here.

1. Original rat AA is more abundant in the selected and most suitable human IgG1 sequence than AA of human graft
2. Original AA frequent in human IgG but not as abundant as grafted (human) AA ( $\geq 15\%$  abundancy)
3. If both AA occur very rarely ( $\leq 1\%$  abundancy)

### 5.7.1 Testing the binding efficiency of different humanised HC and LC PRDX4 antibody sequences

The designed humanised sequences with their respective backmutations were tested in an initial FC-based screening. Therefore, HEK293T cells were co-transfected with two expression plasmids encoding one LC and one HC. Because the LC and HC plasmids co-express mCherry and cerulean, respectively, a successful transfection could be monitored by fluorescence microscopy (Figure 5.19 A).

Three and six days after transfection, the supernatants were harvested and tested for the presence of human IgG in a dot blot (Appendix, see Figure 8.3). All IgG positive supernatants were then investigated for binding activity. To this end, surface PRDX4 positive MDA MB-231 cells were incubated with the supernatants followed by incubation with an  $\alpha$ -human IgG (H + L) Alexa Fluor 647 labelled secondary antibody and were finally tested by FC. Representative histograms of such an experiment are shown in Figure 5.19 C. The three different histograms also visualise the different binding efficiencies of the antibody variants. While some HC-LC combinations showed signal intensities comparable to the ‘only’ chimerised 5H5 positive control AB, others revealed significantly lower signals, indicating a reduced binding affinity due to a conformational modification of the paratope. Summarised data for all HC-LC combinations tested are shown in Figure 5.19 B. Normalised MFI values are shown in a heat map.

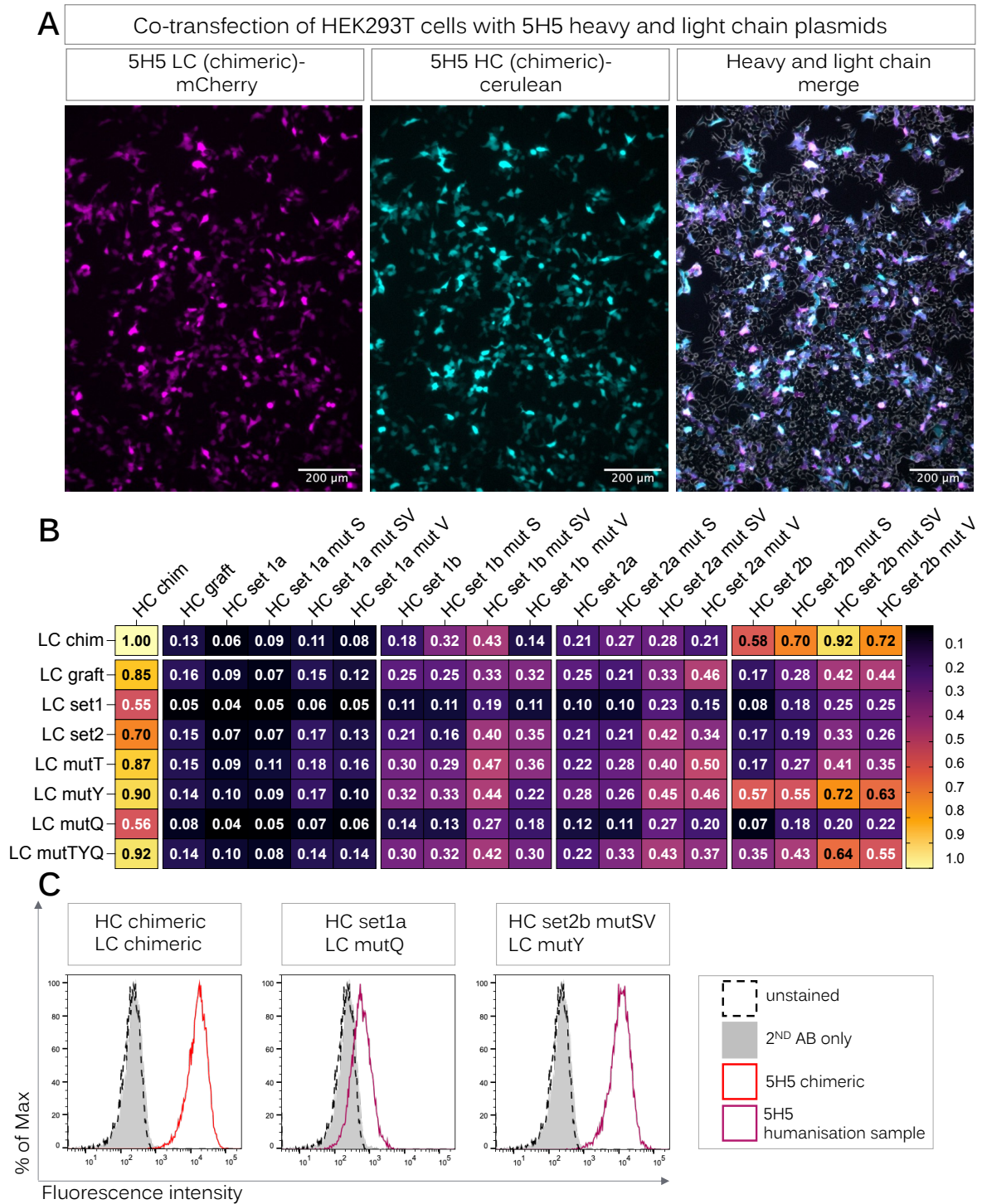


Figure 5.19: FC screening for humanisation of the 5H5 PRDX4 antibody.

**Figure 5.19: FC screening for humanisation of the 5H5 PRDX4 antibody.**

Overall, all 144 possible combination of 18 HC and 8 LC sequences were tested and compared against each other (Appendix, see tables 8.1 and 8.2). HEK293T cells were transiently transfected with one HC and one LC expression plasmid, supernatants of the transfected cells were harvested 3 days and 6 days post transfection and used as primary antibody for the FC staining of MDA MB-231 cells.

**A:** Fluorescence microscopy images of HEK293T cells transfected with HC and LC expression plasmids. **B:** Heat map of all results, normalised to the chimeric MFI values calculated upon FC analysis. **C:** Exemplary FC histograms for the chimeric AB and two humanised variants.

**5.7.2 Measurement of the affinities ( $K_D$ ) of the humanised antibodies**

The five humanised variants that revealed the highest MFI values (Figure 5.19 B, all LC mutY + HC set2b combinations and LC mutTYQ + HC set2b mutSV) were further analysed in a next set of experiments. Therefore, ExpiCHO cells were co-transfected with the respective HC and LC expression plasmids and the antibodies were purified from the supernatants via immunoaffinity binding to protein A. The purification was kindly performed by Dr. Markus Kellner in our group. The concentration of the purified antibodies was assessed, and their binding affinities were evaluated by determining the  $K_D$ , which is the equilibrium constant describing the required molarity of an antibody to achieve a half-maximum binding at the equilibrium (see paragraph 4.2.2).

Therefore 100,000 MDA MB-231 cells were stained with serial dilutions of the purified antibodies, followed by a staining with the  $\alpha$ -human IgG (H + L) Alexa Fluor 647 labelled antibody (see table 3.10) and analysed by FC. The measured MFI values were plotted against the antibody molarity, which was calculated from the antibody concentration and the molecular weight of the antibody (around 150 kDa) and therefrom the  $K_D$ -value could be calculated by non-linear regression fit. Figure 5.20 shows the  $K_D$  of the top five candidates.

Here, the lower right bar chart shows the highest measured MFI values obtained from the different HC and LC combinations. Two combinations (HC set2b/LC mutY and HC set2b mutS/LC mutY) showed lower overall MFI values indicating weaker binding to PRDX4. The  $K_D$  values of all five antibodies tested was in the range between 9 and 13 nM (see table 5.3).

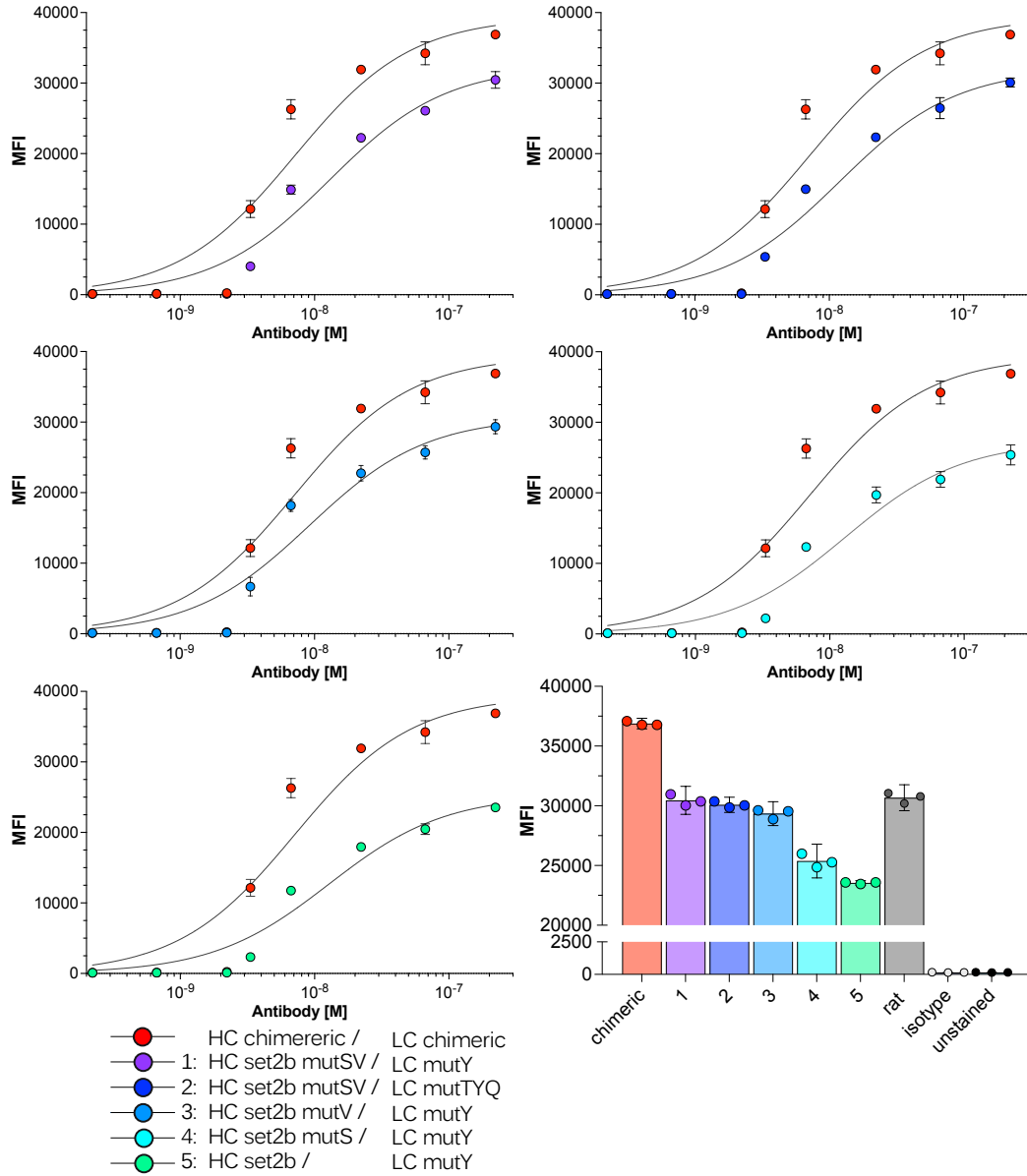


**Figure 5.20:  $K_D$  of the top five humanised HC-LC combinations of antibody 5H5.**

ExpiCHO cells were transfected with different sets of HC and LC expression plasmids, antibodies were purified from supernatants and their concentration was determined. To define the  $K_D$  of the different ABs, MDA MB-231 cells were stained with serial dilutions of the purified antibodies followed by staining with the  $\alpha$ -human IgG (H + L) Alexa Fluor 647 antibody. Upon FC analysis, the measured MFI-values at the different concentrations were used to calculate the  $K_D$  values, which are listed in table 5.3. The lower right graph shows the highest MFI-values measured for the different HC and LC combinations.

**Table 5.3: Calculated  $K_D$  of the top five HC and LC combination for the humanisation of the PRDX4 antibody 5H5.**

plasmid HC 5H5 AB	plasmid LC 5H5 AB	measured $K_D$
chimeric	chimeric	7.116 nM
set2b mutSV	mutY	12.82 nM
set2b mutV	mutTYQ	11.93 nM
set2b mutV	mutY	9.155 nM
set2b	mutY	12.99 nM
set2b mutS	mutY	12.76 nM

## 5.8 An alternatively spliced form of PRDX4 is expressed in human cancer cells

Recently, a testis specific splice variant of PRDX4 has been identified in adult mice. This variant uses an alternative promoter and an alternative exon1 (see Figure 5.21 B). This variant has been predicted in several eutherian mammals, by comparative analysis but it has not been described so far in men [130, 132]. Genes that are expressed during embryonic development and after birth only in testes are often also highly expressed in cancer. These genes are commonly referred to as cancer testis antigens (CTAs). We wished to investigate, whether the predicted testis-specific form of PRDX4 is also detectable in human cancer cell lines and primary tumours. Therefore, different PCR primer pairs were designed, of which the upstream primer is located within the testis-specific exon1 and the downstream primers are located in the regular exons 2,3 or 4 (see table 3.12 and Figure 5.21 A). RNA was isolated from different human cancer cell lines and RT-PCR was performed (see paragraph 4.5.6). The results in Figure 5.21 C show that the testis-specific PRDX4 mRNA is detectable in human cancer cell lines and primary ovarian cancer cells.

## 5.8 AN ALTERNATIVELY SPLICED FORM OF PRDX4 IS EXPRESSED IN HUMAN CANCER CELLS

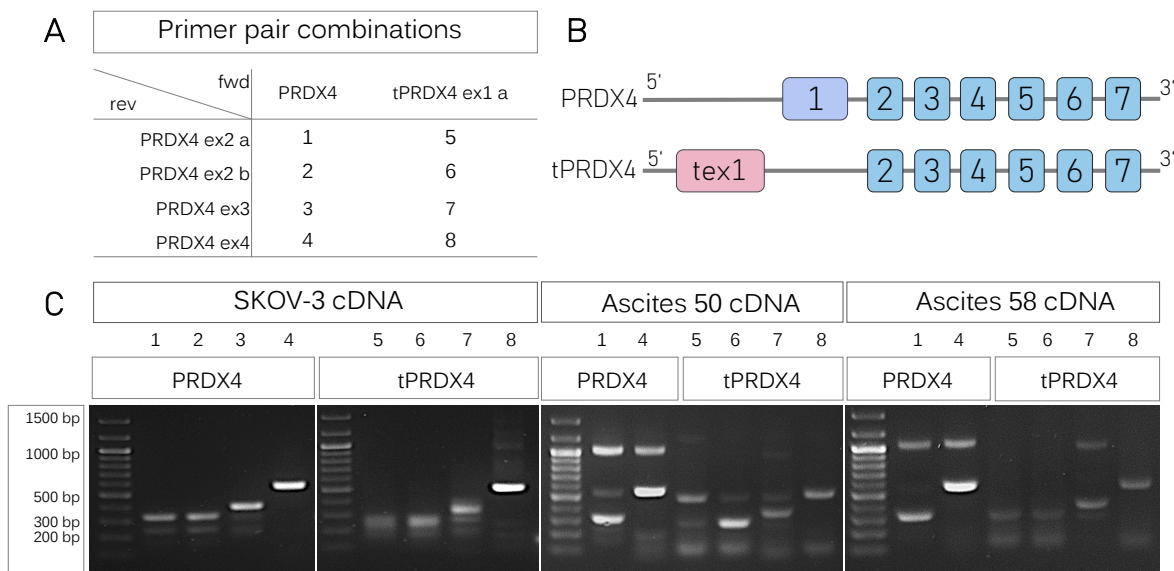


**Figure 5.21: Expression of tPRDX4 in human cancer cells.**

Primer pair combinations (A, see table 3.12) for the detection of PRDX4 and tPRDX4 expression in human cancer cell lines by PCR (C). A scheme of the PRDX4 gene and the tPRDX4 variant is shown in B.

PCR amplified DNA fragments were sent for sequencing to confirm the amplification of the tPRDX4 cDNA. The obtained sequences for the alternatively transcribed exon1 of tPRDX4 were initially aligned to the tPRDX4 sequence of *pan troglodytes*. This alignment showed a single nucleotide variation at position 97 [214] and thus we could identify the tPRDX4-variant in the genome of those sequenced cell lines and primary tumour samples. Additionally, the translated protein sequence of the *pan troglodytes* transcript is identical to a recently described human tPRDX4 protein sequence [214–216].

**Table 5.4: Sequencing results of five different cell lines reveal expression of tPRDX4 in cell lines and primary cancer cells.**

The sequencing results of the five samples aligned to the tPRDX4 sequence [130, 131, 214, 216]. The start of exon2 is marked in blue.

Cell line		DNASequence			
tPRDX4	1	ATGGATCACCGAAGC	CGACTACGGGGCACA	GGCCTGAACCGAATC	CCTGGGACTCAGTCC
A549	1	-----	-----CTCTGGA	GGCCTGAACCGAATC	CCTGGGACTCAGTCC
ES-2	1	-----	-----A	GGCCTGAACCGAATC	CCTGGGACTCAGTCC
Jurkat	1	-----	-----	-----GAACCGAATC	CCTGGGACTCAGTCC
PCI-1	1	-----	-----	-GCCTGAACCGAATC	CCTGGGACTCAGTCC
Ascites 58	1	-----	-----	--CCTGAACCGAATC	CCTGGGACTCAGTCC
tPRDX4	61	CGAGCCCCCGAGTC	CCACTCCCCTTCCAC	GTGCAACAGGAGGCC	AGGGAAGGAGAAGAC
A549	61	CGAGCCCCCGAGTC	CCACTCCCCTTCCAC	GTGCAACAGGAGGCC	AGGGAAGGAGAAGAC
ES-2	61	CGAGCCCCCGAGTC	CCACTCCCCTTCCAC	GTGCAACAGGAGGCC	AGGGAAGGAGAAGAC
Jurkat	61	CGAGCCCCCGAGTC	CCACTCCCCTTCCAC	GTGCAACAGGAGGCC	AGGGAAGGAGAAGAC
PCI-1	61	CGAGCCCCCGAGTC	CCACTCCCCTTCCAC	GTGCAACAGGAGGCC	AGGGAAGGAGAAGAC
Ascites 58	61	CGAGCCCCCGAGTC	CCACTCCCCTTCCAC	GTGCAACAGGAGGCC	AGGGAAGGAGAAGAC
tPRDX4	121	TGGGAGCGAGAGCCA	CCTCGTCAGAGGCCT	CCTATCTATGAGCCA	CCAGAAAGTGAAGAG
A549	121	TGGGAGCGAGAGCCA	CCTCGTCAGAGGCCT	CCTATCTATGAGCCA	CCAGAAAGTGAAGAG
ES-2	121	TGGGAGCGAGAGCCA	CCTCGTCAGAGGCCT	CCTATCTATGAGCCA	CCAGAAAGTGAAGAG
Jurkat	121	TGGGAGCGAGAGCCA	CCTCGTCAGAGGCCT	CCTATCTATGAGCCA	CCAGAAAGTGAAGAG
PCI-1	121	TGGGAGCGAGAGCCA	CCTCGTCAGAGGCCT	CCTATCTATGAGCCA	CCAGAAAGTGAAGAG
Ascites 58	121	TGGGAGCGAGAGCCA	CCTCGTCAGAGGCCT	CCTATCTATGAGCCA	CCAGAAAGTGAAGAG
tPRDX4	181	CTGCCAGATAATGTT	ACGGTTTCCAAGCCA	GCGCCCTACTGGGAA	GGAACAGCTGTGATC
A549	181	CTGCCAGATAATGTT	ATGGTTTCCAAGCCA	GCGCCCTACTGGGAA	GGAACAGCTGTGATC
ES-2	181	CTGCCAGATAATGTT	ATGGTTTCCAAGCCA	GCGCCCTACTGGGAA	GGAACAGCTGTGATC
Jurkat	181	CTGCCAGATAATGTT	ATGGTTTCCAAGCCA	GCGCCCTACTGGGAA	GGAACAGCTGTGATC
PCI-1	181	CTGCCAGATAATGTT	ATGGTTTCCAAGCCA	GCGCCCTACTGGGAA	GGAACAGCTGTGATC
Ascites 58	181	CTGCCAGATAATGTT	ATGGTTTCCAAGCCA	GCGCCCTACTGGGAA	GGAACAGCTGTGATC

### 5.8.1 Successful generation of antibodies targeting tPRDX4

Proteins that are expressed during embryogenesis, but after birth solely in testes and aberrantly in malignant tumours, are collectively referred to as CTAs. Their restricted and specific expression pattern qualify many of them as promising targets for cancer immunotherapeutic approaches [217–219].

## 5.8 AN ALTERNATIVELY SPLICED FORM OF PRDX4 IS EXPRESSED IN HUMAN CANCER CELLS

Given the restricted expression pattern of testis-specific PRDX4 in mice and the positive RT-PCR results described above, it was tempting to investigate tPRDX4 also on the protein level, because it could emerge as a new CTA. For this reason, monoclonal antibodies against tPRDX4 were raised by immunising rats with a peptide (N-GEDWEREPPRQRPP-C) derived from the testis-specific exon1. For the screening of the hybridoma supernatants, a tPRDX4-GFP expression plasmid was cloned as described in paragraph 4.5.5 and HEK293T cells were transfected and put under antibiotic selection to generate a stable tPRDX4-GFP expressing cell line (see paragraph 4.1.5). Cell lysates were generated and the hybridoma supernatants were tested in immunoblots. A scheme of the whole generation process is depicted in Figure 5.22 showing the successful generation of the stable cell line and immunoblot with one tPRDX4 antibody clone that specifically detected the tPRDX4-GFP construct at around 60 kDa.

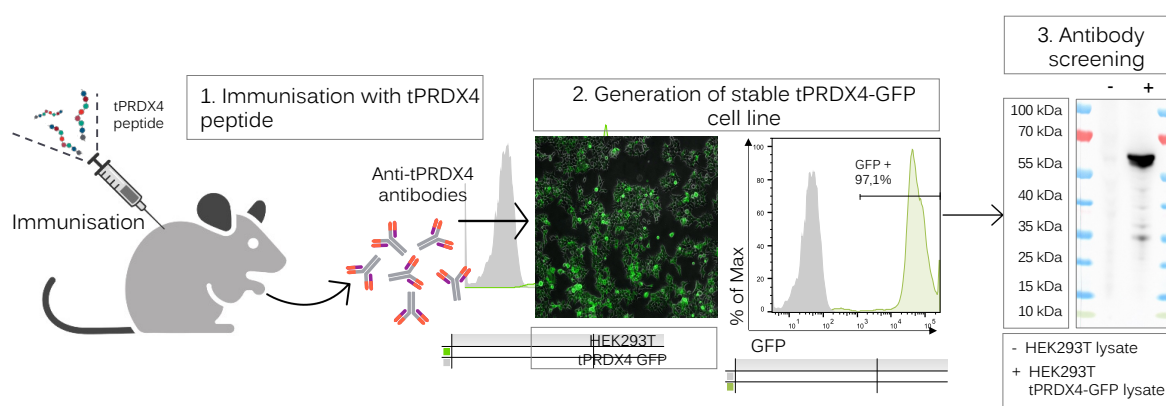


**Figure 5.22: Strategy for the generation of tPRDX4 specific antibodies.**

The tPRDX4 peptide sequence was used for the immunisation of rats (1.) In parallel, an expression plasmid encoding for a tPRDX4-GFP fusion protein was generated (2.). HEK293T cells were transfected and selected, and expression of tPRDX4-GFP protein was revealed by fluorescence microscopy. Lysates of that cell line were generated and the hybridoma supernatants were tested by immunoblotting (3.).

### 5.8.2 Generated antibodies specifically detect tPRDX4

The established tPRDX4 antibodies were further tested in LSCM experiments as described in paragraph 4.3. MDA MB-231 cells were fixed, permeabilized and then stained for PRDX4 (5H5 Alexa Fluor 647, table 3.7, shown in purple), tPRDX4 (15C8, table 3.9 and  $\alpha$ -rat IgG (H + L) Alexa Fluor 568, table 3.10, shown in orange), CD49c for membrane staining (EXO 8F2 Alexa Fluor 488, table 3.7, shown in green) and DAPI for staining of the nuclei (1:5,000, shown in cyan). As shown in Figure 5.23, PRDX4 and CD49c revealed a cell membrane staining, while tPRDX4 was located intracellularly and revealed a punctuated staining pattern implicating location in vesicle-like structures. Thus, PRDX4 and tPRDX4 do not colocalize and probably do not interact.

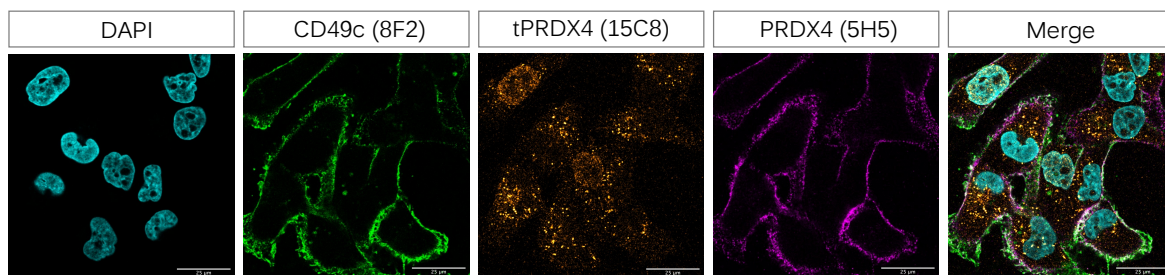


**Figure 5.23: LSCM images show intracellular staining of tPRDX4.**

MDA MB-231 cells were used for LSCM-staining (see paragraph 4.3) using the tPRDX4 (15C8, table 3.9 and  $\alpha$ -rat IgG (H+L) Alexa Fluor 568, table 3.10) PRDX4 (5H5 Alexa Fluor 647, table 3.7), CD49c (EXO 8F2 Alexa Fluor 488, table 3.7) and DAPI (1:5,000).

The specificity of the tPRDX4 antibody was further evaluated by IP experiments. HEK293T cells were transfected with expression plasmids encoding either PRDX4-GFP or tPRDX4-GFP, and cell lysates were prepared two days later. Beads coupled either with 11F2 (PRDX4) or 15C8 (tPRDX4) antibody were incubated with recombinant PRDX4 or CCDC47 protein or with the generated cell lysates. The eluates were subsequently analysed by immunoblots, which were incubated either with PRDX4 antibody (PA3-753, 1:5,000, table 3.8), CCDC47 antibody (HPA029674, 1:2,000, table 3.8) or tPRDX4 antibody (15C8, 1:10, table 3.9).

## 5.8 AN ALTERNATIVELY SPLICED FORM OF PRDX4 IS EXPRESSED IN HUMAN CANCER CELLS

---

The left part of Figure 5.24 shows control cell lysates and protein and the respective signal intensities for PRDX4-GFP (60 kDa) CCDC47 (55 kDa) and tPRDX4 (63 kDa). It is evident that the tPRDX4 antibody 15C8 specifically binds to the tPRDX4-GFP construct and not to endogenous PRDX4 where no signal intensities were detectable (lower left image). As already described in the Figures 5.3 and 5.13, the PRDX4 antibodies bind to PRDX4-GFP, to the recombinant PRDX4-protein and to the endogenous PRDX4 at around 27 kDa. Furthermore, a CCDC47 signal is present for all HEK293T lysates proofing again the interaction between PRDX4 and CCDC47. IPs performed with the 11F2 antibody also bind to the tPRDX4-GFP construct, which also confirms the epitope of the PRDX4 within exons2-7 that are identical in PRDX4 and tPRDX4. In addition, no signal for the CCDC47 recombinant protein could be observed and thereby a direct detection of CCDC47 by the PRDX4 antibody could be excluded. IPs performed with the tPRDX4 antibody 15C8 (right column) did not co-precipitate CCDC47, so that direct interaction between these proteins seems unlikely.

In essence, three tPRDX4 antibody clones were further characterised by 5' RACE-PCR as already described above. Their respective unique sequences of the different clones are listed in the appendix (see table 8.3). It remains to be shown how these antibodies behave on normal and cancerous tissues.

## 5 RESULTS

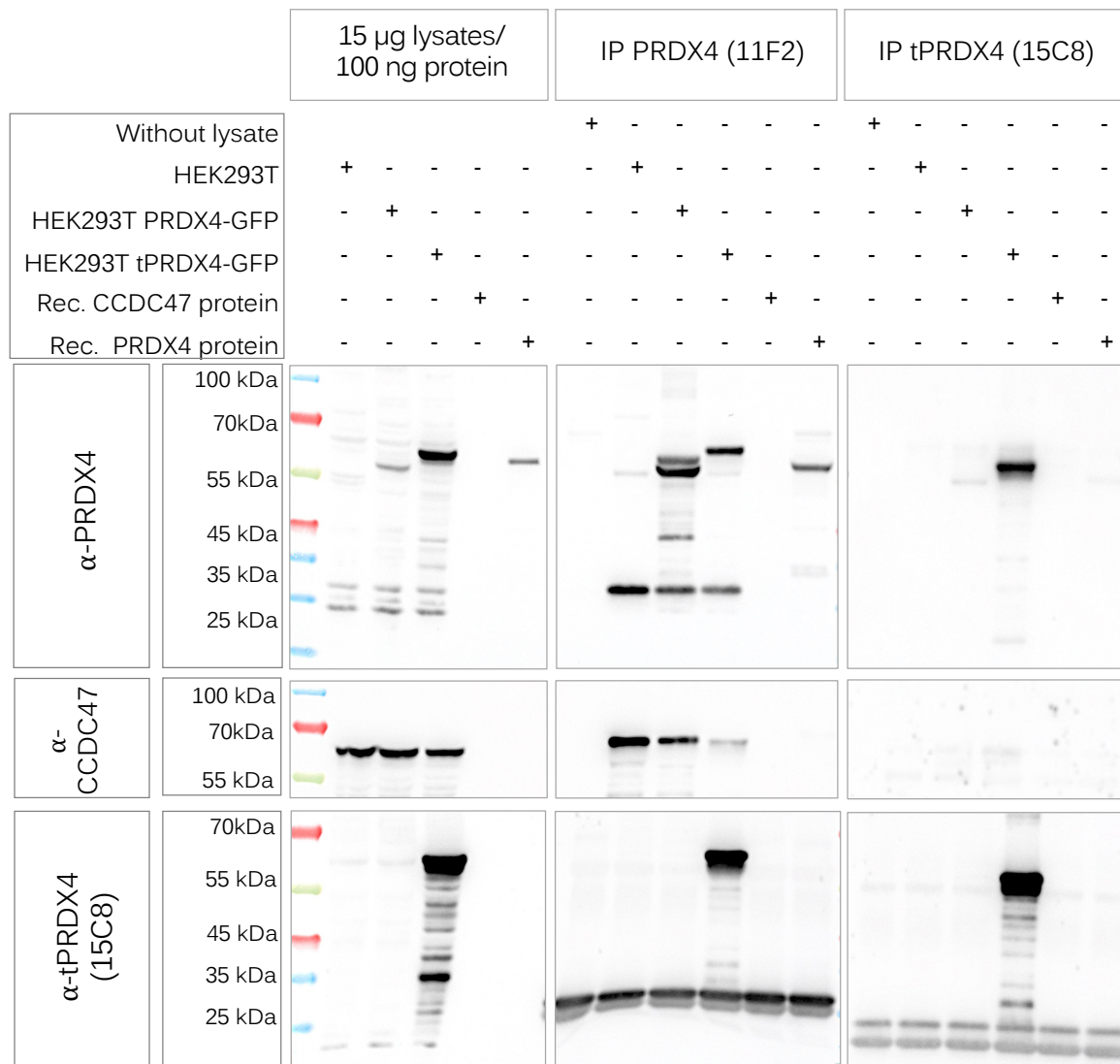


**Figure 5.24: IP experiments revealing specificity of the generated tPRDX4 antibody.**

IP experiments were performed either with the 11F2 PRDX4 antibody or the 15C8 tPRDX4 antibody. The samples were incubated with different lysates from HEK293T cells transfected with the PRDX4-GFP or the tPRDX4-GFP expression plasmids, or with recombinant proteins. Upon IP experiments, immunoblots were performed, stained for PRDX4 (PA3-753, 1:5,000, table 3.8), CCDC47 (HPA029674, 1:2,000, table 3.8) or tPRDX4 (15C8, 1:10, table 3.9).

## 6 Discussion

Therapeutic mAbs offer a great potential for the treatment of tumours because they bind to their respective target molecules in an unprecedented specificity and thus cause relatively little adverse side effects as compared to current treatment regimens like chemotherapies. But as yet, the number of known suitable targets is still small, so that many of patients still cannot benefit. Therefore, the identification of new tumour specific targets is pivotal in order to foster the clinical application of mAbs. To tackle this issue, a new proprietary technique has been developed in our group, that uses extracellular vesicles, isolated from patient samples for immunisation purposes. MAbs obtained by this approach constitute new and promising tools for cancer therapy and diagnostic. Elucidating their specificities can allow a deep insight into tumour biology. Also, most antibodies generated with this technique offer the great advantage of binding target antigens in their native form as proteins present on the EVs used for immunisation are expressed in their native 3D conformation [146].

During this project we successfully generated new monoclonal antibodies against a variety of different targets on the surface of cancer cells. The results show that a considerable part (12 %, see Figure 5.2) of all generated clones bind to the same target protein, namely PRDX4. This unexpected finding highlights PRDX4 as interesting candidate worth for future investigations as it has so far been exclusively described as an ER-resident protein [109]. For this reason, the respective PRDX4 antibody clones were individually analysed and characterised to gain information about their affinity, sequence and binding epitope.

The fact that we could generate mAbs against proteins originally located intracellularly is probably due to tumour derived EVs that harbour tumour neoantigens on their surface. These neoantigens reflect the cell's surface of the tumour cell from which they were shedded from [220]. When proteins originally located intracellularly are exposed to the cell surface of tumour cells [221], those isolated vesicles can lead, upon immunisation, to the generation of mAbs against neoantigens and intracellular proteins.

## 6.1 Successful characterisation and humanisation of PRDX4 antibodies

Upon undoubtedly identifying PRDX4 as target of various antibody clones (Figure 5.3, and 5.4), it was further determined that clone 5H5 showed the strongest binding to PRDX4 upon all AB clones in ELISA experiments (see Figure 5.18). Clone 5H5 is therefore the flag-ship antibody.

Consequently, the antibody sequences of the respective clones were evaluated and compared (see table 5.2). Although, the HC and LC sequences match almost completely, every clone provides a unique sequence. Clonal divergence of the antibodies results from the process of SHM during the process of antibody maturation upon VDJ-recombination [83].

Our antibody clones harbour mutations in the FR as well as in the CDRs, except for CDR3 of the heavy chain, which is completely conserved. The HC CDR3 sequence encompasses the junctions between the combining V D and J genes and is considered the most important CDR for the interaction with the paratope as it possesses the most structural diversity [82, 85]. The differences among our different PRDX4 antibody clones only cause minor changes in the overall antibody affinity and their epitope binding specificity. Furthermore, the conducted blocking assay revealed that all antibody clones have similar blocking capacity and thus have a high chance to bind the same epitope. Even though some clones fail to achieve the same signal reduction, those differences may result from binding to nearby or partially overlapping epitopes or from a lower binding affinity for PRDX4 of these mAb clones.

In further experiments, the region of the exact PRDX4 epitope was characterised by IP and ELISA experiments using PRDX4 deletion constructs (see Figure 5.16, 5.17, and 5.18). Exon1 is thereby of particular interest, as it contains the hydrophobic N-terminal signal sequence, which is responsible for its localisation to the ER membrane [113, 121]. The generated results reveal that the epitope of all antibodies lies most likely within exons2-7, which has been even further confirmed by IP experiments conducted with the 5H5 antibody, where also a pulldown of the exons2-7 construct was observed.

However, no conclusion whether all antibody clones bind the exact same epitope can be drawn from the current data. Because we performed immunisations with antigens present on EVs in their native conformation, it is reasonable to assume, that the majority of the epitopes targeted by our antibodies will be conformational epitopes [90, 91, 222], a fact that unfortunately complicates their identification by conventional technologies.

The exact epitope of the PRDX4 antibody needs to be further evaluated, for example by X-ray crystallography [223] or by an overlapping peptide scan [224]. Due to the current lack of information, this project will be continued in our group. For their clinical application, mAbs have to fulfill several requirements to not elucidate serious side effects, caused by the antibody's immunogenicity in humans leading to its elimination from the body by the immune system [103, 104]. This drawback can be reduced or eliminated through the process of humanisation, which in most cases consists of a grafting of the CDRs into a human Ig backbone [103].

The key challenge in this process lies in maintaining the antibody's specificity, affinity and stability, while making it as 'human' as possible [103, 213]. During this thesis we successfully humanised our best characterised PRDX4 antibody clone 5H5 (see Figure 5.19, 5.20, and table 5.3) and were able to almost completely retain its binding affinity ( $K_D$  value), which is in a low nano-molar range.

## **6.2 PRDX4 is a new potential tumour marker exclusively identified on the surface of tumour cells**

In addition to the functional characterisation of our antibody clones, the underlying biology of the new described surface expression of PRDX4 is of particular interest. As already mentioned above, PRDX4 has been described as a ubiquitously expressed ER-resident protein [114, 120]. It was therefore surprising, that many of the mAbs obtained from our immunisation detected PRDX4 in our initial FC based surface screening (see Figure 5.5 and 5.7).

Interestingly, surface PRDX4 was also detectable *ex vivo* on primary cancer cells isolated from malignant ascites samples (see Figure 5.10), excluding the possibility of an *in vitro* artefact. In contrast, no PRDX4 was present on the surface of human PBMCs, primary FDCs and hepatocytes. The translocation of PRDX4 to the cell surface is therefore most likely a tumour-specific and -intrinsic phenomenon, qualifying the protein as a new tumour-associated target molecule.

Besides PRDX4, also other interesting and promising target proteins on cancer cells were identified in this immunisation experiment, such as serine/arginine repetitive matrix 2 (SRRM2). SRRM2 is localised in nuclear speckles of healthy cells, that co-localise with the Tau protein and is involved in its relocalisation of the complex to the cytoplasm in Alzheimer's disease

[225, 226]. Furthermore, other interesting target proteins such as several integrins, intercellular adhesion molecule 1 (ICAM-1), CD47, epithelial cell adhesion molecule (EpCAM), and basigin (CD147), were identified and all of which need further evaluation. Plenty of those targets have already been described as tumour associated antigens such as CD47, CD147 and EpCAM, which supports the identification power of putative tumour antigens of our technology.

We for example obtained antibodies against CD47, a surface molecule that interacts with integrins [227, 228] and is involved in a variety of physiological processes such as cell migration [229, 230]. To tumour cells, CD47 provides a ‘don’t eat me’ signal to prevent them from phagocytosis by macrophages [230, 231]. CD47 was initially described as a tumour associated antigen for ovarian cancer, but it was also found to be highly overexpressed in multiple other cancer types, where CD47 promotes overall tumour survival [229, 230].

Besides CD47 also antibodies targeting CD147 were identified. CD147 is a transmembrane glycoprotein that is involved in many cellular and immune-related processes [232] and mediates cell-cell and cell-matrix interaction by regulating the synthesis and activity of various matrix metalloproteinases (MMPs) [232, 233]. The protein is overexpressed on the surface of many malignant tumour cells [234] where it promotes tumour proliferation and inhibits apoptosis [233–235].

The fact that we could identify antibodies against accepted tumour antigens is a fundamental proof of concept that our immunisation strategy leads to the generation of antibodies against tumour specific targets and provides an opportunity for the identification of hitherto unknown tumour targets. Interestingly, besides PRDX4, other intracellular targets such as SRRM2, were identified in our flow-cytometric surface screening. This unexpected findings raises several questions, such as why intracellular proteins are translocated and integrated into the plasma membrane of tumour cells and what is the underlying mechanism?

In the literature so-called moonlighting proteins are described [236]. They are a subset of multifunctional proteins, that exhibit more than one physiologically relevant biochemical function [237]. Different biological functions of a protein often come along with an alternative cellular localisation, that can also promote interactions with new binding partners that, in turn, contribute to the evolution of a new function [238].

### 6.3 AUTOANTIBODIES TARGETING PRDX4 AND EVS EXPRESSING PRDX4 ARE PRESENT IN MALIGNANT PATIENT SAMPLES

---

Especially in pathological conditions such as cancer, moonlighting proteins show multiple modes of action such as involvement in the regulation of immune responses and the cellular metabolism, or through alterations in growth factor signalling, leading to the modulation of cell survival and proliferation [238–240]. This phenomenon has been well described. For example, HSP90 is a molecular chaperone localised in the cytoplasm but is also present on the surface of cancer cells. In addition, a secreted form of HSP90 has been described as pro-tumourigenic by contributing to angiogenesis, and cancer invasiveness [239, 241–243]. Also phospholipid hydroperoxide glutathione peroxidase-4 (GPx4), a peroxidase like PRDX4 and also involved in the cellular defense system against oxidative stress, has been described as a moonlighting protein [244]. These observations implicate that also PRDX4 could be a moonlighting protein with hitherto unknown secondary function on the cell surface.

Still, the reason why and when the translocation of PRDX4, or in general intracellular proteins, take place during the evolution of tumour cells is completely unknown. It is neither known when during the transformation of a normal cell to a frank cancer cells this process takes place, nor what the benefit for the tumour cells is. These are fundamental interesting questions to be addressed in future studies.

### **6.3 Autoantibodies targeting PRDX4 and EVs expressing PRDX4 are present in malignant patient samples**

Within this thesis autoantibodies against PRDX4 could be detected in ascites specimens from cancer patients (see Figure 5.12). Autoantibodies are present in all individuals, and their origin and function are only little understood. In general, they occur naturally at only low concentrations in healthy individuals and have weak binding affinities [210, 245]. In contrast, certain high-affinity autoantibodies are a hallmark of autoimmune diseases like multiple sclerosis, [246], psoriatic arthritis [247] or diabetes mellitus type 1 [248].

Several theories attempt to explain the induction of antibodies to cancer cells, such as the over- or ectopic expression of tumour associated antigens [210, 245]. Elevated levels of autoantibodies against tumour associated antigens appear to develop already in early stage disease and therefore emerged as attractive potential biomarkers for diagnosis, prognosis and treatment monitoring [210].

The detection of autoantibodies comes along with several advantages like the possibility to detect cancer prior to the onset of clinical symptoms [249]. They also persist stably as long as the tumour antigen triggers the humoral immune response, and thus can be used as stable detection markers of disease over a long period of time [207, 250, 251]. Importantly, antibodies are present in the peripheral blood, and thus easily accessible and amenable to non-invasive screening and monitoring methods [210, 252, 253].

The fact that we were able to detect PRDX4-specific autoantibodies in malignant ascites samples from patients emphasizes our findings of an ‘abnormal’ expression of the protein in cancer cells. Unfortunately, repeated experiments with serum samples from patients and healthy donors failed to detect those PRDX4-specific autoantibodies in our hands. A reason for that could be a low concentration in combination with a detection technology that was not sensitive enough.

Therefore, it is crucial to establish more sensitive methods such as an ELISA based assay to enhance the detection limit for autoantibodies. In this respect, it is worth mentioning that our group has recently successfully detected such antibodies in sera from cancer patients using immunoblotting. This project will therefore be continued.

Besides the detection of autoantibodies against PRDX4 from malignant ascites samples and its expression on the cell surface of a variety of tumour cell lines, PRDX4 could also be identified on ascites derived EVs (see Figure 5.11). As tumour derived EVs reflect their cellular origin, they contain - besides general EV markers like tetraspanins CD9, CD63, and CD81 - also potential tumour associated proteins and nucleic acids. EVs have emerged as potential circulating biomarkers for cancer detection, and monitoring of disease in progression and recurrence [254, 255].

One potential application of EVs is liquid biopsy, a method initially approved 2016 by the U.S. Food and Drug Administration (FDA) for diagnosis of non-small-cell lung cancer (NSCLC) [256]. However, this may also be used for other types of cancer like prostate, ovarian, breast and glioblastoma [176, 257–262].

## 6.4 Identification of tPRDX4 in human as potential testis cancer antigen

An alternative splice variant has been described for PRDX4 in the testes of mature mice [130, 132]. This variant was predicted for eutherian mammals [130], and was recently also annotated in the human genome (see Figure 5.21 and table 5.4).

CTAs are antigens, which are specifically expressed testicular by germ cells, and aberrantly expressed in various types of cancer [263]. Their stable and specific expression in tumour cells and absence from healthy cells highlight them as attractive targets for cancer therapy and potential biomarkers [218, 264–266]. It has also been shown that CTAs can participate in tumourigenesis and contribute to multiple hallmarks of cancer [12]. CTAs are either located on the X chromosome (CT-X) or on autosomes (so called non-CT-X), whereby CT-X antigens have a more intimate relation with tumours and are also highly expressed on tumour cells elucidating a high immune response [217, 219, 263].

For example, the most prominent and first described CTA is melanoma antigen family 1 (MAGE A1). MAGE A1 has been shown to be expressed in melanoma, bladder, breast and prostate cancer and is known to evoke strong T cell responses [218, 264, 267]. Until now, over 700 CTAs have been identified with ever increasing number [268].

The PRDX4 gene is localised on the X chromosome, and thus its testis specific variant is a potential CT-X. In this work, also tPRDX4 specific mAbs were generated by immunising mice with a peptide derived from the testis specific exon1 (see Figure 5.22, 5.23 and 5.24). In first experiments, those generated antibodies were successfully used in LSCM. The tested tumour cell line revealed only intracellular staining for tPRDX4 as compared to normal PRDX4 which was also found on the surface as shown by LSCM imaging (see Figure 5.14). Recently, the identified tPRDX4 was detected in human blood samples by whole genome sequencing [215, 216]. This expression indicates that its expression in humans is not strictly confined to testes. All the more, its expression profile should be defined by sensitive diagnostic methods such as RT-PCR or immunohistological stainings of in subsequent experiments.

## 6.5 CCDC47 is a novel interaction partner of PRDX4

A variety of PRDX4 interaction partners have been identified, most of them being ER-localised proteins such as endoplasmic reticulum resident protein 44 (ERP44), thioredoxin domain-containing protein 5 (TXNDC5) and PDIA6. The latter two also co-precipitated with PRDX4 in our mass spectrometric experiments [125]. During this project, yet another protein, CCDC47 - also named calumin - was identified as novel PRDX4 interaction partner (see Figure 5.13 and 5.14).

CCDC47 is also an ER-resident transmembrane protein and is involved in  $\text{Ca}^{2+}$  homeostasis. Recently, it was found that CCDC47 forms a heterodimer in combination with a protein termed Asterix. Together they form the so-called PAT-complex. It was further shown that this complex works as an intramembrane chaperone that protects nascent transmembrane domains of proteins against misfolding and degradation. Consequently, this complex promotes the correct insertion of transmembrane proteins into the membrane lipid bilayer [212, 269]. As we could undoubtedly identify CCDC47 as physical interaction partner of PRDX4, it is tempting to speculate that this complex is also involved in the relocation of PRDX4 to the cell surface.

## 7 References

1. Sung, H., Ferlay, J., Siegel, R. L., Laversanne, M., Soerjomataram, I., Jemal, A. & Bray, F. Global cancer statistics 2020: GLOBOCAN estimates of incidence and mortality worldwide for 36 cancers in 185 countries. *CA: a cancer journal for clinicians* **71**, 209–249 (2021).
2. (WHO), W. H. O. *Global health estimates: Leading causes of death, Cause-specific mortality, 2000–2019* <https://www.who.int/data/gho/data/themes/mortality-and-global-health-estimates/ghe-leading-causes-of-death> (2022).
3. Folkman, J. Tumor angiogenesis: therapeutic implications. *New england journal of medicine* **285**, 1182–1186 (1971).
4. Wang, J., Lei, K. & Han, F. Tumor microenvironment: recent advances in various cancer treatments. *Eur Rev Med Pharmacol Sci* **22**, 3855–3864 (2018).
5. Vendramin, R., Litchfield, K. & Swanton, C. Cancer evolution: Darwin and beyond. *The EMBO Journal* **40**, e108389 (2021).
6. Cairns, J. Mutation selection and the natural history of cancer. *Nature* **255**, 197–200 (1975).
7. Nowell, P. C. The Clonal Evolution of Tumor Cell Populations: Acquired genetic lability permits stepwise selection of variant sublines and underlies tumor progression. *Science* **194**, 23–28 (1976).
8. Greaves, M. & Maley, C. C. Clonal evolution in cancer. *Nature* **481**, 306–313 (2012).
9. Cooper, G. *The Cell: A Molecular Approach* 2nd edition Boston University. The Development and Causes of Cancer. *Sunderland (MA): Sinauer Associates* (2000).
10. Sarkar, S., Horn, G., Moulton, K., Oza, A., Byler, S., Kokolus, S. & Longacre, M. Cancer development, progression, and therapy: an epigenetic overview. *International journal of molecular sciences* **14**, 21087–21113 (2013).
11. Hanahan, D. & Weinberg, R. A. Hallmarks of cancer: the next generation. *cell* **144**, 646–674 (2011).
12. Hanahan, D. Hallmarks of Cancer: New Dimensions. *Cancer Discovery* **12**, 31–46 (2022).

## 7 REFERENCES

---

13. Senga, S. S. & Grose, R. P. Hallmarks of cancer—the new testament. *Open biology* **11**, 200358 (2021).
14. Burkhart, D. L. & Sage, J. Cellular mechanisms of tumour suppression by the retinoblastoma gene. *Nature Reviews Cancer* **8**, 671–682 (2008).
15. Mair, B., Konopka, T., Kerzendorfer, C., Sleiman, K., Salic, S., Serra, V., Muellner, M. K., Theodorou, V. & Nijman, S. M. Gain-and loss-of-function mutations in the breast cancer gene GATA3 result in differential drug sensitivity. *PLoS genetics* **12**, e1006279 (2016).
16. Adams, J. M. & Cory, S. The Bcl-2 apoptotic switch in cancer development and therapy. *Oncogene* **26**, 1324–1337 (2007).
17. Lowe, S. W., Cepero, E. & Evan, G. Intrinsic tumour suppression. *Nature* **432**, 307–315 (2004).
18. Carmeliet, P. & Jain, R. K. Angiogenesis in cancer and other diseases. *nature* **407**, 249–257 (2000).
19. Hillen, F. & Griffioen, A. W. Tumour vascularization: sprouting angiogenesis and beyond. *Cancer and Metastasis Reviews* **26**, 489–502 (2007).
20. Patenaude, A., Parker, J. & Karsan, A. Involvement of endothelial progenitor cells in tumor vascularization. *Microvascular research* **79**, 217–223 (2010).
21. Sivaraman Siveen, K., Prabhu, K., Krishnankutty, R., Kuttikrishnan, S., Tsakou, M., Q Alali, F., Dermime, S., M Mohammad, R. & Uddin, S. Vascular endothelial growth factor (VEGF) signaling in tumour vascularization: potential and challenges. *Current Vascular Pharmacology* **15**, 339–351 (2017).
22. Ripperger, T., Gadzicki, D., Meindl, A. & Schlegelberger, B. Breast cancer susceptibility: current knowledge and implications for genetic counselling. *European Journal of Human Genetics* **17**, 722–731 (2009).
23. Negrini, S., Gorgoulis, V. G. & Halazonetis, T. D. Genomic instability—an evolving hallmark of cancer. *Nature reviews Molecular cell biology* **11**, 220–228 (2010).
24. Yao, Y. & Dai, W. Genomic instability and cancer. *Journal of carcinogenesis & mutagenesis* **5** (2014).
25. Tubbs, A. & Nussenzweig, A. Endogenous DNA damage as a source of genomic instability in cancer. *Cell* **168**, 644–656 (2017).
26. Dvorak, H. F. Tumors: wounds that do not heal. *New England Journal of Medicine* **315**, 1650–1659 (1986).

27. Bates, J. P., Derakhshandeh, R., Jones, L. & Webb, T. J. Mechanisms of immune evasion in breast cancer. *BMC cancer* **18**, 1–14 (2018).
28. Swann, J. B., Smyth, M. J., *et al.* Immune surveillance of tumors. *The Journal of clinical investigation* **117**, 1137–1146 (2007).
29. Chen, D. S. & Mellman, I. Oncology meets immunology: the cancer-immunity cycle. *immunity* **39**, 1–10 (2013).
30. Cabrera, T., Fernandez, M. A., Sierra, A., Garrido, A., Herruzo, A., Escobedo, A., Fabra, A. & Garrido, F. High frequency of altered HLA class I phenotypes in invasive breast carcinomas. *Human immunology* **50**, 127–134 (1996).
31. Drake, C. G., Jaffee, E. & Pardoll, D. M. Mechanisms of immune evasion by tumors. *Advances in immunology* **90**, 51–81 (2006).
32. Zugazagoitia, J., Guedes, C., Ponce, S., Ferrer, I., Molina-Pinelo, S. & Paz-Ares, L. Current challenges in cancer treatment. *Clinical therapeutics* **38**, 1551–1566 (2016).
33. Greten, F. R. & Grivennikov, S. I. Inflammation and cancer: triggers, mechanisms, and consequences. *Immunity* **51**, 27–41 (2019).
34. Balkwill, F. & Mantovani, A. Inflammation and cancer: back to Virchow? *The lancet* **357**, 539–545 (2001).
35. Quail, D. F. & Joyce, J. A. Microenvironmental regulation of tumor progression and metastasis. *Nature medicine* **19**, 1423–1437 (2013).
36. DeNardo, D. G., Andreu, P. & Coussens, L. M. Interactions between lymphocytes and myeloid cells regulate pro-versus anti-tumor immunity. *Cancer and Metastasis Reviews* **29**, 309–316 (2010).
37. Motz, G. T. & Coukos, G. Deciphering and reversing tumor immune suppression. *Immunity* **39**, 61–73 (2013).
38. Hockel, M. & Vaupel, P. Tumor hypoxia: definitions and current clinical, biologic, and molecular aspects. *Journal of the National Cancer Institute* **93**, 266–276 (2001).
39. Wigerup, C., Pählman, S. & Bexell, D. Therapeutic targeting of hypoxia and hypoxia-inducible factors in cancer. *Pharmacology & therapeutics* **164**, 152–169 (2016).
40. Koh, M. Y. & Powis, G. Passing the baton: the HIF switch. *Trends in biochemical sciences* **37**, 364–372 (2012).
41. McKeown, S. Defining normoxia, physoxia and hypoxia in tumours—implications for treatment response. *The British journal of radiology* **87**, 20130676 (2014).

42. Thomlinson, R. H. & Gray, L. H. The histological structure of some human lung cancers and the possible implications for radiotherapy. *British journal of cancer* **9**, 539 (1955).
43. Shao, C., Yang, F., Miao, S., Liu, W., Wang, C., Shu, Y. & Shen, H. Role of hypoxia-induced exosomes in tumor biology. *Molecular Cancer* **17**, 1–8 (2018).
44. Muz, B., de la Puente, P., Azab, F. & Azab, A. K. The role of hypoxia in cancer progression, angiogenesis, metastasis, and resistance to therapy. *Hypoxia* **3**, 83 (2015).
45. Warburg, O., Posener, K. & Negelein, E. Über den stoffwechsel der carcinomzelle. *Naturwissenschaften* **12**, 1131–1137 (1924).
46. Wilson, W. R. & Hay, M. P. Targeting hypoxia in cancer therapy. *Nature Reviews Cancer* **11**, 393–410 (2011).
47. Gatenby, R. A. & Gillies, R. J. Why do cancers have high aerobic glycolysis? *Nature reviews cancer* **4**, 891–899 (2004).
48. Denko, N. C. Hypoxia, HIF1 and glucose metabolism in the solid tumour. *Nature Reviews Cancer* **8**, 705–713 (2008).
49. Semenza, G. L. *et al.* HIF-1 mediates metabolic responses to intratumoral hypoxia and oncogenic mutations. *The Journal of clinical investigation* **123**, 3664–3671 (2013).
50. Li, J., Eu, J. Q., Kong, L. R., Wang, L., Lim, Y. C., Goh, B. C. & Wong, A. L. Targeting metabolism in cancer cells and the tumour microenvironment for cancer therapy. *Molecules* **25**, 4831 (2020).
51. Craene, B. D. & Berx, G. Regulatory networks defining EMT during cancer initiation and progression. *Nature Reviews Cancer* **13**, 97–110 (2013).
52. Jing, X., Yang, F., Shao, C., Wei, K., Xie, M., Shen, H. & Shu, Y. Role of hypoxia in cancer therapy by regulating the tumor microenvironment. *Molecular cancer* **18**, 1–15 (2019).
53. Nobre, A. R., Entenberg, D., Wang, Y., Condeelis, J. & Aguirre-Ghiso, J. A. The different routes to metastasis via hypoxia-regulated programs. *Trends in cell biology* **28**, 941–956 (2018).
54. Rohwer, N., Lobitz, S., Daskalow, K., Jöns, T., Vieth, M., Schlag, P., Kemmner, W., Wiedenmann, B., Cramer, T & Höcker, M. HIF-1 $\alpha$  determines the metastatic potential of gastric cancer cells. *British journal of cancer* **100**, 772–781 (2009).

- 
55. Azab, A. K., Hu, J., Quang, P., Azab, F., Pitsillides, C., Awwad, R., Thompson, B., Maiso, P., Sun, J. D., Hart, C. P., *et al.* Hypoxia promotes dissemination of multiple myeloma through acquisition of epithelial to mesenchymal transition-like features. *Blood, The Journal of the American Society of Hematology* **119**, 5782–5794 (2012).
  56. Gilkes, D. M., Semenza, G. L. & Wirtz, D. Hypoxia and the extracellular matrix: drivers of tumour metastasis. *Nature Reviews Cancer* **14**, 430–439 (2014).
  57. Thiery, J. P., Acloque, H., Huang, R. Y. & Nieto, M. A. Epithelial-mesenchymal transitions in development and disease. *cell* **139**, 871–890 (2009).
  58. Bristow, R. G. & Hill, R. P. Hypoxia, DNA repair and genetic instability. *Nature Reviews Cancer* **8**, 180–192 (2008).
  59. Rohwer, N. & Cramer, T. Hypoxia-mediated drug resistance: novel insights on the functional interaction of HIFs and cell death pathways. *Drug Resistance Updates* **14**, 191–201 (2011).
  60. Rabha, B., Bharadwaj, K. K., Pati, S., Choudhury, B. K., Sarkar, T., Kari, Z. A., Edinur, H. A., Baishya, D. & Atanase, L. I. Development of polymer-based nanoformulations for glioblastoma brain cancer therapy and diagnosis: An update. *Polymers* **13**, 4114 (2021).
  61. Kamisawa, T., Wood, L. D., Itoi, T. & Takaori, K. Pancreatic cancer. *The Lancet* **388**, 73–85 (2016).
  62. Monje, M. & Dietrich, J. Cognitive side effects of cancer therapy demonstrate a functional role for adult neurogenesis. *Behavioural brain research* **227**, 376–379 (2012).
  63. Bjornmalm, M., Thurecht, K. J., Michael, M., Scott, A. M. & Caruso, F. Bridging bio–nano science and cancer nanomedicine. *ACS nano* **11**, 9594–9613 (2017).
  64. Pasquier, E., Kavallaris, M. & André, N. Metronomic chemotherapy: new rationale for new directions. *Nature reviews Clinical oncology* **7**, 455–465 (2010).
  65. Bristow, R. E., Tomacruz, R. S., Armstrong, D. K., Trimble, E. L. & Montz, F., *Database of Abstracts of Reviews of Effects (DARE): Quality-assessed Reviews [Internet]* (Centre for Reviews and Dissemination (UK), 2002).
  66. Scholl, S., Asselain, B., Palangie, T., Dorval, T., Jouve, M., Giralt, E. G., Vilcoq, J., Durand, J. & Pouillart, P. Neoadjuvant chemotherapy in operable breast cancer. *European Journal of Cancer and Clinical Oncology* **27**, 1668–1671 (1991).
  67. Pardoll, D. M. The blockade of immune checkpoints in cancer immunotherapy. *Nature Reviews Cancer* **12**, 252–264 (2012).

68. Leach, D. R., Krummel, M. F. & Allison, J. P. Enhancement of antitumor immunity by CTLA-4 blockade. *Science* **271**, 1734–1736 (1996).
69. Cruz, E. & Kayser, V. Monoclonal antibody therapy of solid tumors: clinical limitations and novel strategies to enhance treatment efficacy. *Biologics: targets & therapy* **13**, 33 (2019).
70. Tovey, S., Brown, S, Doughty, J., Mallon, E., Cooke, T. & Edwards, J. Poor survival outcomes in HER2-positive breast cancer patients with low-grade, node-negative tumours. *British journal of cancer* **100**, 680–683 (2009).
71. Wee, P. & Wang, Z. Epidermal growth factor receptor cell proliferation signaling pathways. *Cancers* **9**, 52 (2017).
72. Nahta, R. & Esteva, F. J. Herceptin: mechanisms of action and resistance. *Cancer letters* **232**, 123–138 (2006).
73. Hudis, C. A. Trastuzumab—mechanism of action and use in clinical practice. *New England journal of medicine* **357**, 39–51 (2007).
74. Bou-Assaly, W & Mukherji, S. Cetuximab (erbitux). *American journal of neuroradiology* **31**, 626–627 (2010).
75. Hansel, T. T., Kropshofer, H., Singer, T., Mitchell, J. A. & George, A. J. The safety and side effects of monoclonal antibodies. *Nature reviews Drug discovery* **9**, 325–338 (2010).
76. Behring, E. v. Ueber das zustandekommen der diphtherie-immunität und der tetanus-immunität bei thieren. *Drucke 19. Jh.* (1890).
77. Scott, A. M., Allison, J. P. & Wolchok, J. D. Monoclonal antibodies in cancer therapy. *Cancer Immunity Archive* **12** (2012).
78. Zahavi, D. & Weiner, L. Monoclonal antibodies in cancer therapy. *Antibodies* **9**, 34 (2020).
79. Merino, A. G. Monoclonal antibodies. Basic features. *Neurología (English Edition)* **26**, 301–306 (2011).
80. Parakh, S., King, D., Gan, H. K. & Scott, A. M. Current development of monoclonal antibodies in cancer therapy. *Current Immunotherapeutic Strategies in Cancer*, 1–70 (2020).
81. Stavnezer, J., Guikema, J. E. & Schrader, C. E. Mechanism and regulation of class switch recombination. *Annual review of immunology* **26**, 261 (2008).

- 
82. Regep, C., Georges, G., Shi, J., Popovic, B. & Deane, C. M. The H3 loop of antibodies shows unique structural characteristics. *Proteins: Structure, Function, and Bioinformatics* **85**, 1311–1318 (2017).
  83. Teng, G. & Papavasiliou, F. N. Immunoglobulin somatic hypermutation. *Annu. Rev. Genet.* **41**, 107–120 (2007).
  84. Jung, D., Giallourakis, C., Mostoslavsky, R., Alt, F. W., *et al.* Mechanism and control of V (D) J recombination at the immunoglobulin heavy chain locus. *Annual review of immunology* **24**, 541–570 (2006).
  85. D’Angelo, S., Ferrara, F., Naranjo, L., Erasmus, M. F., Hrabec, P. & Bradbury, A. R. Many routes to an antibody heavy-chain CDR3: necessary, yet insufficient, for specific binding. *Frontiers in immunology* **9**, 395 (2018).
  86. Benichou, J., Glanville, J., Prak, E. T. L., Azran, R., Kuo, T. C., Pons, J., Desmarais, C., Tsaban, L. & Louzoun, Y. The restricted DH gene reading frame usage in the expressed human antibody repertoire is selected based upon its amino acid content. *The Journal of Immunology* **190**, 5567–5577 (2013).
  87. Vidarsson, G., Dekkers, G. & Rispens, T. IgG subclasses and allotypes: from structure to effector functions. *Frontiers in immunology* **5**, 520 (2014).
  88. Muramatsu, M., Kinoshita, K., Fagarasan, S., Yamada, S., Shinkai, Y. & Honjo, T. Class switch recombination and hypermutation require activation-induced cytidine deaminase (AID), a potential RNA editing enzyme. *Cell* **102**, 553–563 (2000).
  89. Lipman, N. S., Jackson, L. R., Trudel, L. J. & Weis-Garcia, F. Monoclonal versus polyclonal antibodies: distinguishing characteristics, applications, and information resources. *ILAR journal* **46**, 258–268 (2005).
  90. Ferdous, S., Kelm, S., Baker, T. S., Shi, J. & Martin, A. C. B-cell epitopes: Discontinuity and conformational analysis. *Molecular immunology* **114**, 643–650 (2019).
  91. Barlow, D., Edwards, M. & Thornton, J. Continuous and discontinuous protein antigenic determinants. *Nature* **322**, 747–748 (1986).
  92. Ponomarenko, J., Bui, H.-H., Li, W., Fusseder, N., Bourne, P. E., Sette, A. & Peters, B. ElliPro: a new structure-based tool for the prediction of antibody epitopes. *BMC bioinformatics* **9**, 1–8 (2008).
  93. Scott, A. M., Wolchok, J. D. & Old, L. J. Antibody therapy of cancer. *Nature reviews cancer* **12**, 278–287 (2012).

94. Li, S., Schmitz, K. R., Jeffrey, P. D., Wiltzius, J. J., Kussie, P. & Ferguson, K. M. Structural basis for inhibition of the epidermal growth factor receptor by cetuximab. *Cancer cell* **7**, 301–311 (2005).
95. Attarwala, H. TGN1412: from discovery to disaster. *Journal of Young Pharmacists* **2**, 332–336 (2010).
96. Mayes, P. A., Hance, K. W. & Hoos, A. The promise and challenges of immune agonist antibody development in cancer. *Nature Reviews Drug Discovery* **17**, 509–527 (2018).
97. Charmsaz, S., Scott, A. M. & Boyd, A. W. Targeted therapies in hematological malignancies using therapeutic monoclonal antibodies against Eph family receptors. *Experimental hematology* **54**, 31–39 (2017).
98. Nimmerjahn, F. & Ravetch, J. V. Fc $\gamma$  receptors as regulators of immune responses. *Nature Reviews Immunology* **8**, 34–47 (2008).
99. Desjarlais, J. R., Lazar, G. A., Zhukovsky, E. A. & Chu, S. Y. Optimizing engagement of the immune system by anti-tumor antibodies: an engineer’s perspective. *Drug discovery today* **12**, 898–910 (2007).
100. Petricevic, B., Laengle, J., Singer, J., Sachet, M., Fazekas, J., Steger, G., Bartsch, R., Jensen-Jarolim, E. & Bergmann, M. Trastuzumab mediates antibody-dependent cell-mediated cytotoxicity and phagocytosis to the same extent in both adjuvant and metastatic HER2/neu breast cancer patients. *Journal of translational medicine* **11**, 1–11 (2013).
101. Tsao, L.-C., Force, J. & Hartman, Z. C. Mechanisms of therapeutic antitumor monoclonal antibodies. *Cancer research* **81**, 4641–4651 (2021).
102. Waldmann, H. Human monoclonal antibodies: the benefits of humanization. *Human Monoclonal Antibodies*, 1–10 (2019).
103. Safdari, Y., Farajnia, S., Asgharzadeh, M. & Khalili, M. Antibody humanization methods—a review and update. *Biotechnology and Genetic Engineering Reviews* **29**, 175–186 (2013).
104. Harding, F. A., Stickler, M. M., Razo, J. & DuBridge, R. *The immunogenicity of humanized and fully human antibodies: residual immunogenicity resides in the CDR regions MAbs* **2** (2010), 256–265.
105. Jones, P. T., Dear, P. H., Foote, J., Neuberger, M. S. & Winter, G. Replacing the complementarity-determining regions in a human antibody with those from a mouse. *Nature* **321**, 522–525 (1986).

- 
106. Lu, R.-M., Hwang, Y.-C., Liu, I.-J., Lee, C.-C., Tsai, H.-Z., Li, H.-J. & Wu, H.-C. Development of therapeutic antibodies for the treatment of diseases. *Journal of biomedical science* **27**, 1–30 (2020).
  107. BioRender. *bioRENDER* <https://biorender.com/> (2022).
  108. Luo, W., Chen, I., Chen, Y., Alkam, D., Wang, Y. & Semenza, G. L. PRDX2 and PRDX4 are negative regulators of hypoxia-inducible factors under conditions of prolonged hypoxia. *Oncotarget* **7**, 6379 (2016).
  109. Nicolussi, A., D'inzeo, S., Capalbo, C., Giannini, G. & Coppa, A. The role of peroxiredoxins in cancer. *Molecular and clinical oncology* **6**, 139–153 (2017).
  110. Rhee, S. G., Kang, S. W., Chang, T.-S., Jeong, W. & Kim, K. Peroxiredoxin, a novel family of peroxidases. *IUBMB life* **52**, 35–41 (2001).
  111. Rhee, S. G., Woo, H. A., Kil, I. S. & Bae, S. H. Peroxiredoxin functions as a peroxidase and a regulator and sensor of local peroxides. *Journal of Biological Chemistry* **287**, 4403–4410 (2012).
  112. Hofmann, B., Hecht, H.-J. & Flohé, L. Peroxiredoxins (2002).
  113. Jia, W., Chen, P. & Cheng, Y. PRDX4 and its roles in various cancers. *Technology in Cancer Research & Treatment* **18**, 1533033819864313 (2019).
  114. Fujii, J., Ikeda, Y., Kurahashi, T. & Homma, T. Physiological and pathological views of peroxiredoxin 4. *Free Radical Biology and Medicine* **83**, 373–379 (2015).
  115. Wood, Z. A., Schröder, E., Harris, J. R. & Poole, L. B. Structure, mechanism and regulation of peroxiredoxins. *Trends in biochemical sciences* **28**, 32–40 (2003).
  116. Martin, K. & Barrett, J. Reactive oxygen species as double-edged swords in cellular processes: low-dose cell signaling versus high-dose toxicity. *Human & experimental toxicology* **21**, 71–75 (2002).
  117. Fulda, S., Gorman, A. M., Hori, O. & Samali, A. Cellular stress responses: cell survival and cell death. *International journal of cell biology* **2010** (2010).
  118. Kwee, J. K. A paradoxical chemoresistance and tumor suppressive role of antioxidant in solid cancer cells: A strange case of Dr. Jekyll and Mr. Hyde. *BioMed research international* **2014** (2014).
  119. Clerkin, J., Naughton, R., Quiney, C & Cotter, T. Mechanisms of ROS modulated cell survival during carcinogenesis. *Cancer letters* **266**, 30–36 (2008).

## 7 REFERENCES

---

120. Okado-Matsumoto, A., Matsumoto, A., Fujii, J. & Taniguchi, N. Peroxiredoxin IV is a secretable protein with heparin-binding properties under reduced conditions. *The Journal of Biochemistry* **127**, 493–501 (2000).
121. Tavender, T. J., Sheppard, A. M. & Bulleid, N. J. Peroxiredoxin IV is an endoplasmic reticulum-localized enzyme forming oligomeric complexes in human cells. *Biochemical Journal* **411**, 191–199 (2008).
122. Zito, E. PRDX4 an endoplasmic reticulum-localized peroxiredoxin at the crossroads between enzymatic oxidative protein folding and nonenzymatic protein oxidation. *Antioxidants & redox signaling* **18**, 1666–1674 (2013).
123. Tavender, T. J. & Bulleid, N. J. Peroxiredoxin IV protects cells from oxidative stress by removing H<sub>2</sub>O<sub>2</sub> produced during disulphide formation. *Journal of cell science* **123**, 2672–2679 (2010).
124. Ikeda, Y., Nakano, M., Ihara, H., Ito, R., Taniguchi, N. & Fujii, J. Different consequences of reactions with hydrogen peroxide and t-butyl hydroperoxide in the hyperoxidative inactivation of rat peroxiredoxin-4. *The Journal of Biochemistry* **149**, 443–453 (2011).
125. Elko, E. A., Manuel, A. M., White, S., Zito, E., van Der Vliet, A., Anathy, V. & Janssen-Heininger, Y. M. Oxidation of peroxiredoxin-4 induces oligomerization and promotes interaction with proteins governing protein folding and endoplasmic reticulum stress. *Journal of Biological Chemistry* **296** (2021).
126. Jain, P., Sayad, A., Mollen, E., Xie, M., Brown, K., Moffat, J., Hedley, D., Boutros, P., Wouters, B. & Koritzinsky, M. PRDX4 as a novel target for pancreatic cancer. *Cancer Research* **79**, 883–883 (2019).
127. Chen, J.-H., Ni, R.-Z., Xiao, M.-B., Guo, J.-G., Zhou, J.-W., *et al.* Comparative proteomic analysis of differentially expressed proteins in human pancreatic cancer tissue (2009).
128. Wei, Q., Jiang, H., Xiao, Z., Baker, A., Young, M. R., Veenstra, T. D. & Colburn, N. H. Sulfiredoxin–peroxiredoxin IV axis promotes human lung cancer progression through modulation of specific phosphokinase signaling. *Proceedings of the National Academy of Sciences* **108**, 7004–7009 (2011).
129. Palande, K. K., Beekman, R., van der Meeren, L. E., Beverloo, H. B., Valk, P. J. & Touw, I. P. The antioxidant protein peroxiredoxin 4 is epigenetically down regulated in acute promyelocytic leukemia. *PLoS One* **6**, e16340 (2011).

- 
130. Yim, S. H., Kim, Y.-J., Oh, S. Y., Fujii, J., Zhang, Y., Gladyshev, V. N. & Rhee, S. G. Identification and characterization of alternatively transcribed form of peroxiredoxin IV gene that is specifically expressed in spermatids of postpubertal mouse testis. *Journal of Biological Chemistry* **286**, 39002–39012 (2011).
  131. Sasagawa, I., Matsuki, S., Suzuki, Y., Iuchi, Y., Tohya, K., Kimura, M., Nakada, T. & Fujii, J. Possible involvement of the membrane-bound form of peroxiredoxin 4 in acrosome formation during spermiogenesis of rats. *European Journal of Biochemistry* **268**, 3053–3061 (2001).
  132. Homma, T., Kurahashi, T., Ishii, N., Shirasawa, N. & Fujii, J. Testis-specific peroxiredoxin 4 variant is not absolutely required for spermatogenesis and fertility in mice. *Scientific reports* **10**, 1–12 (2020).
  133. Tasaki, E., Matsumoto, S., Tada, H., Kurahashi, T., Zhang, X., Fujii, J., Utsumi, T. & Iuchi, Y. Protective role of testis-specific peroxiredoxin 4 against cellular oxidative stress. *Journal of clinical biochemistry and nutrition* **60**, 156–161 (2017).
  134. Raposo, G. & Stoorvogel, W. Extracellular vesicles: exosomes, microvesicles, and friends. *J Cell Biol* **200**, 373–383 (2013).
  135. Van der Pol, E., Böing, A. N., Harrison, P., Sturk, A. & Nieuwland, R. Classification, functions, and clinical relevance of extracellular vesicles. *Pharmacological reviews* **64**, 676–705 (2012).
  136. Ronquist, G. & Brody, I. The prostasome: its secretion and function in man. *Biochimica et biophysica acta* **822**, 203–218 (1985).
  137. Pisitkun, T., Shen, R.-F. & Knepper, M. A. Identification and proteomic profiling of exosomes in human urine. *Proceedings of the National Academy of Sciences of the United States of America* **101**, 13368–13373 (2004).
  138. Caby, M.-P., Lankar, D., Vincendeau-Scherrer, C., Raposo, G. & Bonnerot, C. Exosomal-like vesicles are present in human blood plasma. *International immunology* **17**, 879–887 (2005).
  139. Vella, L., Sharples, R., Lawson, V., Masters, C., Cappai, R & Hill, A. Packaging of prions into exosomes is associated with a novel pathway of PrP processing. *The Journal of pathology* **211**, 582–590 (2007).
  140. Colombo, M., Raposo, G. & Théry, C. Biogenesis, secretion, and intercellular interactions of exosomes and other extracellular vesicles. *Annual review of cell and developmental biology* **30**, 255–289 (2014).

141. Bebelman, M. P., Smit, M. J., Pegtel, D. M. & Baglio, S. R. Biogenesis and function of extracellular vesicles in cancer. *Pharmacology & therapeutics* **188**, 1–11 (2018).
142. Zaborowski, M. P., Balaj, L., Breakefield, X. O. & Lai, C. P. Extracellular vesicles: composition, biological relevance, and methods of study. *Bioscience* **65**, 783–797 (2015).
143. Kerr, J. F., Wyllie, A. H. & Currie, A. R. Apoptosis: a basic biological phenomenon with wideranging implications in tissue kinetics. *British journal of cancer* **26**, 239 (1972).
144. Andaloussi, S. E., Mäger, I., Breakefield, X. O. & Wood, M. J. Extracellular vesicles: biology and emerging therapeutic opportunities. *Nature reviews Drug discovery* **12**, 347 (2013).
145. Morello, M., Minciacchi, V., De Candia, P., Yang, J., Posadas, E., Kim, H., Griffiths, D., Bhowmick, N., Chung, L., Gandellini, P., *et al.* Large oncosomes mediate intercellular transfer of functional microRNA. *Cell cycle* **12**, 3526–3536 (2013).
146. Kalluri, R. & LeBleu, V. S. The biology, function, and biomedical applications of exosomes. *Science* **367**, eaau6977 (2020).
147. Pan, B.-T. & Johnstone, R. M. Fate of the transferrin receptor during maturation of sheep reticulocytes in vitro: selective externalization of the receptor. *Cell* **33**, 967–978 (1983).
148. Théry, C., Ostrowski, M. & Segura, E. Membrane vesicles as conveyors of immune responses. *Nature reviews immunology* **9**, 581 (2009).
149. Robbins, P. D. & Morelli, A. E. Regulation of immune responses by extracellular vesicles. *Nature Reviews Immunology* **14**, 195 (2014).
150. McAndrews, K. M. & Kalluri, R. Mechanisms associated with biogenesis of exosomes in cancer. *Molecular cancer* **18**, 1–11 (2019).
151. Simpson, R. J., Lim, J. W., Moritz, R. L. & Mathivanan, S. Exosomes: proteomic insights and diagnostic potential. *Expert review of proteomics* **6**, 267–283 (2009).
152. Mathivanan, S., Ji, H. & Simpson, R. J. Exosomes: extracellular organelles important in intercellular communication. *Journal of proteomics* **73**, 1907–1920 (2010).
153. Möbius, W, Van Donselaar, E, Ohno-Iwashita, Y, Shimada, Y, Heijnen, H., Slot, J. & Geuze, H. Recycling compartments and the internal vesicles of multivesicular bodies harbor most of the cholesterol found in the endocytic pathway. *Traffic* **4**, 222–231 (2003).

- 
154. Hurley, J. H. ESCRT complexes and the biogenesis of multivesicular bodies. *Current opinion in cell biology* **20**, 4–11 (2008).
  155. Henne, W. M., Buchkovich, N. J. & Emr, S. D. The ESCRT pathway. *Developmental cell* **21**, 77–91 (2011).
  156. Kowal, J., Tkach, M. & Théry, C. Biogenesis and secretion of exosomes. *Current opinion in cell biology* **29**, 116–125 (2014).
  157. Kalluri, R. *et al.* The biology and function of exosomes in cancer. *The Journal of clinical investigation* **126**, 1208–1215 (2016).
  158. Mears, R., Craven, R. A., Hanrahan, S., Totty, N., Upton, C., Young, S. L., Patel, P., Selby, P. J. & Banks, R. E. Proteomic analysis of melanoma-derived exosomes by two-dimensional polyacrylamide gel electrophoresis and mass spectrometry. *Proteomics* **4**, 4019–4031 (2004).
  159. Futter, C. E. & White, I. J. Annexins and endocytosis. *Traffic* **8**, 951–958 (2007).
  160. Valadi, H., Ekström, K., Bossios, A., Sjöstrand, M., Lee, J. J. & Lötvall, J. O. Exosome-mediated transfer of mRNAs and microRNAs is a novel mechanism of genetic exchange between cells. *Nature cell biology* **9**, 654 (2007).
  161. Morelli, A. E., Larregina, A. T., Shufesky, W. J., Sullivan, M. L., Stolz, D. B., Papworth, G. D., Zahorchak, A. F., Logar, A. J., Waang, Z., Watkins, S. C., *et al.* Endocytosis, intracellular sorting, and processing of exosomes by dendritic cells. *Blood* **104**, 3257–3266 (2004).
  162. Cocucci, E. & Meldolesi, J. Ectosomes and exosomes: shedding the confusion between extracellular vesicles. *Trends in cell biology* **25**, 364–372 (2015).
  163. Shifrin, D. A., Beckler, M. D., Coffey, R. J. & Tyska, M. J. Extracellular vesicles: communication, coercion, and conditioning. *Molecular biology of the cell* **24**, 1253–1259 (2013).
  164. Feng, D., Zhao, W.-L., Ye, Y.-Y., Bai, X.-C., Liu, R.-Q., Chang, L.-F., Zhou, Q. & Sui, S.-F. Cellular internalization of exosomes occurs through phagocytosis. *Traffic* **11**, 675–687 (2010).
  165. Barrès, C., Blanc, L., Bette-Bobillo, P., André, S., Mamoun, R., Gabius, H.-J. & Vidal, M. Galectin-5 is bound onto the surface of rat reticulocyte exosomes and modulates vesicle uptake by macrophages. *Blood* **115**, 696–705 (2010).

## 7 REFERENCES

---

166. Camussi, G., Deregibus, M.-C., Bruno, S., Grange, C., Fonsato, V. & Tetta, C. Exosome/ microvesicle-mediated epigenetic reprogramming of cells. *American journal of cancer research* **1**, 98 (2011).
167. Gatti, S., Bruno, S., Deregibus, M. C., Sordi, A., Cantaluppi, V., Tetta, C. & Camussi, G. Microvesicles derived from human adult mesenchymal stem cells protect against ischaemia–reperfusion-induced acute and chronic kidney injury. *Nephrology Dialysis Transplantation* **26**, 1474–1483 (2011).
168. Kurywchak, P., Tavormina, J. & Kalluri, R. The emerging roles of exosomes in the modulation of immune responses in cancer. *Genome medicine* **10**, 1–4 (2018).
169. Raposo, G., Nijman, H. W., Stoorvogel, W., Liejendekker, R., Harding, C. V., Melief, C. J. & Geuze, H. J. B lymphocytes secrete antigen-presenting vesicles. *Journal of Experimental Medicine* **183**, 1161–1172 (1996).
170. Clayton, A., Mitchell, J. P., Mason, M. D., Tabi, Z., *et al.* Human tumor-derived exosomes selectively impair lymphocyte responses to interleukin-2. *Cancer research* **67**, 7458–7466 (2007).
171. Baj-Krzyworzeka, M., Szatanek, R., Węglarczyk, K., Baran, J. & Zembala, M. Tumour-derived microvesicles modulate biological activity of human monocytes. *Immunology letters* **113**, 76–82 (2007).
172. Simhadri, V. R., Reiners, K. S., Hansen, H. P., Topolar, D., Simhadri, V. L., Nohroudi, K., Kufer, T. A., Engert, A. & von Strandmann, E. P. Dendritic cells release HLA-B-associated transcript-3 positive exosomes to regulate natural killer function. *PloS one* **3**, e3377 (2008).
173. Taylor, D. D. & Gerçel-Taylor, C. MicroRNA signatures of tumor-derived exosomes as diagnostic biomarkers of ovarian cancer. *Gynecologic oncology* **110**, 13–21 (2008).
174. Rabinowits, G., Gerçel-Taylor, C., Day, J. M., Taylor, D. D. & Kloecker, G. H. Exosomal microRNA: a diagnostic marker for lung cancer. *Clinical lung cancer* **10**, 42–46 (2009).
175. Skog, J., Würdinger, T., Van Rijn, S., Meijer, D. H., Gainche, L., Curry, W. T., Carter, B. S., Krichevsky, A. M. & Breakefield, X. O. Glioblastoma microvesicles transport RNA and proteins that promote tumour growth and provide diagnostic biomarkers. *Nature cell biology* **10**, 1470–1476 (2008).
176. Nilsson, J., Skog, J., Nordstrand, A., Baranov, V., Mincheva-Nilsson, L., Breakefield, X. & Widmark, A. Prostate cancer-derived urine exosomes: a novel approach to biomarkers for prostate cancer. *British journal of cancer* **100**, 1603–1607 (2009).

- 
177. Melo, S. A., Luecke, L. B., Kahlert, C., Fernandez, A. F., Gammon, S. T., Kaye, J., LeBleu, V. S., Mittendorf, E. A., Weitz, J., Rahbari, N., *et al.* Glypican-1 identifies cancer exosomes and detects early pancreatic cancer. *Nature* **523**, 177–182 (2015).
178. Thakur, B. K., Zhang, H., Becker, A., Matei, I., Huang, Y., Costa-Silva, B., Zheng, Y., Hoshino, A., Brazier, H., Xiang, J., *et al.* Double-stranded DNA in exosomes: a novel biomarker in cancer detection. *Cell research* **24**, 766–769 (2014).
179. Kosaka, N., Yoshioka, Y., Fujita, Y., Ochiya, T., *et al.* Versatile roles of extracellular vesicles in cancer. *The Journal of clinical investigation* **126**, 1163–1172 (2016).
180. Andreola, G., Rivoltini, L., Castelli, C., Huber, V., Perego, P., Deho, P., Squarcina, P., Accornero, P., Lozupone, F., Lugini, L., *et al.* Induction of lymphocyte apoptosis by tumor cell secretion of FasL-bearing microvesicles. *The Journal of experimental medicine* **195**, 1303–1316 (2002).
181. Fernandes Ribeiro, M., Zhu, H., W Millard, R. & Fan, G.-C. Exosomes function in pro-and anti-angiogenesis. *Current angiogenesis* **2**, 54–59 (2013).
182. Park, J. E., Tan, H. S., Datta, A., Lai, R. C., Zhang, H., Meng, W., Lim, S. K. & Sze, S. K. Hypoxic tumor cell modulates its microenvironment to enhance angiogenic and metastatic potential by secretion of proteins and exosomes. *Molecular & cellular proteomics* **9**, 1085–1099 (2010).
183. Tao, S.-C. & Guo, S.-C. Role of extracellular vesicles in tumour microenvironment. *Cell Communication and Signaling* **18**, 1–24 (2020).
184. Psaila, B. & Lyden, D. The metastatic niche: adapting the foreign soil. *Nature Reviews Cancer* **9**, 285–293 (2009).
185. Peinado, H., Alečković, M., Lavotshkin, S., Matei, I., Costa-Silva, B., Moreno-Bueno, G., Hergueta-Redondo, M., Williams, C., García-Santos, G., Ghajar, C. M., *et al.* Melanoma exosomes educate bone marrow progenitor cells toward a pro-metastatic phenotype through MET. *Nature medicine* **18**, 883–891 (2012).
186. Mashouri, L., Yousefi, H., Aref, A. R., Molaei, F., Alahari, S. K., *et al.* Exosomes: composition, biogenesis, and mechanisms in cancer metastasis and drug resistance. *Molecular cancer* **18**, 1–14 (2019).
187. Corrado, C., Raimondo, S., Chiesi, A., Ciccia, F., De Leo, G. & Alessandro, R. Exosomes as intercellular signaling organelles involved in health and disease: basic science and clinical applications. *International journal of molecular sciences* **14**, 5338–5366 (2013).

188. Safaei, R., Larson, B. J., Cheng, T. C., Gibson, M. A., Otani, S., Naerdemann, W. & Howell, S. B. Abnormal lysosomal trafficking and enhanced exosomal export of cisplatin in drug-resistant human ovarian carcinoma cells. *Molecular cancer therapeutics* **4**, 1595–1604 (2005).
189. Scientific, T. F. *ExpiCHO-S Cells are derived from a non-engineered subclone that has been screened and isolated from CHO-S Chinese hamster ovary (CHO) cells* <https://www.thermofisher.com/order/catalog/product/A29127> (2022).
190. Graham, F., Smiley, J., Russell, W. & Nairn, R. Characteristics of a human cell line transformed by DNA from human adenovirus type 5. *Journal of General Virology* **36**, 59–72 (1977).
191. Hanahan, D. Studies on transformation of *Escherichia coli* with plasmids. *Journal of molecular biology* **166**, 557–580 (1983).
192. Schindelin, J., Arganda-Carreras, I., Frise, E., Kaynig, V., Longair, M., Pietzsch, T., Preibisch, S., Rueden, C., Saalfeld, S., Schmid, B., *et al.* Fiji: an open-source platform for biological-image analysis. *Nature methods* **9**, 676–682 (2012).
193. Chemogenomix. *abYsis Integrated antibody sequence and structure analysis* <http://www.abysis.org/abysis/index.html> (2022).
194. Scientific, T. F. *Stable Trnasfection* <https://www.thermofisher.com/de/de/home/references/gibco-cell-culture-basics/transfection-basics/transfection-methods/stable-transfection.html> (2022).
195. Life technologies, I. *5' RACE System for Rapid Amplification of cDNA Ends, Version 2.0* [https://www.thermofisher.com/document-connect/document-connect.html?url=https%3A%2F%2Fassets.thermofisher.com%2FTFS-Assets%2FLSG%2Fmanuals%2F5prime\\_race\\_man.pdf](https://www.thermofisher.com/document-connect/document-connect.html?url=https%3A%2F%2Fassets.thermofisher.com%2FTFS-Assets%2FLSG%2Fmanuals%2F5prime_race_man.pdf) (2022).
196. NEB. *PCR Protocol for Phusion HF DNA Polymerase* <https://international.neb.com/protocols/0001/01/01/pcr-protocol-m0530> (2022).
197. QIAGEN. *Ni-NTA Agarose* <https://www.qiagen.com/us/products/discovery-and-translational-research/protein-purification/tagged-protein-expression-purification-detection/ni-nta-agarose/> (2022).
198. Dragovic, R. A., Gardiner, C., Brooks, A. S., Tannetta, D. S., Ferguson, D. J., Hole, P., Carr, B., Redman, C. W., Harriss, A. L., Dobson, P. J., *et al.* Sizing and phenotyping of cellular vesicles using Nanoparticle Tracking Analysis. *Nanomedicine: Nanotechnology, Biology and Medicine* **7**, 780–788 (2011).

199. Battke, C., Kremmer, E., Mysliwietz, J., Gondi, G., Dumitru, C., Brandau, S., Lang, S., Vullo, D., Supuran, C. & Zeidler, R. Generation and characterization of the first inhibitory antibody targeting tumour-associated carbonic anhydrase XII. *Cancer Immunology, Immunotherapy* **60**, 649–658 (2011).
200. Kellner, M., von Neubeck, B., Czogalla, B., Feederle, R., Vick, B., Jeremias, I. & Zeidler, R. A Novel Anti-CD73 Antibody That Selectively Inhibits Membrane CD73 Shows Antitumor Activity and Induces Tumor Immune Escape. *Biomedicines* **10**, 825 (2022).
201. Kahlert, C. & Kalluri, R. Exosomes in tumor microenvironment influence cancer progression and metastasis. *Journal of molecular medicine* **91**, 431–437 (2013).
202. Bertout, J. A., Patel, S. A. & Simon, M. C. The impact of O<sub>2</sub> availability on human cancer. *Nature Reviews Cancer* **8**, 967–975 (2008).
203. Schulte, J. Peroxiredoxin 4: a multifunctional biomarker worthy of further exploration. *BMC medicine* **9**, 1–5 (2011).
204. Skou, J. C. The influence of some cations on an adenosine triphosphatase from peripheral nerves. *Biochimica et biophysica acta* **23**, 394–401 (1957).
205. Lingrel, J. B. Na<sup>+</sup>, K<sup>+</sup>-ATPase. *J Biol Chem* **269**, 19659–19662 (1994).
206. Morth, J. P., Pedersen, B. P., Buch-Pedersen, M. J., Andersen, J. P., Vilsen, B., Palmgren, M. G. & Nissen, P. A structural overview of the plasma membrane Na<sup>+</sup>, K<sup>+</sup>-ATPase and H<sup>+</sup>-ATPase ion pumps. *Nature reviews Molecular cell biology* **12**, 60–70 (2011).
207. Baldwin, R. Immunity to transplanted tumour: the effect of tumour extracts on the growth of homologous tumours in rats. *British Journal of Cancer* **9**, 646 (1955).
208. Pedersen, J. W. & Wandall, H. H. Autoantibodies as biomarkers in cancer. *Laboratory Medicine* **42**, 623–628 (2011).
209. Von Kleist, S. & Burtin, P. On the specificity of autoantibodies present in colon cancer patients. *Immunology* **10**, 507 (1966).
210. Yadav, S., Kashaninejad, N., Masud, M. K., Yamauchi, Y., Nguyen, N.-T. & Shid-diky, M. J. Autoantibodies as diagnostic and prognostic cancer biomarker: Detection techniques and approaches. *Biosensors and Bioelectronics* **139**, 111315 (2019).
211. Zhang, M., Yamazaki, T., Yazawa, M., Treves, S., Nishi, M., Murai, M., Shibata, E., Zorzato, F. & Takeshima, H. Calumin, a novel Ca<sup>2+</sup>-binding transmembrane protein on the endoplasmic reticulum. *Cell Calcium* **42**, 83–90 (2007).

## 7 REFERENCES

---

212. Chitwood, P. J. & Hegde, R. S. An intramembrane chaperone complex facilitates membrane protein biogenesis. *Nature* **584**, 630–634 (2020).
213. Clavero-Álvarez, A., Di Mambro, T., Perez-Gaviro, S., Magnani, M. & Bruscolini, P. Humanization of antibodies using a statistical inference approach. *Scientific reports* **8**, 1–11 (2018).
214. National Library of Medicine, U. & National Center of Biotechnology Information, B. *Nucleotide Pan troglodytes peroxiredoxin 4 (PRDX4) transcript variant X3 mRNA XM016943945* [https://www.ncbi.nlm.nih.gov/nuccore/XM\\_016943945.1](https://www.ncbi.nlm.nih.gov/nuccore/XM_016943945.1) (2022).
215. National Library of Medicine, U. & National Center of Biotechnology Information, B. *peroxiredoxin 4, Homo sapiens, KAI2598897.1* <https://www.ncbi.nlm.nih.gov/protein/KAI2598897.1?report=genpept> (2022).
216. Zimin, A. V., Shumate, A., Shinder, I., Heinz, J., Puiu, D., Pertea, M. & Salzberg, S. L. A reference-quality, fully annotated genome from a Puerto Rican individual. *Genetics* **220**, iyab227 (2022).
217. Simpson, A. J., Caballero, O. L., Jungbluth, A., Chen, Y.-T. & Old, L. J. Cancer/testis antigens, gametogenesis and cancer. *Nature Reviews Cancer* **5**, 615–625 (2005).
218. Krishnadas, D. K., Bai, F. & Lucas, K. G. Cancer testis antigen and immunotherapy. *ImmunoTargets and therapy* **2**, 11 (2013).
219. Meng, X., Sun, X., Liu, Z. & He, Y. A novel era of cancer/testis antigen in cancer immunotherapy. *International Immunopharmacology* **98**, 107889 (2021).
220. Mathew, M., Zade, M., Mezghani, N., Patel, R., Wang, Y. & Momen-Heravi, F. Extracellular vesicles as biomarkers in cancer immunotherapy. *Cancers* **12**, 2825 (2020).
221. Weidle, U. H., Maisel, D., Klostermann, S., Schiller, C. & Weiss, E. H. Intracellular proteins displayed on the surface of tumor cells as targets for therapeutic intervention with antibody-related agents. *Cancer genomics & proteomics* **8**, 49–63 (2011).
222. Huang, J. & Honda, W. CED: a conformational epitope database. *BMC immunology* **7**, 1–8 (2006).
223. Long, F., Fong, R. H., Austin, S. K., Chen, Z., Klose, T., Fokine, A., Liu, Y., Porta, J., Sapparapu, G., Akahata, W., *et al.* Cryo-EM structures elucidate neutralizing mechanisms of anti-chikungunya human monoclonal antibodies with therapeutic activity. *Proceedings of the National Academy of Sciences* **112**, 13898–13903 (2015).

- 
224. Linnebacher, M., Lorenz, P., Koy, C., Jahnke, A., Born, N., Steinbeck, F., Wollbold, J., Latzkow, T., Thiesen, H.-J. & Glocker, M. O. Clonality characterization of natural epitope-specific antibodies against the tumor-related antigen topoisomerase IIa by peptide chip and proteome analysis: a pilot study with colorectal carcinoma patient samples. *Analytical and bioanalytical chemistry* **403**, 227–238 (2012).
225. Lester, E., Ooi, F. K., Bakkar, N., Ayers, J., Woerman, A. L., Wheeler, J., Bowser, R., Carlson, G. A., Prusiner, S. B. & Parker, R. Tau aggregates are RNA-protein assemblies that mislocalize multiple nuclear speckle components. *Neuron* **109**, 1675–1691 (2021).
226. McMillan, P. J., Strovast, T. J., Baum, M., Mitchell, B. K., Eck, R. J., Hendricks, N., Wheeler, J. M., Latimer, C. S., Keene, C. D. & Kraemer, B. C. Pathological tau drives ectopic nuclear speckle scaffold protein SRRM2 accumulation in neuron cytoplasm in Alzheimer’s disease. *Acta neuropathologica communications* **9**, 1–14 (2021).
227. Brown, E. J. & Frazier, W. A. Integrin-associated protein (CD47) and its ligands. *Trends in cell biology* **11**, 130–135 (2001).
228. Reinhold, M. I., Lindberg, F. P., Plas, D., Reynolds, S., Peters, M. G. & Brown, E. J. In vivo expression of alternatively spliced forms of integrin-associated protein (CD47). *Journal of cell science* **108**, 3419–3425 (1995).
229. Jaiswal, S., Jamieson, C. H., Pang, W. W., Park, C. Y., Chao, M. P., Majeti, R., Traver, D., van Rooijen, N. & Weissman, I. L. CD47 is upregulated on circulating hematopoietic stem cells and leukemia cells to avoid phagocytosis. *Cell* **138**, 271–285 (2009).
230. Chao, M. P., Weissman, I. L. & Majeti, R. The CD47–SIRP $\alpha$  pathway in cancer immune evasion and potential therapeutic implications. *Current opinion in immunology* **24**, 225–232 (2012).
231. Oldenborg, P.-A., Zheleznyak, A., Fang, Y.-F., Lagenaur, C. F., Gresham, H. D. & Lindberg, F. P. Role of CD47 as a marker of self on red blood cells. *Science* **288**, 2051–2054 (2000).
232. Weidle, U. H., Scheuer, W., Eggle, D., Klostermann, S. & Stockinger, H. Cancer-related issues of CD147. *Cancer genomics & proteomics* **7**, 157–169 (2010).
233. Grass, G. D. & Toole, B. P. How, with whom and when: an overview of CD147-mediated regulatory networks influencing matrix metalloproteinase activity. *Bioscience Reports* **36** (2016).

## 7 REFERENCES

---

234. Landras, A., Reger de Moura, C., Jouenne, F., Lebbe, C., Menashi, S. & Mourah, S. CD147 is a promising target of tumor progression and a prognostic biomarker. *Cancers* **11**, 1803 (2019).
235. Yan, L., Zucker, S. & Toole, B. P. Roles of the multifunctional glycoprotein, emmprin (basigin; CD147), in tumour progression. *Thrombosis and haemostasis* **93**, 199–204 (2005).
236. Jeffery, C. J. Moonlighting proteins. *Trends in biochemical sciences* **24**, 8–11 (1999).
237. Jeffery, C. J. Protein moonlighting: what is it, and why is it important? *Philosophical Transactions of the Royal Society B: Biological Sciences* **373**, 20160523 (2018).
238. Adamo, A., Frusteri, C., Pallotta, M. T., Pirali, T., Sartoris, S. & Ugel, S. Moonlighting proteins are important players in cancer immunology. *Frontiers in immunology* **11**, 613069 (2021).
239. Min, K.-W., Lee, S.-H. & Baek, S. J. Moonlighting proteins in cancer. *Cancer letters* **370**, 108–116 (2016).
240. Lv, L. & Lei, Q. Proteins moonlighting in tumor metabolism and epigenetics. *Frontiers of Medicine* **15**, 383–403 (2021).
241. Whitesell, L. & Lindquist, S. L. HSP90 and the chaperoning of cancer. *Nature Reviews Cancer* **5**, 761–772 (2005).
242. Isaacs, J. S., Xu, W. & Neckers, L. Heat shock protein 90 as a molecular target for cancer therapeutics. *Cancer cell* **3**, 213–217 (2003).
243. Eustace, B. K., Sakurai, T., Stewart, J. K., Yimlamai, D., Unger, C., Zehetmeier, C., Lain, B., Torella, C., Henning, S. W., Beste, G., *et al.* Functional proteomic screens reveal an essential extracellular role for hsp90 $\alpha$  in cancer cell invasiveness. *Nature cell biology* **6**, 507–514 (2004).
244. Scheerer, P., Borchert, A., Krauss, N., Wessner, H., Gerth, C., Höhne, W. & Kuhn, H. Structural basis for catalytic activity and enzyme polymerization of phospholipid hydroperoxide glutathione peroxidase-4 (GPx4). *Biochemistry* **46**, 9041–9049 (2007).
245. Caron, M., Choquet-Kastylevsky, G. & Joubert-Caron, R. Cancer immunomics using autoantibody signatures for biomarker discovery. *Molecular & Cellular Proteomics* **6**, 1115–1122 (2007).
246. Genain, C. P., Cannella, B., Hauser, S. L. & Raine, C. S. Identification of autoantibodies associated with myelin damage in multiple sclerosis. *Nature medicine* **5**, 170–175 (1999).

- 
247. Yuan, Y., Qiu, J., Lin, Z.-T., Li, W., Haley, C., Mui, U. N., Ning, J., Tying, S. K. & Wu, T. Identification of novel autoantibodies associated with psoriatic arthritis. *Arthritis & Rheumatology* **71**, 941–951 (2019).
248. Taplin, C. E. & Barker, J. M. Autoantibodies in type 1 diabetes. *Autoimmunity* **41**, 11–18 (2008).
249. Chapman, C. J., Thorpe, A. J., Murray, A., Parsy-Kowalska, C. B., Allen, J., Stafford, K. M., Chauhan, A. S., Kite, T. A., Maddison, P. & Robertson, J. F. Immunobiomarkers in Small Cell Lung Cancer: Potential Early Cancer Signals Autoantibodies in Small Cell Lung Cancer. *Clinical Cancer Research* **17**, 1474–1480 (2011).
250. Zaenker, P., Gray, E. S. & Ziman, M. R. Autoantibody production in cancer—the humoral immune response toward autologous antigens in cancer patients. *Autoimmunity reviews* **15**, 477–483 (2016).
251. Tan, H. T., Low, J., Lim, S. G. & Chung, M. C. Serum autoantibodies as biomarkers for early cancer detection. *The FEBS journal* **276**, 6880–6904 (2009).
252. Aggarwal, A. Role of autoantibody testing. *Best Practice & Research Clinical Rheumatology* **28**, 907–920 (2014).
253. Arif, S., Qudsia, S., Urooj, S., Chaudry, N., Arshad, A. & Andleeb, S. Blueprint of quartz crystal microbalance biosensor for early detection of breast cancer through salivary autoantibodies against ATP6AP1. *Biosensors and Bioelectronics* **65**, 62–70 (2015).
254. Möller, A. & Lobb, R. J. The evolving translational potential of small extracellular vesicles in cancer. *Nature Reviews Cancer* **20**, 697–709 (2020).
255. Keller, S., Ridinger, J., Rupp, A.-K., Janssen, J. W. & Altevogt, P. Body fluid derived exosomes as a novel template for clinical diagnostics. *Journal of translational medicine* **9**, 1–9 (2011).
256. Kwapisz, D. The first liquid biopsy test approved. Is it a new era of mutation testing for non-small cell lung cancer? *Annals of translational medicine* **5** (2017).
257. Soung, Y. H., Ford, S., Zhang, V. & Chung, J. Exosomes in cancer diagnostics. *Cancers* **9**, 8 (2017).
258. Xu, R., Rai, A., Chen, M., Suwakulsiri, W., Greening, D. W. & Simpson, R. J. Extracellular vesicles in cancer—implications for future improvements in cancer care. *Nature reviews Clinical oncology* **15**, 617–638 (2018).

## 7 REFERENCES

---

259. Moon, P.-G., Lee, J.-E., Cho, Y.-E., Lee, S. J., Jung, J. H., Chae, Y. S., Bae, H.-I., Kim, Y.-B., Kim, I.-S., Park, H. Y., *et al.* Identification of Developmental Endothelial Locus-1 on Circulating Extracellular Vesicles as a Novel Biomarker for Early Breast Cancer Detection. *Clinical cancer research* **22**, 1757–1766 (2016).
260. Khan, S., Jutzy, J. M., Valenzuela, M. M. A., Turay, D., Aspe, J. R., Ashok, A., Mirshahidi, S., Mercola, D., Lilly, M. B. & Wall, N. R. Plasma-derived exosomal survivin, a plausible biomarker for early detection of prostate cancer (2012).
261. Shao, H., Chung, J., Balaj, L., Charest, A., Bigner, D. D., Carter, B. S., Hochberg, F. H., Breakefield, X. O., Weissleder, R. & Lee, H. Protein typing of circulating microvesicles allows real-time monitoring of glioblastoma therapy. *Nature medicine* **18**, 1835–1840 (2012).
262. Liu, J., Chen, Y., Pei, F., Zeng, C., Yao, Y., Liao, W. & Zhao, Z. Extracellular vesicles in liquid biopsies: potential for disease diagnosis. *BioMed Research International* **2021** (2021).
263. Caballero, O. L. & Chen, Y.-T. Cancer/testis antigens: potential targets for immunotherapy. *Innate Immune Regulation and Cancer Immunotherapy*, 347–369 (2009).
264. Scanlan, M. J., G Simpson, A. J. & Old, L. J. The cancer/testis genes: review, standardization, and commentary. *Cancer immunity* **4** (2004).
265. Salmaninejad, A., Zamani, M. R., Pourvahedi, M., Golchehre, Z., Hosseini Bereshneh, A. & Rezaei, N. Cancer/testis antigens: expression, regulation, tumor invasion, and use in immunotherapy of cancers. *Immunological investigations* **45**, 619–640 (2016).
266. Scanlan, M. J., Gure, A. O., Jungbluth, A. A., Old, L. J. & Chen, Y.-T. Cancer/testis antigens: an expanding family of targets for cancer immunotherapy. *Immunological reviews* **188**, 22–32 (2002).
267. Chaux, P., Luiten, R., Demotte, N., Vantomme, V., Stroobant, V., Traversari, C., Russo, V., Schultz, E., Cornelis, G. R., Boon, T., *et al.* Identification of five MAGE-A1 epitopes recognized by cytolytic T lymphocytes obtained by in vitro stimulation with dendritic cells transduced with MAGE-A1. *The Journal of Immunology* **163**, 2928–2936 (1999).
268. Yang, P., Qiao, Y., Meng, M. & Zhou, Q. Cancer/Testis Antigens as Biomarker and Target for the Diagnosis, Prognosis, and Therapy of Lung Cancer. *Frontiers in Oncology* **12** (2022).

269. Yamamoto, S., Yamazaki, T., Komazaki, S., Yamashita, T., Osaki, M., Matsubayashi, M., Kidoya, H., Takakura, N., Yamazaki, D. & Kakizawa, S. Contribution of calumen to embryogenesis through participation in the endoplasmic reticulum-associated degradation activity. *Developmental biology* **393**, 33–43 (2014).



## 8 Appendix

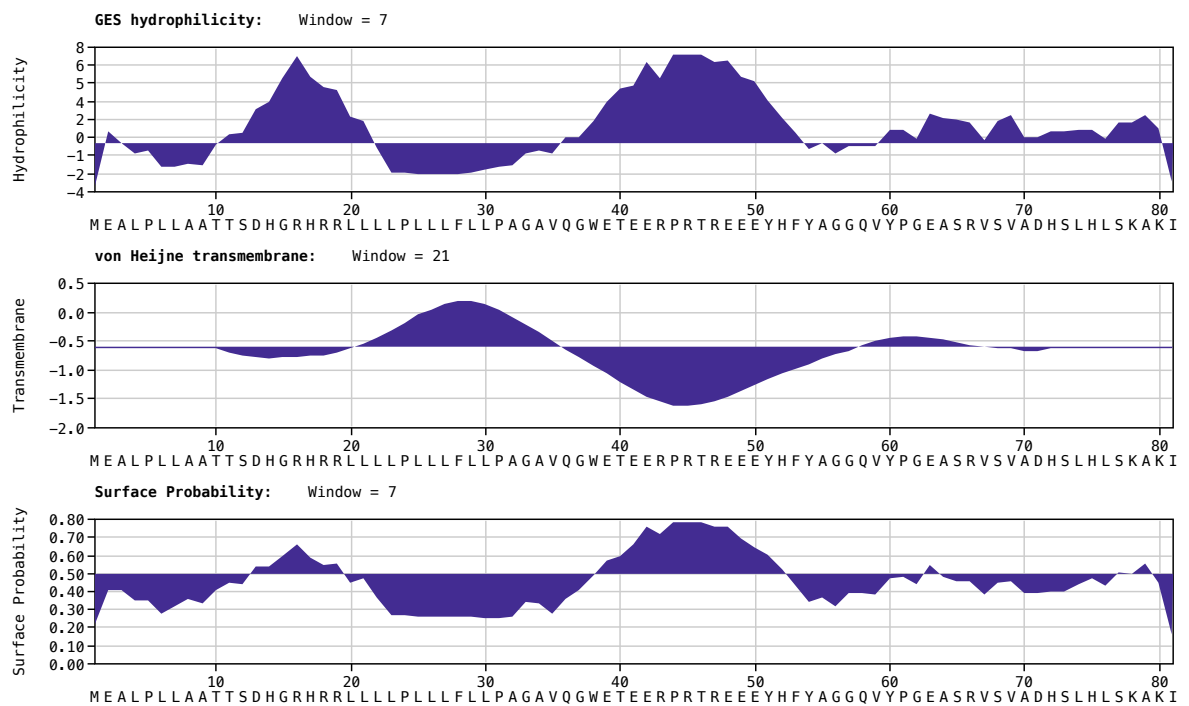


**Figure 8.1: Computational analysis of PRDX4 exon1.**

PRDX4 exon 1 comprises a hydrophobic signal sequence followed by a hydrophilic stretch.  
Created with Macvector (see table 3.19).

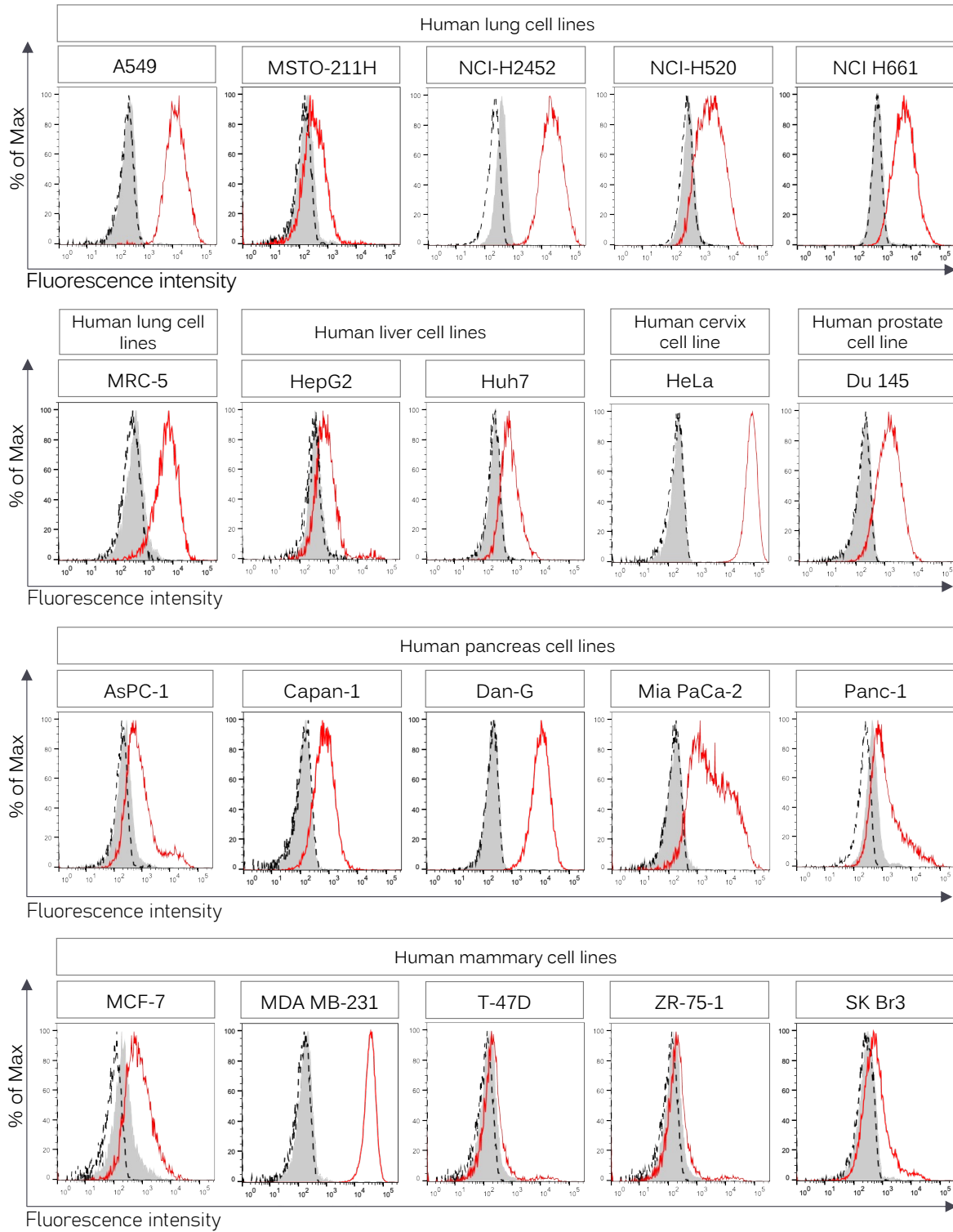
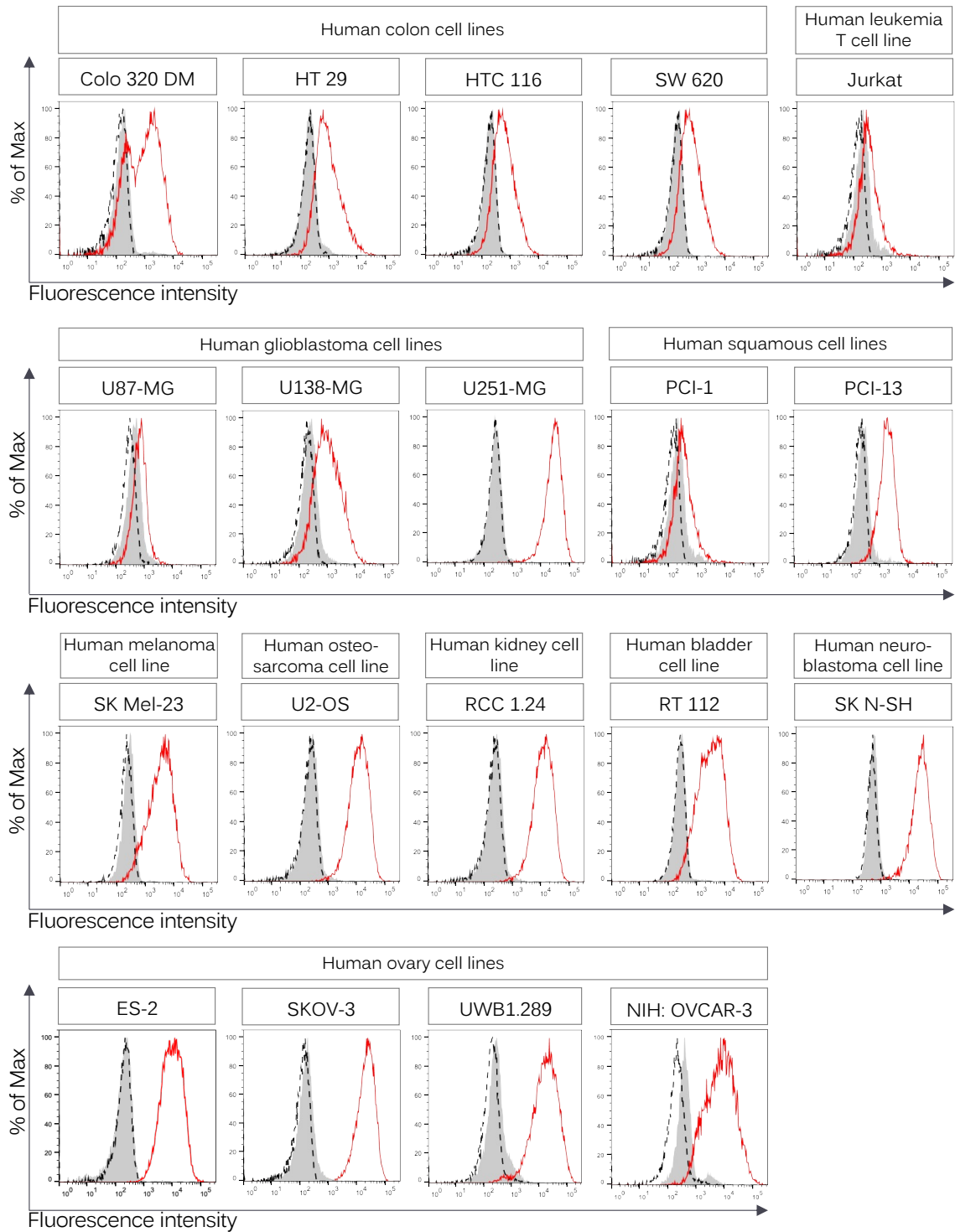
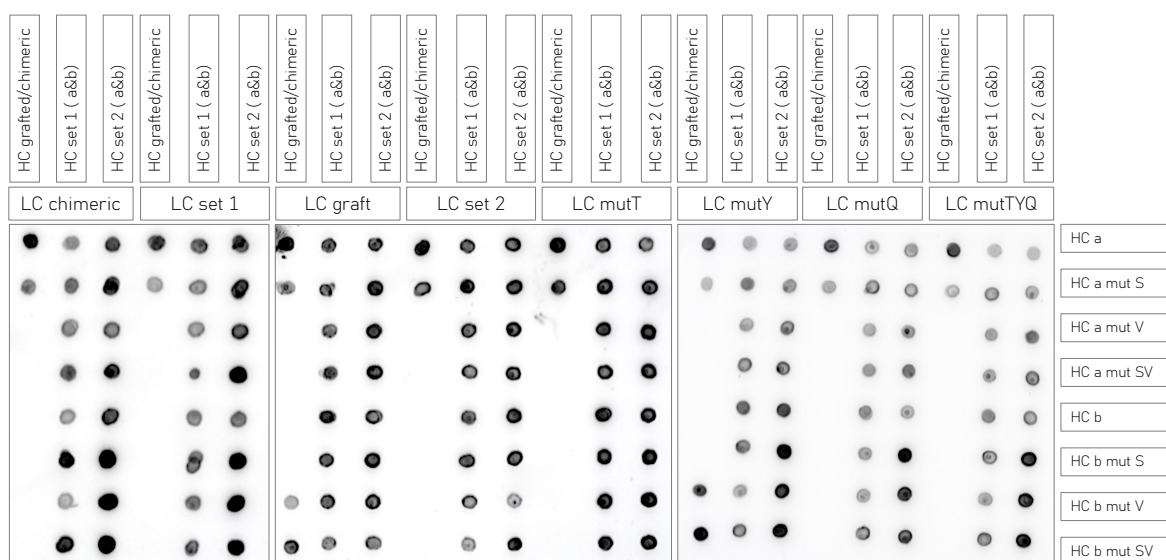


Figure 8.2: PRDX4 surface expression on different cell lines.



**Figure 8.2: PRDX4 surface expression on different cell lines.**

Each cell line was stained using the OCA2E 5H5 antibody (see table 3.9) followed by staining with  $\alpha$ -rat IgG (H + L) Alexa Flour 647 antibody (see table 3.10).



**Figure 8.3: Dot Blot of humanisation of antibody 5H5.**

Dot blot of supernatants upon cotransfection with 5H5 heavy and light chain plasmids. For all samples, 2  $\mu$ L supernatant were pipetted onto the nitrocellulose membrane, blocked and incubated with  $\alpha$ -human-HRP antibody (1:2,000) and analysed using the Fusion FX6 device.

**Table 8.1: Plasmid sequences of the evaluated backmutations for the humanisation of the OCA2E 5H5 antibody heavy chain.**

The backmutations of the different sets are marked in different colors. Black = fully humanised, purple = set1 backmutations, blue = set2 backmutations, orange = additional backmutations ‘S’ and/or ‘V’ included upon an insufficient first round of tests.

plasmid	Protein Sequence.
	<b>Heavy chain</b>
chimeric	QVQLQQSGAELVRPGTSVKLSCKASGYTFTSNHMHWIKETTGQGLEWIGIINPGNGGSRFNVKFKGKATLTVDKSSTTA <sup>S</sup> FMQLSSLTPEDSAVYYCARGNPASFDYWGQGMVTVSS
graft	QVQLVQSGAEVKKPGASVKV <sup>S</sup> SCKASGYTFTSNHMHWVRQAPGQGLEW <sup>M</sup> GIINPGNGGSRFNVKFKGRVTMTRD <sup>T</sup> TSTSTVY <sup>M</sup> ELSSLR <sup>S</sup> EDTAVYYCARGNPASFDYWGQGLVTVSS
set1a	QVQLVQSGAEVKKPGASVKV <sup>S</sup> SCKASGYTFTSNHMHWVRQAPGQGLEW <sup>M</sup> GIINPGNGGSRFNVKFKGRVTMTRD <sup>T</sup> TSTSTAY <sup>M</sup> ELSSLR <sup>S</sup> EDTAVYYCARGNPASFDYWGQGLVTVSS
set1a mutS	QVQLVQSGAEVKKPGASVKV <sup>S</sup> SCKASGYTFTSNHMHWVRQAPGQGLEW <sup>M</sup> GIINPGNGGSRFNVKFKGRVTMTRD <sup>T</sup> SS <sup>T</sup> AY <sup>M</sup> ELSSLR <sup>S</sup> EDTAVYYCARGNPASFDYWGQGLVTVSS
set1a mutV	QVQLVQSGAEVKKPGASVKV <sup>S</sup> SCKASGYTFTSNHMHWVRQAPGQGLEW <sup>M</sup> GIINPGNGGSRFNVKFKGRVTMTRD <sup>T</sup> TSTSTVY <sup>M</sup> ELSSLR <sup>S</sup> EDTAVYYCARGNPASFDYWGQGLVTVSS
set1a mutSV	QVQLVQSGAEVKKPGASVKV <sup>S</sup> SCKASGYTFTSNHMHWVRQAPGQGLEW <sup>M</sup> GIINPGNGGSRFNVKFKGRVTMTRD <sup>T</sup> SS <sup>T</sup> VY <sup>M</sup> ELSSLR <sup>S</sup> EDTAVYYCARGNPASFDYWGQGLVTVSS
set1b	QVQLVQSGAEVKKPGASVKLSCKASGYTFTSNHMHWVRQAPGQGLEWIGIINPGNGGSRFNVKFKGRVTMTRD <sup>T</sup> TSTSTAY <sup>M</sup> QLSSLR <sup>S</sup> EDTAVYYCARGNPASFDYWGQGLVTVSS
set1b mutS	QVQLVQSGAEVKKPGASVKLSCKASGYTFTSNHMHWVRQAPGQGLEWIGIINPGNGGSRFNVKFKGRVTMTRD <sup>T</sup> SS <sup>T</sup> AY <sup>M</sup> QLSSLR <sup>S</sup> EDTAVYYCARGNPASFDYWGQGLVTVSS
set1b mutV	QVQLVQSGAEVKKPGASVKLSCKASGYTFTSNHMHWVRQAPGQGLEWIGIINPGNGGSRFNVKFKGRVTMTRD <sup>T</sup> TSTSTVY <sup>M</sup> QLSSLR <sup>S</sup> EDTAVYYCARGNPASFDYWGQGLVTVSS
set1b mutSV	QVQLVQSGAEVKKPGASVKLSCKASGYTFTSNHMHWVRQAPGQGLEWIGIINPGNGGSRFNVKFKGRVTMTRD <sup>T</sup> SS <sup>T</sup> VY <sup>M</sup> QLSSLR <sup>S</sup> EDTAVYYCARGNPASFDYWGQGLVTVSS
set2a	QVQLVQSGAELVKPGASVKLSCKASGYTFTSNHMHWVRQAPGQGLEWIGIINPGNGGSRFNVKFKGRVTMTRD <sup>T</sup> TSTSTAY <sup>M</sup> QLSSLR <sup>S</sup> EDTAVYYCARGNPASFDYWGQGLVTVSS
set2a mutS	QVQLVQSGAELVKPGASVKLSCKASGYTFTSNHMHWVRQAPGQGLEWIGIINPGNGGSRFNVKFKGRVTMTRD <sup>T</sup> SS <sup>T</sup> AY <sup>M</sup> QLSSLR <sup>S</sup> EDTAVYYCARGNPASFDYWGQGLVTVSS
set2a mutV	QVQLVQSGAELVKPGASVKLSCKASGYTFTSNHMHWVRQAPGQGLEWIGIINPGNGGSRFNVKFKGRVTMTRD <sup>T</sup> TSTSTVY <sup>M</sup> QLSSLR <sup>S</sup> EDTAVYYCARGNPASFDYWGQGLVTVSS
set2a mutSV	QVQLVQSGAELVKPGASVKLSCKASGYTFTSNHMHWVRQAPGQGLEWIGIINPGNGGSRFNVKFKGRVTMTRD <sup>T</sup> SS <sup>T</sup> VY <sup>M</sup> QLSSLR <sup>S</sup> EDTAVYYCARGNPASFDYWGQGLVTVSS
set2b	QVQLVQSGAELVKPGASVKLSCKASGYTFTSNHMHWIRQAPGQGLEWIGIINPGNGGSRFNVKFKGRVTMTVD <sup>T</sup> TSTSTAY <sup>M</sup> QLSSLT <sup>S</sup> EDTAVYYCARGNPASFDYWGQGLVTVSS
set2b mutS	QVQLVQSGAELVKPGASVKLSCKASGYTFTSNHMHWIRQAPGQGLEWIGIINPGNGGSRFNVKFKGRVTMTVD <sup>T</sup> SS <sup>T</sup> AY <sup>M</sup> QLSSLT <sup>S</sup> EDTAVYYCARGNPASFDYWGQGLVTVSS
set2b mutV	QVQLVQSGAELVKPGASVKLSCKASGYTFTSNHMHWIRQAPGQGLEWIGIINPGNGGSRFNVKFKGRVTMTVD <sup>T</sup> TSTSTVY <sup>M</sup> QLSSLT <sup>S</sup> EDTAVYYCARGNPASFDYWGQGLVTVSS
set2b mutSV	QVQLVQSGAELVKPGASVKLSCKASGYTFTSNHMHWIRQAPGQGLEWIGIINPGNGGSRFNVKFKGRVTMTVD <sup>T</sup> SS <sup>T</sup> VY <sup>M</sup> QLSSLT <sup>S</sup> EDTAVYYCARGNPASFDYWGQGLVTVSS

**Table 8.2: Plasmid sequences of the evaluated backmutations for the humanisation of the OCA2E 5H5 antibody light chain.**

The backmutations of the different sets are marked in different colors. Black = fully humanised, purple = set1 backmutations, blue = set2 backmutations, orange = additional backmutations ‘T’, ‘Y’ or ‘Q’, or all included upon an insufficient first round of tests.

plasmid	Protein Sequence
<b>Light chain</b>	
chimeric	DIQMTQSPSFLSASVGDRVTINCRASENIYKYLWYQQK <b>F</b> GEAPKRLIYNTNTLETG <b>I</b> PSRFSGSGSGT <b>D</b> F <del>FT</del> LTISSLQPEDFATY <b>F</b> CLQHSNFPFTFG <b>S</b> GTKLEIKRA
graft	DIQMTQSPSSLASVGDRVTITCRASENIYKYLWYQQK <b>P</b> GKAPKRLIYNTNTLETG <b>V</b> PSRFSGSGSGT <b>E</b> F <del>FT</del> LTISSLQPEDFATY <b>Y</b> CLQHSNFPFTFG <b>Q</b> GTKLEIKRA
set1	DIQMTQSPSSLASVGDRVTITCRASENIYKYLWYQQK <b>P</b> GKAPKRLIYNTNTLETG <b>V</b> PSRFSGSGSGT <b>D</b> F <del>FT</del> LTISSLQPEDFATY <b>Y</b> CLQHSNFPFTFG <b>Q</b> GTKLEIKRA
set2	DIQMTQSPSSLASVGDRVTITCRASENIYKYLWYQQK <b>P</b> GKAPKRLIYNTNTLETG <b>I</b> PSRFSGSGSGT <b>E</b> F <del>FT</del> LTISSLQPEDFATY <b>Y</b> CLQHSNFPFTFG <b>Q</b> GTKLEIKRA
mutT	DIQMTQSPSSLASVGDRVTI <b>N</b> CRASENIYKYLWYQQK <b>P</b> GKAPKRLIYNTNTLETG <b>V</b> PSRFSGSGSGT <b>E</b> F <del>FT</del> LTISSLQPEDFATY <b>Y</b> CLQHSNFPFTFG <b>Q</b> GTKLEIKRA
mutY	DIQMTQSPSSLASVGDRVTITCRASENIYKYLWYQQK <b>P</b> GKAPKRLIYNTNTLETG <b>V</b> PSRFSGSGSGT <b>E</b> F <del>FT</del> LTISSLQPEDFATY <b>F</b> CLQHSNFPFTFG <b>Q</b> GTKLEIKRA
mutQ	DIQMTQSPSSLASVGDRVTITCRASENIYKYLWYQQK <b>P</b> GKAPKRLIYNTNTLETG <b>V</b> PSRFSGSGSGT <b>E</b> F <del>FT</del> LTISSLQPEDFATY <b>Y</b> CLQHSNFPFTFG <b>S</b> GTKLEIKRA
mutTYQ	DIQMTQSPSSLASVGDRVTI <b>N</b> CRASENIYKYLWYQQK <b>P</b> GKAPKRLIYNTNTLETG <b>V</b> PSRFSGSGSGT <b>E</b> F <del>FT</del> LTISSLQPEDFATY <b>F</b> CLQHSNFPFTFG <b>S</b> GTKLEIKRA

**Table 8.3: Identified protein sequences of three tPRDX4 antibody clones.**

Immunoglobulin heavy and light chain sequences were obtained by 5' RACE-PCR technique. CDR-regions are marked in red. All three antibodies analysed show different sequences for their respective HC and LC sequences.

AB clone	Protein Sequence
<b>Heavy chain</b>	
1H1	QVQLKESGPRVQPSQTLSTCTVSGFSLR <b>NNGVI</b> WVRQPPGKGLEW <b>MTI</b> WEDENT <b>NYNSVLK</b> SRLTFSRDTSK <b>SQVFL</b> NMNNLQTEDTAMYFCAR <b>DRFDY</b> WGQGVMTVSS
15C8	QVQLQQSGAELVKPGSSVKMSCKASGYTFT <b>SYI</b> FWIKQSPGQGLEW <b>IGR</b> IGPGSGDT <b>NYNEK</b> FKGKATFTVDKSSSTAYMQLSSLTPEDTAVYYCARE <b>SMDA</b> WGQGTSVTVSS
19A4	QVQLKESGPGLVQPSQTLSTCTVSGFSL <b>TRYI</b> HWVRQPPGKGLEW <b>LGM</b> WNDGDT <b>SYNSGLK</b> SRLSISRDTSK <b>SQVFL</b> KLNSLQTEDTATYYCAR <b>VSHGY</b> WGQGVLTVSS
<b>Light chain</b>	
1H1	EIVLTQGALPNPVPSGESASITC <b>QSSKSL</b> LHRNGK <b>TYLN</b> WYLQRPGQSPQLLIY <b>WMSTRAS</b> GVSDRFSGSGSGTDFTLKISSVEAEDVAVYYC <b>QQFLEYPL</b> TFGSGTKLEIKRA
15C8	DIVMTQTPSSQAVSTGEKVTMT <b>CKSSQS</b> LLYSEN <b>KKNYLA</b> WYQKPGQSPKLLIY <b>WASTRKS</b> GVDPDRFIGSGSGTDFTLTISVQAEDLAVYYC <b>QQYYNFPL</b> TFGSGTKLEIKRA
19A4	DVVLVTPPTLSATIGQSVSIS <b>CRSSQS</b> LLHSNG <b>NTYLH</b> WLLQRPGQSPQLLIY <b>SVYRLQS</b> GVPNRFSGSGSGTDFTLKISGVEAEDLGVYYC <b>VQGT</b> HVPNTFGAGTKLELRRAD



# Danksagung

An dieser Stelle möchte ich mich ganz herzlich bei einigen Personen bedanken, ohne die diese Arbeit nicht möglich gewesen wäre.

Zu allererst vielen Dank an Prof. Dr. Reinhard Zeidler für das spannende Projekt, die hervorragende wissenschaftliche Betreuung. Danke für die Unterstützung, die vielen Diskussionen und Ideen die dieses Projekt erst so interessant gestaltet haben.

Zudem einen besonderen Dank an Prof. Dr. Rainer Glaß und Prof. Dr. Irmela Jeremias für die exzellente beratende Unterstützung meines Projektes als Mitglieder meines Promotionskomitees.

Des Weiteren ein großes Danke an das gesamte Labor 205. Danke an Judith und Sanni für die unendliche Hilfsbereitschaft bei allerlei großen und kleinen Belangen, den immer "fachlichen" Austausch im Labor und das gute Miteinander. Danke an Kathrin für die gute Zusammenarbeit. Danke an Markus, unseren Klonierungsexperten für die ständigen großen und kleinen Hilfestellungen sobald es ans Klonieren ging. Danke an Johannes, für die vielen "Montagsmorgen"-Gespräche und guten Optimierungsideen im Laboralltag.

Ein Danke auch an unsere "Adoptiv-Zeidlers" Alex und Tanja für die vielen Gespräche über Gott und die Welt und manchmal auch über Wissenschaftliches.

Einen Dank auch an die Arbeitsgruppe "Monoklonale Antikörper Core Facility" für die Durchführung der Immunisierungen sowie die Reinigung der vielen, vielen Antikörper.

Einen riesengroßen Dank an meine Familie für die bedingungslose Unterstützung über die ganzen Jahre des Studiums. Zu guter Letzt möchte ich mich von ganzem Herzen bei meinem Partner Sebastian bedanken, der mich immer emotional untertützt hat - egal wie anstrengend es war - und auch viel wissenschaftlichen Input aus einer anderen Sichtweise geliefert hat, den ich sonst bestimmt übersehen hätte.